Department of Physics
Indian Institute of Technology Guwahati
Ph.D. Thesis

Exploring BSM Physics Through Doublet Extensions of the Higgs Sector

Shibananda Sahoo

Thesis Supervisor: Prof. Poulose Poulose

March, 2019

Exploring BSM Physics Through Doublet Extensions of the Higgs Sector

A Thesis submitted for the award of the degree of
Doctor of Philosophy in Physics
by

Shibananda Sahoo

Thesis Supervisor: **Prof. Poulose Poulose**

Department of Physics
Indian Institute of Technology Guwahati
Guwahati - 781039, Assam, India

March, 2019

Statement

The work contained in the thesis entitled "**Exploring BSM Physics Through Doublet Extensions of the Higgs Sector**" has been carried out at the Department of Physics, Indian Institute of Technology Guwahati, India by me under the supervision of Prof. Poulose Poulose. The material of this thesis has not been submitted elsewhere for any other degree. Works presented in the thesis are all my own unless referenced to the contrary in the thesis.

(Shibananda Sahoo) Date:
March, 2019
Department of Physics
Indian Institute of Technology Guwahati
Guwahati - 781039, India

Disclaimer

The bibliography included in this thesis is, by no means complete but contains the ones which are consulted thoroughly by me. I apologize for inadvertently missing out some of the research papers, review articles and other scientific documents pertaining to the focus of this thesis which should also have been cited.

Certificate

It is certified that the work contained in the thesis entitled "**Exploring BSM Physics Through Doublet Extensions of the Higgs Sector**" by Mr. Shibananda Sahoo (Roll No - 126121016), a Ph.D. student in the Department of Physics, Indian Institute of Technology Guwahati is carried out under my supervision and has not been submitted elsewhere for the award of any other degree.

(Dr. Poulose Poulose) Date:
March, 2019
Professor
Department of Physics
Indian Institute of Technology Guwahati
Guwahati - 781039, India

To

Dibyajanani Maa

and

Lord Sri Aurobindo

Acknowledgement

I am highly indebted to my supervisor Prof. Poulose Poulose for giving me an oppurtunity to carry out the work under his guidance. He always motivated me to take this work as a challenge. Best thing about him, his friendly behaviour which made me comfortable with him for the entire period. I am fortunate enough to get a supervisor like him.

I would also like to thank my Doctoral committee members Dr. Arunansu Sil, Dr. Udit Raha, Dr. Subhaditya Bhattacharya, Dr. K.V.Srikanth for giving me numerous comments and valuable suggestions during my PhD tenure. I want to thank my collaborators Dr. Satendra Kumar, Prof. K. Sridhar, Dr. Debasish Borah, Dr. Soumya Sadhukhan, Dr. Baradhwaj Coleppa, Prof. Benjamin Fuks. It was quite wonderful experience while collaborating with them. I have learnt many things from the collaborative discussions. I am specially grateful to Dr. Debasish Borah for his immense help and support during the entire period. I am thankful to Prof. Girish Sampath Setlur, Dr. Charudatt Y. Kadolkar, Dr. Tarak Nath Dey, Prof. Subhradip Ghosh for their excellent lectures during the course work days. I am very much thankful to Dr. Tapan Mishra for his constant motivation during last phase of my PhD tenure. I am also thankful to present HoD Prof. Subhradip Ghosh and former HoD Prof. Saurabh Basu for all the help and support during my entire PhD career. I also thank all the members of our HEP Journal Club at IITG. I have learnt many things from the discussions in the journal club meetings. I extend my gratitude to all the faculty members and staff of the Department of Physics, who supported me in several ways during this period. I am grateful to Mr. Basab Purkayastha and Mr. Hemanta Medhi for their timely help to resolve the technical issues.

I am thankful to my 2012 batchmates Abhijit, Bibhuti, Omkar, Rahul, Ramiz, Kallol, Sourav, Ashis, Koushik, Sudinda, Anabilda, , Venkat, Prahlad, Ram, Junmoni. I would like to thank my research group friends: Biswaranjan, Deepanjali, Subhasish, Dr. Rashidul Islam, Sreemanti, Suresh. I thank all my seniors: Ranjan bhai, Bhagaban bhai, Brahma bhai, Debashish bhai, Bisuda, Biplobda, Sandeep

bhai, Bapada, Amitda, Vishwajit Bhaiya, Nitin. I am also thankful to my juniors: Ghanashyam, Goutam, Purushottam, Rishav, Dibyendu, Kajal. I am fortunate enough to get some good buddies in hostel: Anand, Pratap, Rasmi bhai, Himadri bhai, Pradeep bhai, Kajwal, Chitta, Saibal, Sritam, Soumya, Ranjan, Ramesh, Bighna, Uttam, Ankan, Rupak, Sangram, Pankaj, Swarup, Sudarshan, Ramesh Ana, Swarup RJ.

I must also mention that I had very good friends in my M.Sc. days Abhaya Bhai, Kasinath, Kishora, Mihir bhai, Pragati, Sudipta, Jitendra, Saroj bhai, Suryakanta, Nirakar, Jogesh, Biswaranjan, Dipu, Bikash, Naba Bhai from whom I have learnt many things related to academic as well as non-academic issues. I am specially thankful to Kasinath who always helped me to clarify my silly doubts and also for his critical comments on the thesis. I am very much thankful my village friends: Satya, Ugra, Kula, Susanta, Chagulu, Ramei, Santosh, Kuna, Kusunu, Titu, Prasanta (Kha), Chandan, Bishnu, Akshaya, Anta Bhai, Ranjan Bhai, Atula Bhai, Kula Bhai, Sakuntala Apa for their constant support and encouragement.

I am thankful to my colleagues from GM University: Pati Sir, Acharya Sir, Niranjan Sir, Prasanti Madam, from Dhenkanal College: Rashmi Madam, Sujaya Sir, Baral Sir, Ramesh Sir, Debasis Sir, Ranjit Sir, Debaraj Sir, Pati Sir, Khillar Sir, Rajanikant Sir, Pandaba Sir, Dilip Sir, Bibhu Sir, Sarangi Sir, Rana Sir, Padhy Sir, Sanjeet Sir, Padmakanta Sir, Pal Sir, Biswa Sir, Aditya Sir, Gopi Sir, Kalandi Sir, Manju Madam, Ranjita Madam, Namrata Madam, Namita Madam, Surekha Madam, Priyanka Madam, Swagatika Madam, Rinarani Madam. I would also like to thank Dhenkanal College supporting staff members : Pothal Sir, Singh Sir, Khuntia Babu, Bhoi Babu, Rama bhai for their help and support.

I want to thank all my teachers from School days to PhD: Bailochan Sir, Late Chintamani Sir, Shishir Sir, Mayadhar Sir, Gobinda Sir, Basanta Sir, Purastam Sir, Raghu Sir, Mutu Sir, Krushna Sir, Padhi Sir, Chitta Sir, Rama Sir, Prasanna Sir, Tuna Sir, Kalipad Sir, PET Sir, Sridhar Sir, Sriram Sir, Sukanta Sir, Damodar Sir, Karamadev Sir, Swapna Madam, Pramod Sir, Mishra Sir, Prasanta Sir, Barik Sir, Khare Madam, LP Singh Sir for their inspiration throughout my entire career.

Special thanks to Subas from whom I have learnt many things, Kathia Bhai who always encouraged to study properly, Tanmaya bhai who always helped me in the tough periods and Chandini(Anand's Wife) for all the moral support and tasty foods.

I am also thankful to my supervisor's wife Ms. Stavelin who had always inspired to finish PhD soon and their sweet kids Hasvid and Onella for all the fun moments.

In the end, I would like to thank my family members: Bou, Bapa, Majianma, Late

Ratna Dada, Bina Sanama, Late Mahia Dada, Gaya Dada, Bhama Sanama, Late my grandfather Chintamani, Late my grandmother Kasani, my sisters: Mina, Rina, Lina, Pinky, Mama, Sima, Kandhei and Chinky, my brothers: Piku bhai, Papu bhai, Dipu, Kunu, my Bhaujas: Sanju, Pami and the sweetest kid of our family: Om. I am really thankful my sister Rina who has sacrificed her entire career for our family. I am also thankful to my relatives: Piesa, Nani, Kodanda Piesa, Para Nani, Rabi Nana, Mandakini, Chinmaya, Babi, Dillip, Niru, Nini, Debunu, Gania Bhai, Siria Bhai, Bhasa Bhai, Bidya Bhai. I am very thankful to my sweet Aei and Late Aja who spent their entire life for the sake of our family.

I would like to gratefully acknowledge to MHRD, Government of India for the research fellowship and to DST for the travel grant to attend the conference Scalars 2017 which held at University of Warsaw, Poland. I am very much grateful to DHE, Government of Odisha for granting leave to me to complete the remaining part of thesis work.

Last but not the least I thank to Almighty for his help during those tough and hard fought days.

March, 2019 *Shibananda Sahoo*

Acronyms

LHC	:	Large Hadron Collider
ATLAS	:	A Toroidal LHC Apparatus
CMS	:	Compact Muon Solenoid
SM	:	Standard Model
2HDM	:	Two Higgs Doublet Model
IHDM	:	Inert Higgs Doublet Model
DM	:	Dark Matter
GeV	:	Giga electron Volt
BSM	:	Beyond Standard Model
EW	:	Electroweak
QCD	:	Quantum ChromoDynamics
VEV	:	Vacuum Expectation Value
SSB	:	Spontaneous Symmetry Breaking
EWSB	:	Electroweak Symmetry Breaking
GUT	:	Grand Unified Theory
SUSY	:	Supersymmetry
MSSM	:	Minimal Supersymmetric Standard Model
NMSSM	:	Next-to-Minimal Supersymmetric Model
ExD	:	Extra Dimensions
EGMs	:	Extended Gauge Models
DOFs	:	Degress of Freedoms

ggF	:	gluon gluon Fusion
MET	:	Missing Transverse Energy
LEP	:	Large Electron Positron Collider
ILC	:	International Linear Collider
BR	:	Branching Ratio
BP	:	Benchmark Points
VBF	:	Vector Boson Fusion
h.c.	:	Hermitian Conjugate
UFO	:	Universal FeynRule Output
VLL	:	Vector like Leptons
LFV	:	Lepton Flavour Violation
TeV	:	Tera electron Volt
EWPD	:	Electroweak Precision Data
RGE	:	Renormalization Group Evolution

Abstract

In the year 2012, two collaborations of LHC, ATLAS and CMS independently observed a new particle known as Standard Model (SM)-like Higgs boson. This discovery confirms Higgs mechanism as the way of Electroweak Symmetry Breaking. The Higgs boson was predicted by Peter Higgs and Francois Englert in 1964 to break the electroweak symmetry spontaneously, for which they received nobel prize in 2013. Although the discovery completes the particle spectrum of the SM, it opens the door for the beyond the SM Higgs sector as the observed particle can be accommodated in a natural way in many attractive multi-Higgs scenarios. But the confirmation of these models depends on observing other scalars of the models. Our main aim in this thesis is to explore the implications of some of the multi-Higgs models.

Out of the several multi-Higgs models, two Higgs doublet model (2HDM) is the most popular and simpler model. In this model, SM Higgs sector is extended by another Higgs doublet. As a result, the model has four physical Higgs bosons i.e. H, A, $H^{\pm}$ in addition to SM-like Higgs boson h^0. Current experiments are looking for the signatures of these additional scalars. So, from phenomenological point of view, it is worthwhile to explore the signatures of the additional scalars.

In our first work, we perform a model independent analysis focusing on the cascade decay of a heavy Higgs. In particular, we have studied $gg \to H_2 \to H_1 Z \to h^0 ZZ$. with $h^0 \to b\bar{b}$ and two Z's decaying to leptons in one case. In another case, out of two Z's, one Z decay to leptons, another Z decaying to bottom-antibottom pair with $h^0 \to b\bar{b}$. So the final state signatures consists either of four leptons and two b-jets (4l2b) or of two leptons and four b-jets (2l4b). With selected benchmark points in the parameter space, consistent with all know experimental observations, we perform the analysis to device event selection methods aimed at enhancing signal over the expected background. The 5σ discovery reach of the possible new physics effect are then translated into the constraints on the parameters of the Type II 2HDM.

In our second work, we consider an inert version of 2HDM, popularly known as

inert higgs doublet model (IHDM). With the additional Z_2 symmetry, the lightest neutral scalar of this model is stable, which is a candidate for dark matter (DM). We try to probe heavier charged Higgs masses via final state of dijet and missing transverse energy beyond what could be probed through the leptonic and semi-leptonic final state processes available in the literature. The analysis is being performed for a selected set of benchmark points in the parameter space obtained from the scan satisfying all the relevant constraints. The best case scenario is that of a charged Higgs having mass 200 GeV with DM mass 65 GeV with a signal significance 2σ at an integrated luminosity of about 3000 fb^{-1}.

Explaining DM and non-zero neutrino mass in a single framework is a pressing task among modern particle physicists. In our final work, we make an attempt in this direction. We explain DM and non-zero neutrino mass in a single framework by extending the IHDM with addition of three copies of right handed neutrinos and three copies of charged vector-like leptons. With the assumption of tiny Higgs-DM coupling, inspired from the null results of direct detection experiments, we reproduce the correct relic abundance by tuning the additional couplings of DM. The collider implications of this extended IHDM is quite interesting in comparison to pure IHDM.

Summarizing, we focus on the multi-Higgs sector aiming to probe the additional scalars of the models at the LHC, and investigate the DM phenomenology from collider perspective in one of the models. We also make the connection of DM with neutrino mass in a single framework.

List of Publications

Journal Publications

⋆1. Baradhwaj Coleppa, Benjamin Fuks, P. Poulose, **Shibananda Sahoo** "Seeking Heavy Higgs Bosons through Cascade Decays",*Published in Phys.Rev.D***97** *(2018) no.7, 075007.* arxiv:1712.06593

⋆2 Debasish Borah, Soumya Sadhukhan, **Shibananda Sahoo** "Lepton Portal Limit of Inert Higgs Doublet Dark Matter with Radiative Neutrino Mass", *Published in Phys.Lett. B***771** *(2017) 624-632.* arxiv: 1703.08674

3. Sher Alam, Subhasish Behera, Satendra Kumar, **Shibananda Sahoo** "Constraining Capability of Zγh Production at ILC", *Published in Int.J.Mod.Phys. A* **32** *(2017) no.02n03, 1750017.* arxiv: 1701.08250

⋆4 P. Poulose, **Shibananda Sahoo**, K. Sridhar "Exploring the Inert Doublet Model through the dijet plus missing transverse energy channel at the LHC", *Published in Phys.Lett. B***765** *(2017) 300-306.* arxiv: 1604.03045

5. Debasish Borah, **Shibananda Sahoo**, Sudhanwa Patra "Subdominant left-right scalar dark matter as origin of the 750GeV di-photon excess at LHC", *Published in Int.J.Mod.Phys. A* **31** *(2016) no.17, 1650097.* arxiv:1601.01828

6. Satendra Kumar, P. Poulose, **Shibananda Sahoo** "Study of Higgs-gauge boson anomalous couplings through $e^-e^+ \to W^-W^+H$ at ILC", *Published in Phys.Rev. D***91** *(2015) no.7, 073016.* arxiv:1501.03283

N.B. Publications marked with ⋆ are included in the thesis

Conference Publication

7. P. Poulose, **Shibananda Sahoo**, K. Sridhar "Searching the Inert Scalars Through the Dijet Plus Missing Transverse Energy Final States at High Luminosity LHC",*Published in Springer Proc.Phys.* **203 (2018) 411-414**

Schools/Workshops/Conferences attended

1. **Preparatory SERC School** held at Tezpur University, Assam during June 17-July 13 in 2013.
2. **Discussion Meeting on EWSB and Flavours in the light of LHC** held at IIT Guwahati, Assam during February 20-22 in 2014.
3. **Sangam@ 2014:Instructional Workshop in Particle Physics** held at HRI, Allahabad, during March 24-29 in 2014.
4. **XXI DAE-BRNS High Energy Physics Symposium** held at IIT Guwahati, Assam during 8-12 December in 2016.
5. **Sangam@ 2016:Instructional Workshop in Particle Physics** held at HRI, Allahabad, during February 12-15 in 2016.
6. **XXII DAE-BRNS High Energy Physics Symposium** held at Delhi University, Delhi during 12-16 December in 2016.
7. **XXXI SERC Main School** held at Kalyani University, West Bengal during 9th-23th January in 2017.
8. **Collider Physics Workshop: Events, Analysis, QCD** held at IIT Guwahati, Assam during 27th-31st March in 2017.
9. **SCALARS 2017** held at University of Warsaw, Poland during 30th November-3th December in 2017.
10. **GIAN Course on Electroweak Symmetry Breaking, Flavour Physics and BSM** held at IIT Guwahati, Assam during 18-22 December in 2017.

Contents

List of Figures

List of Tables

Chapter 1

Introduction

In this chapter, we present a short note on the Standard Model (SM) of particle physics, and discuss some of its major difficulties. We then go ahead to introduce ideas going beyond the SM addressing some of these issues. Further, we present the main motivations of the thesis work and discuss in details the beyond Standard Model (BSM) scenarios considered for this, vis the two Higgs doublet model (2HDM) as well as its inert version. Then, we outline the content of the upcoming chapters.

Unlocking the secrets of nature is one of the primary goals of a scientific brain. The scientific curiosity of human civilization leads to manifestation of many beautiful theories with SM being the most successful theory in describing fundamental particles and their interactions. Most of its predictions are well tested by experiments. But this model lacks the qualities of being the supreme theory of nature. Now, the next daunting task among the particle physicists, is to look for that complete theory which will include qualities that the SM lacks. In this thesis, we address some of these issues.

This chapter is organized in the following way. Firstly, we describe the SM along with its difficulties. Then, we discuss some of the models beyond the SM and briefly highlight the contents of the upcoming chapters.

1.1 Standard Model of Particle Physics

Combining the electroweak (EW) theory proposed by Glashow, Weinberg and Salam [1–3] with quantum chromodynamics (QCD), SM beautifully describes fundamental interactions between the particles. It is built on the mathematical framework of

quantum field theory, incorporating local gauge invariance. The gauge group of SM is $SU(3)_C \otimes SU(2)_L \otimes U(1)_Y$. This gauge symmetry forbids mass terms in the Lagrangian, both for fermions and gauge bosons. But, the masses can be generated through "Higgs mechanism" which is discussed in the following subsection. The SM includes in its particle spectrum, three generations of quarks, three generations of leptons and the Higgs boson, the most elusive one along with the gauge bosons which mediate the interactions. We have listed all the fundamental fields of SM and their representations under the gauge group in Table 1.1.

	Fields	$SU(3)_C \otimes SU(2)_L \otimes U(1)_Y$
Quarks	$Q \equiv \begin{pmatrix} u_L^i \\ d_L^i \end{pmatrix}, \begin{pmatrix} c_L^i \\ s_L^i \end{pmatrix}, \begin{pmatrix} t_L^i \\ b_L^i \end{pmatrix},$	(3, 2, 1/3)
	$u_R^i,\ c_R^i,\ t_R^i,$	(3, 1, 4/3)
	$d_R^i,\ s_R^i,\ b_R^i$	(3, 1, -2/3)
Leptons	$L \equiv \begin{pmatrix} \nu_{eL} \\ e_L \end{pmatrix}, \begin{pmatrix} \nu_{\mu L} \\ \mu_L \end{pmatrix}, \begin{pmatrix} \nu_{\tau L} \\ \tau_L \end{pmatrix},$	(1, 2, -1)
	$e_R,\ \mu_R,\ \tau_R$	(1, 1, -2)
Gauge Bosons	G_μ^a ,	(8, 1, 0)
	$W_\mu^\pm,\ W_\mu^3,$	(1, 3, 0)
	B_μ	(1, 1, 0)
Scalar	$\Phi \equiv \begin{pmatrix} \phi^+ \\ \phi^0 \end{pmatrix}$	(1, 2, 1)

Table 1.1: SM fields and their charges under the gauge group. Here $i = r, g, b$ and $a = 1, 2, .., 8$.

As it can be seen from Table 1.1, left handed fermionic fields are doublets under $SU(2)_L$ whereas right handed fermionic fields are singlets under $SU(2)_L$. The quarks are triplets under $SU(3)_C$ whereas the leptons are singlets under $SU(3)_C$. The gauge bosons are known as mediators by which various interactions are mediated. The electromagnetic interaction is mediated by photon. Weak interaction is mediated by $W^\pm$ and Z whereas strong interaction is mediated by gluons (G_μ^a). Both the photon and Z boson are orthogonal combinations of W_μ^3 and B_μ given in Table 1.1.

Now we can write the SM Lagrangian given by

$$\mathcal{L}_{SM} = \mathcal{L}_{Gauge} + \mathcal{L}_{Fermion} + \mathcal{L}_{Yukawa} + \mathcal{L}_{Scalar}, \tag{1.1}$$

where

$$\mathcal{L}_{Gauge} = -\frac{1}{4}W^{k\mu\nu}W^{k}_{\mu\nu} - \frac{1}{4}B^{\mu\nu}B_{\mu\nu} - \frac{1}{4}G^{a}_{\mu\nu}G^{\mu\nu a}. \tag{1.2}$$

Here, $W^{k}_{\mu\nu}$, $B_{\mu\nu}$ and $G^{a}_{\mu\nu}$ are the field strength tensors of gauge fields of $SU(2)_L$, $U(1)_Y$ and $SU(3)_C$ respectively. The field strength tensors are given as

$$W^{k}_{\mu\nu} = \partial_\mu W^{k}_{\nu} - \partial_\nu W^{k}_{\mu} + g\epsilon_{klm}W^{l}_{\mu}W^{m}_{\nu}, \tag{1.3}$$

$$B_{\mu\nu} = \partial_\mu B_\nu - \partial_\nu B_\mu \tag{1.4}$$

and

$$G^{a}_{\mu\nu} = \partial_\mu G^{a}_{\nu} - \partial_\nu G^{a}_{\mu} + g_s f_{abc}G^{b}_{\mu}G^{c}_{\nu}. \tag{1.5}$$

Here g and g_s are the coupling constants of $SU(2)_L$ and $SU(3)_C$ gauge groups. ϵ_{klm} and f_{abc} are the structure constants of $SU(2)_L$ and $SU(3)_C$ respectively.

The Lagrangian for the fermion kinetic term is

$$\mathcal{L}_{Fermion} = \sum_{\psi} i\bar{\psi}\gamma^\mu D_\mu \psi, \tag{1.6}$$

where $\psi = Q, L, l_R, q_R$ with $l_R = e_R, \mu_R, \tau_R$ and $q_R = u_R, d_R, c_R, s_R, t_R, b_R$. The covariant derivatives for different fermionic fields are given by

$$i\bar{Q}\gamma^\mu D_\mu Q = i\bar{Q}\gamma^\mu(\partial_\mu - ig\frac{\sigma^k}{2}W^{k}_{\mu} - ig'\frac{Y}{2}B_\mu - ig_s\frac{\lambda^a}{2}G^{a}_{\mu})Q, \tag{1.7}$$

$$i\bar{L}\gamma^\mu D_\mu L = i\bar{L}(\partial_\mu - ig\frac{\sigma^k}{2}W^{k}_{\mu} - ig'\frac{Y}{2}B_\mu)L, \tag{1.8}$$

$$i\bar{q}_R\gamma^\mu D_\mu q_R = i\bar{q}_R\gamma^\mu(\partial_\mu - ig'\frac{Y}{2}B_\mu - ig_s\frac{\lambda^a}{2}G^{a}_{\mu})q_R \tag{1.9}$$

and

$$i\bar{l}_R\gamma^\mu D_\mu l_R = i\bar{l}_R\gamma^\mu(\partial_\mu - ig'\frac{Y}{2}B_\mu)l_R. \tag{1.10}$$

Here σ^k (with k = 1, 2, 3) are the Pauli matrices, Y known as hypercharge, is the generator of $U(1)_Y$ group. λ^a (with a = 1, 2, ..., 8) are the Gell-Mann matrices,

known as generators of $SU(3)_C$ gauge group.

The Yukawa interaction in the SM can be written as

$$\mathcal{L}_{Yukawa} = -\sum_{m,n}(Y_d^{mn}\bar{Q^m}\Phi d_R^m + Y_u^{mn}\bar{Q^m}\tilde{\Phi}u_R^n + Y_l^{mn}\bar{L^m}\Phi e_R^n) + h.c., \tag{1.11}$$

where $\tilde{\Phi} = \mathrm{i}\sigma_2\ \Phi^*$ and $m, n = 1, 2, 3$ stand for three generations of fermions. $Y_{d,u,l}^{mn}$ are complex Yukawa couplings.

We discuss the Lagrangian corresponding to the scalar ($\mathcal{L}_{Scalar}$) in the subsection 1.1.1. We also describe how EW symmetry is broken by a scalar doublet which leads to masses of gauge bosons and fermions.

1.1.1 Higgs Mechanism

Higgs mechanism is one of the main pillars of SM. It was suggested by R. Brout, F. Englert, P. Higgs, G. S. Gurlanik, C. R. Hagen and T.W.B. Kibble [4–6] in 1964. All known massive particles are expected to acquire their masses through Higgs mechanism.[1] This mechanism introduces a scalar field in the SM through the Lagrangian with the well-known Higgs potential given by $V(\Phi)$. The Lagrangian corresponding to the scalar is given by

$$\mathcal{L}_{scalar} = \mathcal{L}_{Kinetic-Scalar} + V(\Phi), \tag{1.12}$$

with

$$\mathcal{L}_{Kinetic-Scalar} = (D_\mu\Phi)^\dagger(D^\mu\Phi), \tag{1.13}$$

where D_μ is the covariant derivative associated with the scalar field, given by,

$$D_\mu = \partial_\mu - ig\frac{\sigma^k}{2}W_\mu^k - ig'\frac{Y}{2}B_\mu. \tag{1.14}$$

The scalar potential $V(\Phi)$ can be written as

$$V(\Phi) = \mu^2(\Phi^\dagger\Phi) + \lambda(\Phi^\dagger\Phi)^2, \tag{1.15}$$

where

$$\Phi = \begin{pmatrix} \phi^+ \\ \\ \phi^0 \end{pmatrix} \tag{1.16}$$

[1] Neutrinos could be an exception where the origin of mass may be more complicated.

is a doublet under $SU(2)_L$. In Eq. (1.15) μ^2, λ are parameters of our theory, with $\lambda > 0$. For $\mu^2 > 0$, the theory simply describes a scalar field with mass μ. But, the alternative case $\mu^2 < 0$ needs a special attention. In this case, Φ gets a vacuum expectation value (VEV) which is different from zero denoted by

$$\langle \Phi \rangle^2 = v^2, \tag{1.17}$$

with $v{=}\sqrt{-\mu^2/\lambda}$. Now we have to expand the field around one minimum. After the expansion around the minimum, the field can be written as,

$$\Phi = \sqrt{\frac{1}{2}} \begin{pmatrix} w_1(x) + i w_2(x) \\ v + h(x) + i w_3(x) \end{pmatrix}, \tag{1.18}$$

where $w_1(x), w_2(x), w_3(x), h(x)$ are real scalar fields. The preference of choosing one vacuum over another for expansion breaks the symmetry. This is technically called as spontaneous symmetry breaking (SSB). Here $h(x)$ is the field corresponding to the physical Higgs particle. The remaining three degrees of freedom reappear as longitudinal components of massive gauge bosons after choosing a specific $SU(2)_L$ gauge transformation. The same gauge transformation modifies Φ to,

$$\Phi = \sqrt{\frac{1}{2}} \begin{pmatrix} 0 \\ v + h(x) \end{pmatrix}. \tag{1.19}$$

From the potential, we can obtain the mass and various couplings of physical Higgs boson. The mass, trilinear and quadrilinear Higgs self-couplings are given by

$$m_h = \sqrt{-2\mu^2},\ \lambda_{hhh} = \frac{-\mu^2}{v} = \frac{m_h^2}{2v},\ \lambda_{hhhh} = \frac{-\mu^2}{v^2} = \frac{m_h^2}{2v^2}. \tag{1.20}$$

This means that the whole Higgs sector of SM is parametrised in terms of m_h and v. SM is unable to predict the value of m_h. This is fixed from the experiments. The measurements of self-couplings are important to probe the shape of the Higgs potential, which is an important test of electroweak symmetry breaking (EWSB). These measurements are challenging, because the processes involving these couplings have a very low cross section. Search for the physical Higgs boson took place for several decades. Finally, with great efforts of experimentalists LHC discovered a particle, which is similar to the predicted physical Higgs boson, in 2012 [7, 8]. For

the validity of their theory, F. Englert and P. Higgs got the nobel prize in 2013.

The same Higgs doublet is also responsible for masses of gauge bosons as well as fermions. The gauge boson mass term arises from kinetic term given in the Eq. (1.13) after substituting the expression for Φ as given in Eq. (1.19). Diagonalising the mass matrix one can get,

$$m_{W^\pm}^2 = \frac{1}{4}g^2v^2, \qquad m_Z^2 = \frac{1}{4}(g^2+g\prime^2)v^2 \qquad \text{and} \qquad m_A^2 = 0, \tag{1.21}$$

where $W^\pm$ is the linear combination of W^1 and W^2, whereas Z and A (photon) are linear combinations of W^3 and B as given below,

$$W_\mu^\pm = \frac{1}{\sqrt{2}}(W_\mu^1 \mp iW_\mu^2), \tag{1.22}$$

$$Z_\mu = \frac{-g\prime B_\mu + gW_\mu^3}{\sqrt{g^2+g\prime^2}}, \tag{1.23}$$

and

$$A_\mu = \frac{gB_\mu + g\prime W_\mu^3}{\sqrt{g^2+g\prime^2}}. \tag{1.24}$$

We can not simply add mass terms for fermions because it violates gauge invariance. But we can get the mass of fermions through the same Higgs doublet which is responsible for masses of gauge bosons. If we replace Eq. (1.19) in Eq. (1.11), then one can obtain masses for the fermions through,

$$\mathcal{L}_{mass} = -\sum_{m,n}(\bar{d}_L^m M_d^{mn} d_R^n + \bar{u}_L^m M_u^{mn} u_R^n + \bar{e}_L^m M_l^{mn} e_R^n) + h.c., \tag{1.25}$$

where $M_f = Y_f v/\sqrt{2}$ where $f = u, d, l$ denoting the mass matrices for up-type quarks, down-type quarks and charged leptons respectively.

Although, SM is very successful in describing nature but still it has a lot of failures. We highlight some of those in the next section.

1.2 Drawbacks of SM

1.2.1 Hierarchy Problem

The observed Higgs mass is roughly 125 GeV. The expression for m_h given in Eq. (1.20) is a tree level relation. But, after including higher order quantum correc-

tions to the square of the mass, the relation is altered. The dominant loop diagrams are given by top quark, W, Z and h exchange in the loop as shown in Figure 1.1. All other divergent diagrams do not contribute much, because of small coupling constants. For a cutoff value Λ, the contributions become [9]

$$m_h^2 = (m_h^{tree})^2 + \frac{3\Lambda^2}{8\pi^2}\left[-y_t^2 + \frac{g^2}{6} + \frac{\lambda^2}{6}\right], \tag{1.26}$$

where y_t is Yukawa coupling of top quark, g is the $SU(2)_L$ gauge coupling, λ is the Higgs self-coupling. The above expression clearly shows quadratically divergent behaviour. Now if we choose the cut-off scale Λ to be the GUT scale, $M_{GUT} \sim 10^{16}$ GeV, or the Planck Scale $M_P \sim 10^{19}$ GeV, then we have to adjust the value of the couplings to an order of 28 to 34 to get a correction to an order of 10^4 GeV. The problem of fine-tuning arises because of the hierarchy between the EW scale and the scale of new physics. This difficulty is popularly known as hierarchy problem. SM does not have any explanation to this hierarchy problem.

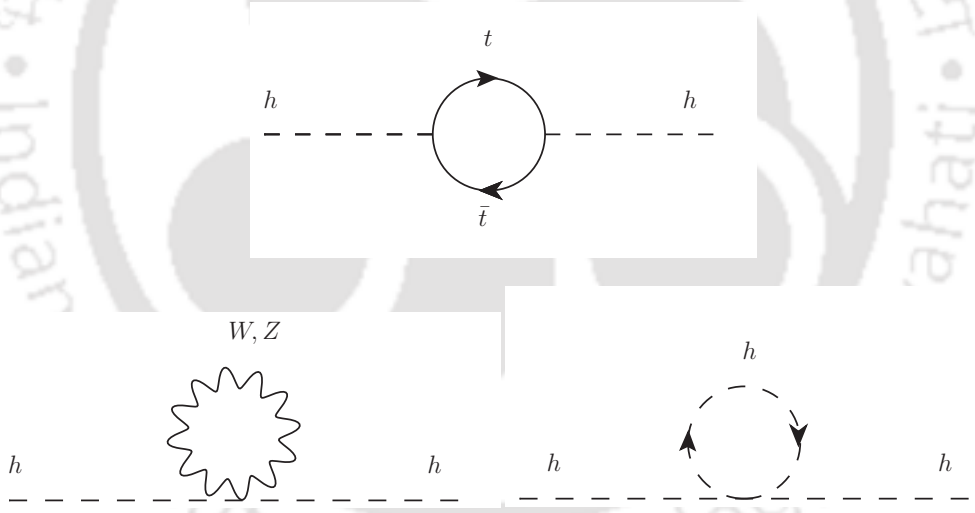

Figure 1.1: Loop Contributions to Higgs Mass.

1.2.2 Dark Matter & Dark Energy

Although SM is very successful in describing particles and their interactions that only belongs to 5% of the total matter content of the universe. Rest matter content of the universe is still unknown and mysterious. It is widely believed that some unknown form of matter, named as, dark matter (DM) contribute to 27% to the total matter content of the universe. Although there are ample of strong evidences

of the DM, there is no discovery till date. Another ingredient, which contributes largely to the content of the universe is dark energy. Still, we do not have much understanding of it in the current scenario.

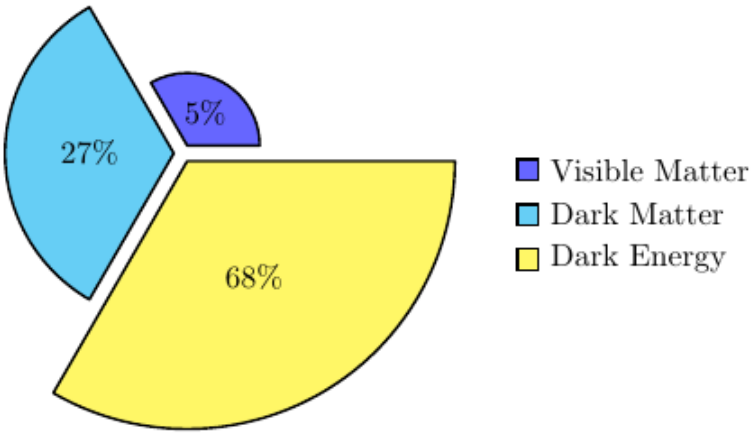

Figure 1.2: Content of Universe.

1.2.3 Neutrino Mass

As we have mentioned earlier, SM is unable to explain the non-zero tiny mass of neutrino as we cannot write gauge invariant mass term for the neutrinos. To explain the non-zero neutrino mass, we need to extend the particle content of the SM which is now a days favourite way of building a new physics model.

1.2.4 Electroweak Symmetry Breaking

SM does not tell us the exact nature of EWSB although it achieves by introducing a scalar doublet. There is no reason to believe this is the only way of EWSB. A deeper understanding of EWSB is necessary to pinpoint its nature.

Modern particle physics is on the way to search for the theory which will provide answer to the problems we mentioned in the previous section. There are many attempts in the different directions. We discuss some of the approaches in the next section.

1.3 Different Approaches to BSM

In this section, we describe some of the models beyond the SM.

1.3.1 Two Higgs Doublet Model

Though the SM successfully describes most of elementary particles phenomenology, the Higgs sector of SM is not experimentally well explored yet. In the SM, the Higgs sector is minimal with one doublet complex scalar field. One of the simplest extensions of SM compatible with gauge invariance is to add another doublet to SM Higgs doublet. This model is popularly known as 2HDM. Several motivations are there to introduce the second doublet. The primary motivation is to explain fermion mass hierarchy. In the SM, both the top quark and bottom quark get their masses from same doublet. But, there is a mass hierarchy between these two quarks. This hierarchy is quite unnatural. In the 2HDM, they get mass from two different doublets. So, the hierarchy could be more natural.

Inert Higgs Doublet Model

This model is a frontline candidate for dark matter models. Its Higgs sector contains SM-like Higgs boson with another doublet scalar field providing some additional Higgs bosons. With some modifications, this has the potential to provide leptogenesis and provides insight into the neutrino mass generation. It is basically a 2HDM with an additional Z_2 symmetry imposed on the potential. Due to this additional symmetry linear term with one doublet does not appear in the potential. In this model only one doublet acquires VEV. Since the other doublet has neither a VEV nor direct couplings to fermions, it is called inert. So, this model as a whole is called as inert Higgs doublet model (IHDM).

1.3.2 Supersymmetry

Arguably, the most well-known candidate for BSM is the supersymmetric extension of the SM. Supersymmetry (SUSY) is a space-time symmetry which relates fermions and bosons. Each fermion has a superpartner which is a boson and vice-versa. The superpartners of fermions are called “sfermions”, more specifically squarks and sleptons. The fermionic superpartners of gauge bosons are called “gauginos”. A partner differs from its superpartner in spin quantum number by half unit. Although no superpartner is observed till now, there are several motivations which force us

to believe in SUSY. Some popular SUSY models are briefly discussed in next two paragraphs.

MSSM

The minimal supersymmetric standard model (MSSM) [10, 11] is the minimal extension of SM with the incorporation of supersymmetry. By introducing SUSY partners to every particle in the SM spectrum, the MSSM is directly obtained from the SM. The gauge theory of MSSM is based on the SM gauge group. SUSY must be a broken symmetry since no scalars have been discovered having same mass with any of the known fermions. As there is no clear understanding of the origin of SUSY breaking, the MSSM Lagrangian contains some soft susy breaking terms to parametrize SUSY breaking. An additional R-parity conservation rule is imposed on the superpotential of MSSM so that the lightest supersymmetric particle would be stable. The Higgs sector of MSSM is similar to the 2HDM.

Beyond MSSM

Although the signatures of MSSM is yet to realize, some non-minimal extensions of SUSY to SM also exists. By adding another singlet superfield to MSSM, we get the next-to-minimal supersymmetric standard model (NMSSM) [10, 11]. An $U(1)^{'}$ extended models (UMSSM) [12] can be built by adding an extra gauge symmetry $U(1)^{'}$ to MSSM. All these SUSY models will loose their importance if no sparticles observed in the next few decades.

1.3.3 Other Alternatives

Besides the above mentioned models, several other alternatives are proposed to look beyond the SM. Among these, the most fascinating ones are the models related to extra dimensions (ExD) [13]. The idea of ExD comes from string theory. Though the presence of ExD is unclear, still the search for ExD is an alive option for experiments. Like the extension of Higgs sector of SM, extended gauge models (EGMs) [14] are also pursued. Another popular choice among the theorists is the models those depend on dynamical symmetry breaking [15].

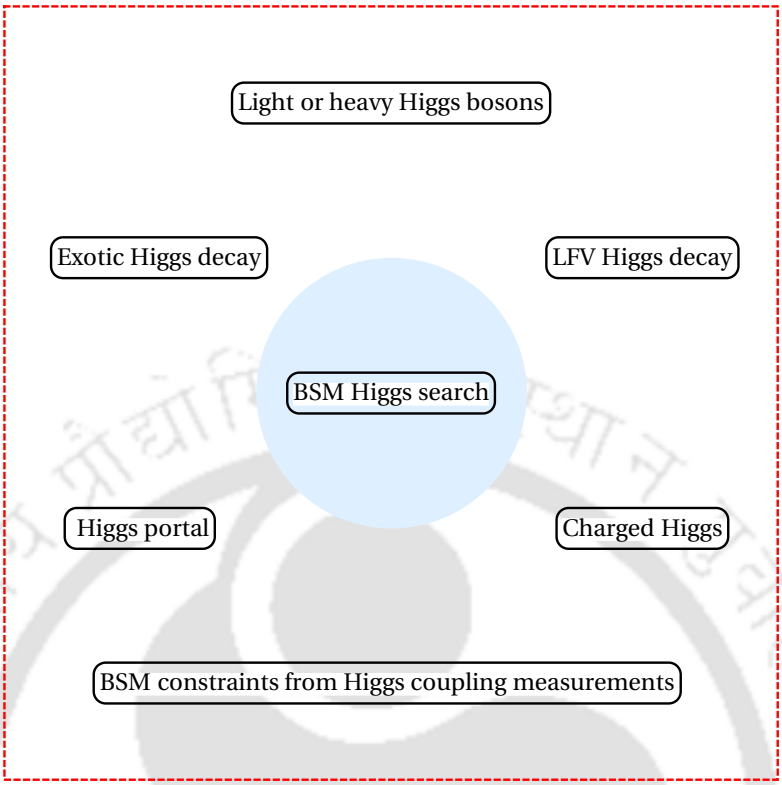

Figure 1.3: Different BSM Higgs search approaches.

1.4 Main Focus of the Thesis

As mentioned previously, the drawbacks of SM force us to look for the new physics. There are many aspects of searching physics beyond the SM, some of which are introduced in the previous section. In this thesis, we focus on the Higgs sector. Even within the Higgs sector, there are many areas one can look for as given in Figure 1.3 . Out of several BSM Higgs search areas, we take up a few in this thesis. Explicitly, we focus on searches including heavier neutral Higgs bosons in one of the studies carried out in this thesis. In another study, we concentrate on probing charged Higgs bosons of heavier masses. In the final work, we address neutrino mass and DM in a single framework.

1.5 Details of Two Higgs Doublet Model

In this section, we discuss the details of 2HDM including its kinetic and Yukawa sector.

Potential

In SM, the Higgs potential is unique. But in 2HDM, this is not so. The potential [16] compatible with gauge invariance is given by

$$V(\Phi_1,\Phi_2) = -\mu_1^2\hat{A} - \mu_2^2\hat{B} - \mu_3^2\hat{C} - \mu_4^2\hat{D} + \lambda_1'\hat{A}^2 + \lambda_2'\hat{B}^2 + \lambda_3'\hat{C}^2 + \lambda_4'\hat{D}^2 + \lambda_5'\hat{A}\hat{B} + \lambda_6'\hat{A}\hat{C} + \lambda_7'\hat{B}\hat{C} + \lambda_8'\hat{A}\hat{D} + \lambda_9'\hat{B}\hat{D} + \lambda_{10}'\hat{C}\hat{D}, \quad (1.27)$$

where $\hat{A} = \Phi_1^\dagger\Phi_1, \hat{B} = \Phi_2^\dagger\Phi_2, \hat{C} = (\Phi_1^\dagger\Phi_2 + \Phi_2^\dagger\Phi_1)/2 = \mathrm{Re}(\Phi_1^\dagger\Phi_2), \hat{D} = -i(\Phi_1^\dagger\Phi_2 - \Phi_2^\dagger\Phi_1)/2 = \mathrm{Im}(\Phi_1^\dagger\Phi_2)$. Here Φ_1, Φ_2 are doublets under $SU(2)_L$ i.e.

$$\Phi_1 = \begin{pmatrix} \phi_1^+ \\ \phi_1^0 \end{pmatrix} = \begin{pmatrix} \phi_1 + i\phi_2 \\ \phi_3 + i\phi_4 \end{pmatrix}, \qquad \Phi_2 = \begin{pmatrix} \phi_2^+ \\ \phi_2^0 \end{pmatrix} = \begin{pmatrix} \phi_5 + i\phi_6 \\ \phi_7 + i\phi_8 \end{pmatrix}, \quad (1.28)$$

with hypercharges $Y_1 = Y_2 = 1$. This potential looks much more complicated than the Higgs potential in SM. In this potential, we have fourteen free parameters. We can reduce the number of parameters by demanding the potential to be invariant under certain suitable symmetry. If charge is conserved and we forbid CP violation in the Higgs sector, then after the SSB

$$\langle\Phi_1\rangle = \begin{pmatrix} 0 \\ \frac{v_1}{\sqrt{2}} \end{pmatrix}, \qquad \langle\Phi_2\rangle = \begin{pmatrix} 0 \\ \frac{v_2}{\sqrt{2}} \end{pmatrix}. \quad (1.29)$$

The potential can be minimized by equating the first derivative to zero i.e.

$$\frac{\partial V}{\partial \phi_i} = 0. \quad (1.30)$$

Also, the elements of the mass matrix are given by

$$M_{ij}^2 = \frac{1}{2}\frac{\partial^2 V}{\partial\phi_i\partial\phi_j}. \quad (1.31)$$

With the VEV, the neutral component of two doublets can be written as

$$\Phi_1 = \begin{pmatrix} \phi_1^+ \\ \frac{h_1+v_1+i\phi_4}{\sqrt{2}} \end{pmatrix}, \Phi_2 = \begin{pmatrix} \phi_2^+ \\ \frac{h_2+v_2+i\phi_8}{\sqrt{2}} \end{pmatrix}. \quad (1.32)$$

We can obtain various physical mass eigen states and the Goldstone bosons (massless) from the gauge eigen states. It is achieved by diagonalizing the mass matrix by choosing a unitary transformation. This rotation of gauge eigen states to mass eigen states is given below.

$$\begin{pmatrix} H^0 \\ h^0 \end{pmatrix} = \begin{pmatrix} \cos\alpha & \sin\alpha \\ -\sin\alpha & \cos\alpha \end{pmatrix} \begin{pmatrix} h_1 \\ h_2 \end{pmatrix} \tag{1.33}$$

$$\begin{pmatrix} G^+ \\ H^+ \end{pmatrix} = \begin{pmatrix} \cos\beta & \sin\beta \\ -\sin\beta & \cos\beta \end{pmatrix} \begin{pmatrix} \phi_1^+ \\ \phi_2^+ \end{pmatrix} \tag{1.34}$$

$$\begin{pmatrix} G^0 \\ A^0 \end{pmatrix} = \begin{pmatrix} \cos\beta & \sin\beta \\ -\sin\beta & \cos\beta \end{pmatrix} \begin{pmatrix} \phi_4 \\ \phi_8 \end{pmatrix}, \tag{1.35}$$

where α is the mixing angle between two neutral CP-even Higgs (h^0, H^0) and $\tan\beta = v_2/v_1$ is the ratio of two VEVs.

Now it is the suitable time for counting the degrees of freedom (DOFs). Initially we have 8 DOFs because of two complex doublets. So after SSB, the DOFs should be same. Because, our theory respects the conservation of DOFs. After SSB, our theory contains five Higgs bosons : two CP-even Higgs, one CP-odd Higgs (A^0), two charged Higgs ($H^\pm$) with three Goldstone bosons ($G^\pm$,G^0). These Goldstone bosons reappear as longitudinal modes of massive gauge bosons ($W^\pm$, Z^0).

Next, we move into the kinetic sector to understand the interaction between the Higgs bosons and the gauge bosons.

Kinetic Sector

The structure of the Lagrangian corresponding to kinetic sector is quite similar to that of the SM. We can write the Lagrangian ($\mathcal{L}_{kin}$) as

$$\mathcal{L}_{kin} = (D_\mu\Phi_1)^\dagger(D^\mu\Phi_1) + (D_\mu\Phi_2)^\dagger(D^\mu\Phi_2), \tag{1.36}$$

where $D_\mu = \partial_\mu - ig\frac{\sigma^k}{2}W_\mu^k - ig'\frac{Y}{2}B_\mu$ with $k = 1, 2, 3$.

From this Lagrangian, we can derive the masses of gauge bosons.

$$M_{W^\pm}^2 = \frac{1}{4}g^2(v_1^2 + v_2^2), \;\; W_\mu^\pm = \frac{W_\mu^1 \mp iW_\mu^2}{\sqrt{2}} \tag{1.37}$$

and

$$M_Z^2 = \frac{1}{4}(g^2 + g\prime^2)(v_1^2 + v_2^2) = \frac{M_W^2}{\cos^2\theta_W}, \tag{1.38}$$

where

$$Z_\mu = \cos\theta_W W_\mu^3 - \sin\theta_W B_\mu. \tag{1.39}$$

Here θ_W is the Weinberg mixing angle. The above expressions for the masses of vector bosons coincide with the SM ones if $v_1^2 + v_2^2 = v^2$(where v=246 GeV is the VEV of the Higgs doublet of SM). Since the value of v^2 is known, we are getting the constraint $v_1^2 + v_2^2 = v^2$.

This Lagrangian($\mathcal{L}_{kin}$) provides us information about the interactions of Higgs bosons with gauge bosons. The interaction vertices can be obtained by expanding the Lagrangian in terms of the mass eigen states of Higgs bosons and gauge bosons. Some of the allowed vertices are ZH^+H^-, $h^0H^0H^0$, ZH^0A^0, ZA^0h^0 etc. Some other vertices, which do not appear at tree level, but radiatively genarated at one loop, are A^0gg, H^0gg, h^0gg etc. These vertices are very important for study because gluon-gluon fusion is one of the major production channels for neutral Higgs bosons at LHC. Furthermore the couplings of 2HDM sector satisfy the relation [17]

$$g^2_{h^0VV} + g^2_{H^0VV} = g^2_{h_{SM}VV}, \tag{1.40}$$

where $V = W, Z$. In terms of two angles α and β, the couplings are given by

$$g_{h^0VV} = g_{h_{SM}VV}\, sin(\beta - \alpha), \qquad g_{H^0VV} = g_{h_{SM}VV}\, cos(\beta - \alpha). \tag{1.41}$$

One additional feature of 2HDM with respect to SM is the existence of gauge boson-Higgs-Higgs coupling. Thus it is clear that the Higgs sector of 2HDM is fairly complex compared to that of the SM, in terms of both the number of physical Higgs bosons, as well as their various interactions.

Yukawa Sector Of 2HDM

Yukawa sector is very important for fundamental fermions (Quarks and Leptons), because they get masses through the Yukawa Lagrangian. Depending on which doublet is allowed or not allowed to couple the up-type quarks, down-type quarks and the leptons, the 2HDM can be distinguished in different types.

The two most popular versions are the Type-I 2HDM and the Type-II 2HDM. In Type-I 2HDM, only one Higgs doublet couples to fermions. Here we can see

that Higgs fermiophobic, bosophobic scenarios [16] will appear. If these scenarios are discovered in the near future, then this opens a window to new physics. In Type-II 2HDM, one Higgs doublet (e.g. Φ_1) couples to the Q = 2/3 quarks and another Higgs doublet (e.g. Φ_2) couples to the Q = −1/3 quarks and leptons. This model nicely explains fermion mass hierarchy. The suppression and enhancement of couplings differentiate these two models. Depending on the interchange of the lepton couplings, two additional versions come in to the picture. In the "lepton-specific" model (Type-X), all of the quarks couple to one doublet and the leptons couple to other doublet. In the "flipped" model (Type-Y) the Q = 2/3 quarks and leptons couple to one doublet while the Q = −1/3 quarks couple to the other.

These different types of models arise because of Φ_1 and Φ_2 have various choices to couple with the fundamental fermions. For simplicity, we listed the choices in a table.

Fermions / Types	up quarks	down quarks	leptons
Type-I	✓	✓	✓
Type-II	✓	×	×
Lepton-specific	✓	✓	×
Flipped	✓	×	✓

Table 1.2: Different Types of 2HDM. Here ✓ denotes coupling to Φ_1 and × denotes coupling to Φ_2.

In the next section, we discuss the inert version of 2HDM, popularly known as IHDM.

1.6 Essential Details of IHDM

The IHDM [18] has one additional scalar doublet (under $SU(2)_L$), compared to the SM. This additional scalar, denoted by Φ_2 is odd under a discrete Z_2 symmetry imposed, while all the SM fields are even under this new symmetry. This Z_2 symmetry prohibits the Yukawa interactions of Φ_2 with the SM fields. The inert doublet, however, does have direct interaction with the gauge fields. A consequence of the Z_2 symmetry is that the lightest particle state belonging to Φ_2 is stable, and thus providing a candidate for dark matter. Denoting the SM scalar doublet as Φ_1, the

scalar potential respecting $SU(2)_L \otimes U(1)_Y$ gauge invariance is given by

$$V(\Phi_1,\Phi_2) = \mu_1^2|\Phi_1|^2 + \mu_2^2|\Phi_2|^2 + \frac{\lambda_1}{2}|\Phi_1|^4 + \frac{\lambda_2}{2}|\Phi_2|^4 + \lambda_3|\Phi_1|^2|\Phi_2|^2 + \lambda_4|\Phi_1^\dagger\Phi_2|^2 + \left\{\frac{\lambda_5}{2}(\Phi_1^\dagger\Phi_2)^2 + h.c.\right\}. \quad (1.42)$$

In the CP-conserved version, the parameters μ_1^2, μ_2^2, λ_1, λ_2, λ_3, λ_4, λ_5 are considered to be real. In the version with exact Z_2 symmetry, Φ_2 does not acquire any non-zero VEV, and therefore, only the SM field, Φ_1 takes part in the EWSB. After the EWSB these scalar doublets may be written in the following form in the unitary gauge.

$$\Phi_1 = \begin{pmatrix} 0 \\ \frac{v+h}{\sqrt{2}} \end{pmatrix}, \Phi_2 = \begin{pmatrix} H^+ \\ \frac{H+iA}{\sqrt{2}} \end{pmatrix}, \quad (1.43)$$

where $v = 246$ GeV is the vacuum expectation value of Φ_1. Apart from the SM-like Higgs h, this presents a neutral scalar, H, a neutral pseudo scalar, A,(the lighter of which is a possible candidate dark matter) and two charged Higgs bosons $H^\pm$, with the other degrees of freedom of Φ_1 becoming part of the massive gauge bosons through the Higgs mechanism. The masses of these physical scalars can be written in terms of parameters of the potential and v as

$$\begin{aligned} m_h^2 &= \lambda_1 v^2, \qquad m_{H^\pm}^2 = \mu_2^2 + \frac{1}{2}\lambda_3 v^2, \\ m_H^2 &= \mu_2^2 + \frac{1}{2}(\lambda_3+\lambda_4+\lambda_5)v^2 = m_{H^\pm}^2 + \frac{1}{2}(\lambda_4+\lambda_5)\,v^2 \\ \text{and} \qquad m_A^2 &= \mu_2^2 + \frac{1}{2}(\lambda_3+\lambda_4-\lambda_5)v^2 = m_{H^\pm}^2 + \frac{1}{2}(\lambda_4-\lambda_5)\,v^2. \end{aligned} \quad (1.44)$$

We discuss the constraints on these parameters in the working chapters along with the previous studies in the model. Now, we move to sum up the content of working chapters.

1.7 Outline Of Chapters

In this section, we briefly mention the outline of remaining chapters.

In Chapter 2, we investigate the LHC discovery prospects for a heavy Higgs boson decaying into the SM Higgs boson and additional weak bosons. We consider a generic model-independent new physics configuration where this decay proceeds

via a cascade involving other intermediate scalar bosons and focus on an LHC final-state signature comprised either of four b-jets and two charged leptons or of four charged leptons and two b-jets. We design two analyses of the corresponding signals, and demonstrate that a 5σ discovery at the 14 TeV LHC is possible for various combinations of the parent and daughter Higgs boson masses at different integrated luminosities. We moreover find that the SM backgrounds can be sufficiently rejected to guarantee the reconstruction of the parent Higgs boson mass. We apply our analyses to the Type-II 2HDM and identify the regions of the parameter space to which the LHC is sensitive.

In Chapter 3, we propose that the dijet plus missing transverse energy (MET) channel at the LHC will be an effective way of searching for the scalar particles of the IHDM. This channel receives contributions from gauge boson fusion, and $t-$channel production, along with contributions from H^+ associated production. We perform the analysis including study of the SM background with assumed systematic uncertainty, and optimise the selection criteria employing suitable cuts on the kinematic variables to maximise the signal significance. We find that with high luminosity option of the LHC, this channel has the potential to probe the IHDM in the mass range of up to about 400 GeV, which is not accessible through other leptonic channels. In a scenario with light dark matter of mass about 65 GeV, charged Higgs in the mass range of around 200 GeV provides the best possibility with a signal significance of about 2σ at an integrated luminosity of about 3000 fb^{-1}.

In Chapter 4, we study an extension of the IHDM by three copies of right handed neutrinos and heavy charged leptons such that both the inert Higgs doublet and the heavy fermions are odd under the Z_2 symmetry of the model. The neutrino masses are generated at one loop in the scotogenic fashion. Assuming the neutral scalar of the inert Higgs to be the dark matter candidate, we particularly look into the region of parameter space where dark matter relic abundance is primarily governed by the inert Higgs coupling with the leptons. This corresponds to tiny Higgs portal coupling of dark matter as well as large mass splitting within different components of the inert Higgs doublet suppressing the coannihilations. Such lepton portal couplings can still produce the correct relic abundance even if the Higgs portal couplings are arbitrarily small. Such tiny Higgs portal couplings may be responsible for suppressed dark matter nucleon cross section as well as tiny invisible branching ratio of the standard model Higgs, to be probed at ongoing and future experiments. We also briefly discuss the collider implications of such a scenario.

In Chapter 5, we summarize the studies that has been carried out in the thesis.

Chapter 2

Cascade decay of a Heavy Higgs

This chapter is devoted to the study of cascade decay of a heavy Higgs in the context of LHC. We investigate the decay by considering two important final states through model independent way. Further, we interpret the results obtained in the context of Type-II 2HDM.

The discovery of a Higgs boson whose properties are consistent with the expectations of the SM has undoubtedly been the triumph of the LHC thus far [7, 8, 19, 20]. While it is clear that the Higgs boson plays a central role in the breaking of the electroweak symmetry, there is still room for a non-minimal Higgs sector with a more involved TeV scale structure than what could be expected from the SM alone. Moreover, the proof of existence of the Higgs boson has provided an additional tool to narrow down the possibilities for new physics, additional constraints on the new physics parameter spaces being imposed by enforcing predictions of the production cross section and decay branching ratios to agree with the measured values. However, the Higgs boson could also be a perfect laboratory for uncovering new physics in cases where new heavier particles could decay into it, enhancing its indirect production rate.

One attractive minimal scenario along these lines is the so-called 2HDM where the SM Higgs sector is extended by a second weak doublet of Higgs fields [21, 22]. Although numerous not-so-minimal options including the supersymmetric versions like the MSSM [23, 24] or the NMSSM [12] fall in the category of multi-Higgs models, we shall focus on the minimal setup of the 2HDM here. The physical spectrum here contains, on top of the SM particles including the Higgs boson h^0, a heavy neutral scalar H^0, a pseudoscalar particle A as well as a pair of charged Higgs bosons $H^{\pm}$. A general feature of heavier Higgs bosons consists in the dominance of Higgs-to-Higgs

decays in association with a weak boson as soon as they are kinematically open [25–27]. This has consequently motivated the search for the corresponding signals in LHC data by both the ATLAS [28–31] and CMS [32–34] collaborations, as well as a series of theoretical works both in the 2HDM [35–48] and other (less minimal) new physics models [49–54].

In this chapter, we generalize this concept of Higgs-to-Higgs decays when several weak bosons arise from the cascade [55, 56], like when in the 2HDM, the heaviest scalar Higgs boson H^0 decays via a lighter pseudoscalar state A into the SM Higgs boson, $H^0 \to AZ \to h^0ZZ$. We further consider h^0 decays into leptons or jets originating from the fragmentation of b-quarks, as the latter consists of the dominant decay mode of the SM Higgs boson. In particular, we focus on a final state signature made of either four leptons and two b-jets, or of two leptons and four b-jets, and we analyze the corresponding LHC prospects. We first consider a simplified model approach (Section 2.1) that can easily be reinterpreted in terms of specific model featuring an extended Higgs sector. In Section 2.2, we take the example of the Type-II 2HDM and translate our findings in the corresponding parameter space. We summarize our work and present our conclusions in Section 2.3.

2.1 A Simplified Model for Analysing Higgs Cascade Decay Signals

In this section, we present the possible scenario with heavier Higgs bosons with mass splittings enabling cascade decay of the heavier ones to the SM Higgs boson.

2.1.1 Theoretical Framework, Benchmark Scenarios and Simulation Setup

In order to determine the LHC sensitivity to Higgs-to-Higgs cascade decays, we make use of a simplified model where the SM is minimally extended in terms of new particles and couplings. In practice, we complement the SM field content by two additional scalar bosons, so that the scalar part of the particle spectrum now contains the observed SM-like Higgs boson h^0 and two new states that we denote by H_1 and H_2. In our convention, H_1 is the lighter boson and H_2 the heavier one, and the couplings of the new scalars to the Z-boson are kept generic. Whilst their strengths are in principle free parameters, they are traded, in the analyses detailed in the next subsections, for the signal cross sections (see below for more details).

We assume varied mass differences between the two new states and the SM Higgs boson, so that we define four different scenarios that we name **BP1**, **BP2**, **BP3** and **BP4** and for which the heavy scalar masses m_{H_1} and m_{H_2} read

$$\begin{aligned} \textbf{BP1}: &\quad m_{H_1} = 250 \text{ GeV}, &\quad m_{H_2} = 400 \text{ GeV}, \\ \textbf{BP2}: &\quad m_{H_1} = 600 \text{ GeV}, &\quad m_{H_2} = 1000 \text{ GeV}, \\ \textbf{BP3}: &\quad m_{H_1} = 250 \text{ GeV}, &\quad m_{H_2} = 1000 \text{ GeV}, \\ \textbf{BP4}: &\quad m_{H_1} = 400 \text{ GeV}, &\quad m_{H_2} = 600 \text{ GeV}. \end{aligned} \tag{2.1}$$

This choice of benchmark points allows us to capture various features that could arise from distinct mass-splitting options. In the **BP1** scenario, there is not much available phase space for both the $H_2 \to ZH_1$ and $H_1 \to h^0 Z$ decays and thus these occur close to threshold. In contrast, the larger mass splittings featured by the **BP2** configuration, in which $m_{H_2} \gg m_{H_1} \gg m_{h^0}$, implies that both the H_1 and H_2 decays proceed far from threshold, the decay products being thus expected to feature a larger amount of transverse momentum p_T. The third scenario **BP3** consists of an intermediate case where only the $H_1 \to Zh^0$ decay occurs close to threshold. Finally, in the fourth scenario **BP4**, both decays occur far from threshold, but the mass splitting is reduced compared to the **BP2** case.

The different mass splittings between the h^0, H_1 and H_2 states probed in our benchmarks are expected to impact the kinematic properties of the leptons and b-jets originating from the decays of the final state SM Higgs boson and Z-bosons. As a consequence, their study could provide handles for unraveling new physics at the LHC. In the following, we consider the production of the heaviest Higgs boson H_2 through gluon fusion, and its subsequent decays into lighter Higgs states and Z-bosons,

$$pp \to H_2 \to H_1 Z \to h^0 Z Z \ . \tag{2.2}$$

Whilst we focus on the dominant Higgs boson decay mode $h^0 \to b\bar{b}$, we consider Z-boson decays into a lepton pair $Z \to \ell^+\ell^-$ and into a bottom-antibottom pair $Z \to b\bar{b}$. Omitting a final state signature comprised of six b-jets, given the huge associated multijet background and the difficulties induced by the combinatorics to reconstruct all intermediate particles, the final state signatures of interest therefore consist of a system made either of four leptons and two b-jets ($4\ell 2b$) or of two leptons and four b-jets ($2\ell 4b$).

As mentioned above, the signal cross section is taken as a free parameter which correspondingly allows us to ignore the actual strengths of the Z-boson couplings

to the new scalar bosons. As a benchmark, we make use of a fiducial signal cross sections $\sigma_{\rm fid}$ fixed to

$$\begin{aligned} \sigma_{\rm fid}(pp \to H_2 \to H_1 Z \to h^0 ZZ \to 4\ell 2b) &= 5 \text{ fb} \\ \text{and } \sigma_{\rm fid}(pp \to H_2 \to H_1 Z \to h^0 ZZ \to 2\ell 4b) &= 5 \text{ fb} \ , \end{aligned} \tag{2.3}$$

which consist of values lying in the ball park of what could be achieved in a phenomenologically-viable model.

Hard-scattering signal events at a collision center-of-mass energy of 14 TeV are generated by means of the MadGraph5_aMC@NLO platform [57]. Practically, we convolute the signal leading-order matrix elements, as automatically obtained from the 2HDM UFO [58] model available from the FeynRules repository [59, 60], with the leading-order set of NNPDF parton densities version 3.0 [61]. The dependence on the numerical values of the different coupling strengths being factorized out by an appropriate choice of the fiducial cross section, the sole model dependence consists of the Lorentz structure of the various interactions of the Z-boson with Higgs bosons. This restriction is however compatible with a large variety of popular multi-Higgs models. The simulation of the SM background proceeds analogously, using instead the SM UFO library shipped with MadGraph5_aMC@NLO.

The simulation of the parton showering and hadronization is performed by means of the Pythia 6 program [62], and we include the simulation of the response of a typical LHC detector as modeled by Delphes 3 [63], relying on the CMS-MA5tune parameterization of the detector [64]. The resulting detector-level objects are then reconstructed by applying the anti-k_T jet algorithm [65]. More precisely, this is achieved by making use of the MadAnalysis 5 framework [66, 67] to simulate the detector effects and reconstruct the events (through an interface to FastJet [68]), such a framework being also used to implement the analyses described in the next subsections.

2.1.2 Probing Higgs Cascades in the $4\ell 2b$ final state

In this section, we focus on the process of Eq. (2.2) when both Z-bosons decay leptonically,

$$pp \to H_2 \to H_1 Z \to h^0 ZZ \to b\bar{b}\ \ell_1^+\ell_1^-\ \ell_2^+\ell_2^- \ . \tag{2.4}$$

The signal under consideration is thus made of one pair of b-jets and two pairs of opposite-sign same-flavor leptons. In our analysis, we restrict ourselves to lepton

Background	$ZZb\bar{b}$	$t\bar{t}Z$	$t\bar{t}W$	$WWZb\bar{b}$	$WWWb\bar{b}$
$\sigma\times$ BR	0.1 fb	1.2 fb	2.3 fb	1.2 fb	2.1 fb

Table 2.1: Leading-order cross section for the different SM processes contributing to the background of our $4\ell + 2b$ analysis. They include the relevant branching ratios and the preselection cuts of Eq. (2.5) and Eq. (2.6).

and jet candidates whose transverse momentum (p_T^ℓ and p_T^j) and pseudorapidity (η^ℓ and η^j) satisfy

$$p_T^j > 20 \text{ GeV}, \qquad p_T^\ell > 10 \text{ GeV}, \qquad |\eta^j| < 5 \qquad \text{and} \qquad |\eta^\ell| < 2.5 \ . \tag{2.5}$$

Moreover, we omit from the analysis any pair of jet candidates that would not be well separated from each other as well as any lepton that would be too close to a jet. In practice, we impose that the angular distance in the transverse plane between two jets (ΔR_{jj}) and the one between a jet and a lepton ($\Delta R_{\ell j}$) satisfy

$$\Delta R_{jj} > 0.4 \qquad \text{and} \qquad \Delta R_{\ell j} > 0.4 \ . \tag{2.6}$$

The dominant contributions to the SM background hence arise from $ZZb\bar{b}$, $t\bar{t}V$ and $WWVb\bar{b}$ production, with V being a W-boson or a Z-boson. Including the branching ratio (BR) corresponding to the $4\ell 2b$ final state, the leading-order cross sections as returned by MadGraph5_aMC@NLO are given in Table 2.1.

We implement a flavor-blind analysis in order to increase the signal statistics, although we ignore tau leptons as those objects are more complicated to reconstruct. We hence focus on leptons of the first two generations, so that $\ell_1, \ell_2 = e, \mu$ in Eq. (2.4), and we require the presence of two positively-charged and two negatively-charged leptons,

$$N(\ell^+) = N(\ell^-) = 2 \ . \tag{2.7}$$

The corresponding signal selection efficiency is about 40%, many leptons being missed as lying outside the acceptance of the detector or being too soft for being correctly reconstructed. The corresponding background rejection factor is slightly below 7, as many of the background components do not yield a tetraleptonic signal.

Although the signal is expected to feature the presence of two b-jets, b-tagging is not perfect. Harder b-jets are indeed more easily correctly reconstructed than softer b-jets. Moreover, for scenarios where the mass splitting between the Higgs

bosons is large, the produced SM Higgs boson is often boosted. The two b-jets are therefore not resolved, and a single b-jet is instead reconstructed. It consequently turns out that only 10–20% of the surviving signal events contain two tagged b-jets. For the **BP2** and **BP4** scenarios, the mass splittings between the different Higgs states is large and b-jets are more efficiently tagged, the signal selection efficiency being larger. In contrast, the selection efficiency is found to be smaller for the two other scenarios, as the $H_1 \to h^0 Z$ decay proceeds almost at threshold.

On the other hand, 40–50% of the signal events are tagged as single-b-jet events, and a significant fraction of them do not feature any tagged b-jets at all. In order to recover the large number of signal events featuring a single b-jet, we consider two independent signal regions in which we respectively require 2 and 1 b-tagged jet,

$$N(b) = 2 \qquad \text{or} \qquad N(b) = 1. \tag{2.8}$$

This cut allows for reducing the background by a factor of about 10 and 2.5 in the two and one jet cases respectively.

As shown in Table 2.2 and 2.3 for an integrated luminosity of 1000 fb^{-1}, about 200–500 and 900–1300 signal events are expected to respectively populate the $N(b) = 2$ and $N(b) = 1$ signal regions, to be compared with 230 and 800 background events (including a conservative K-factor of 2). From this stage, background rejection can be improved by restricting the missing transverse energy $\not{E}_T$ in the event,

$$\not{E}_T < 50 \text{ GeV}. \tag{2.9}$$

This selection leaves the signal barely unaffected as it is expected to be fully visible, and reduces the background by an extra factor of 3. The surviving background events are mostly originating from $t\bar{t}Z$ and $WWZb\bar{b}$ production. In the $N(b) = 2$ signal region, an extra selection can be imposed as the invariant mass of the dijet system m_{bb} has to be compatible with the mass of the Higgs boson,

$$90 \text{ GeV} < m_{bb} < 150 \text{ GeV}. \tag{2.10}$$

Finally, we make use of the different properties of the leading lepton ℓ_1 and next-to-leading lepton ℓ_2 for the signal and the background (as illustrated in Figure 2.1 for the **BP2** scenario) to further improve the senstivity, enforcing

$$p_T(\ell_1) > 75 \text{ GeV} \qquad \text{and} \qquad p_T(\ell_2) > 50 \text{ GeV}. \tag{2.11}$$

	Selection step	**BP1**	**BP2**	**BP3**	**BP4**	Background
0	Initial	5000	5000	5000	5000	13636
1	$N(\ell^+) = N(\ell^-) = 2$	1993	2723	1979	2373	1992
2	$N(b) = 2$	206	490	260	340	231
3	$\not{E}_T < 50$ GeV	203	415	220	321	66
4	90 GeV $< m_{bb} <$ 150 GeV	160	344	174	257	16
5	$p_T(\ell_1) > 75$ GeV $p_T(\ell_2) > 50$ GeV	–	200	59	37	2

Table 2.2: Number of events surviving each selection step for the four considered benchmark scenarios, as well as for the SM background. The results are normalized to an integrated luminosity of 1000 fb^{-1} and include a conservative K-factor of 2 for the background. Results are presented for the $N(b) = 2$ signal region.

	Selection step	**BP1**	**BP2**	**BP3**	**BP4**	Background
0	Initial	5000	5000	5000	5000	13636
1	$N(\ell^+) = N(\ell^-) = 2$	1993	2723	1979	2373	1992
2	$N(b) = 1$	884	1310	910	1115	818
3	$\not{E}_T < 50$ GeV	871	1122	782	1060	242
4	$p_T(\ell_1) > 75$ GeV $p_T(\ell_2) > 50$ GeV	–	650	296	163	20

Table 2.3: Number of events surviving each selection step for the four considered benchmark scenarios, as well as for the SM background. The results are normalized to an integrated luminosity of 1000 fb^{-1} and include a conservative K-factor of 2 for the background. Results are presented for the $N(b) = 1$ signal region.

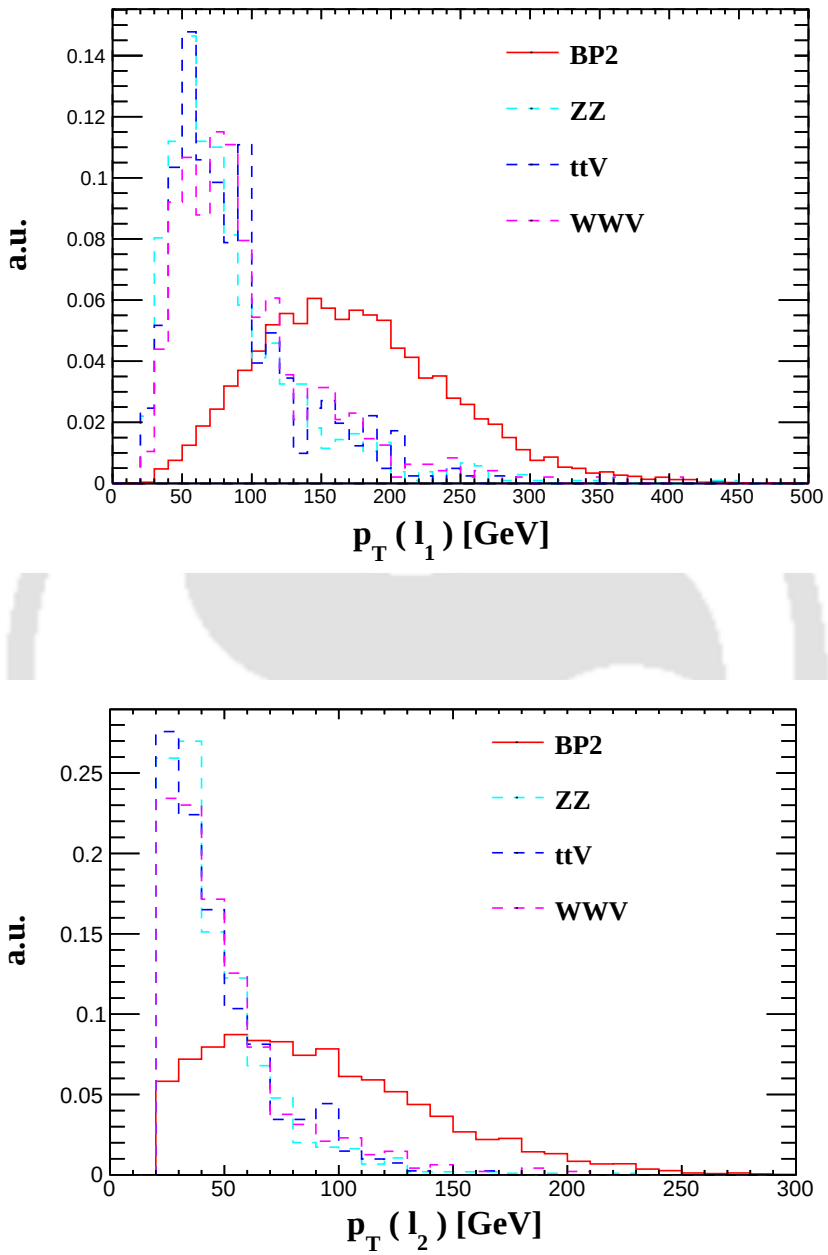

Figure 2.1: Normalised p_T distributions of the leading (upper panel) and next-to-leading (lower panel) leptons, both for the signal corresponding to the **BP2** scenario and the dominant background contributions, in the case of the $N_b = 2$ signal region.

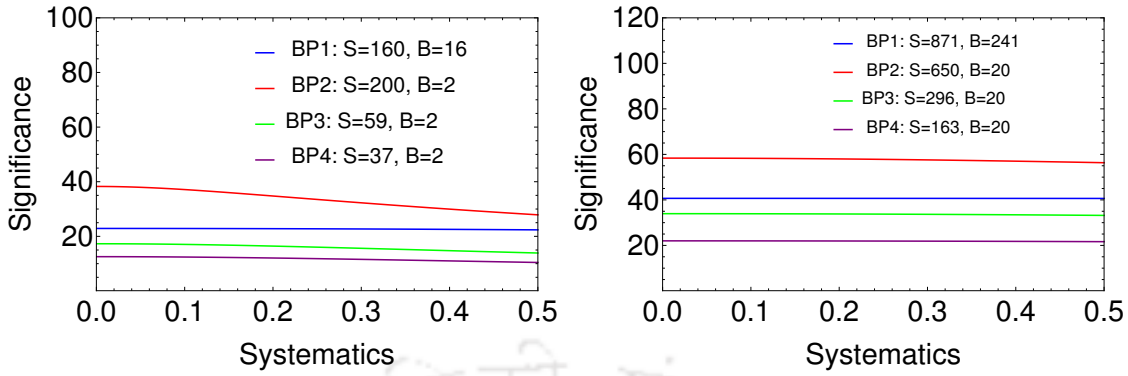

Figure 2.2: LHC significance, as defined by Eq. (2.12), to the considered Higgs cascade decays for the four considered benchmark scenarios and assuming a luminosity of 1000 fb^{-1}. We show results for the $N(b) = 2$ (left panel) and $N(b) = 1$ (right panel) signal regions, and calculate the dependence of the significance on the level of systematic uncertainties taken as $\Delta_B = xB$ (with x being shown on the horizontal axis).

These two last cuts yield a basically background-free environment. The corresponding signal selection efficiencies are usually large, except for scenarios featuring a small mass splitting such as in the **BP1** configuration. We will therefore ignore this cut for what concerns the **BP1** configuration.

In addition to the conservative K-factor of 2 that has been included in the background numbers to model higher-order effects, we assess the potential effects of the systematic uncertainties of Δ_B by computing the signal significance as [69]

$$Z = \sqrt{2}\left((S+B)\ \ln\left[\frac{(S+B)\ (B+\Delta_B^2)}{B^2+(S+B)\ \Delta_B^2}\right] - \frac{B^2}{\Delta_B^2}\ln\left[1+\frac{\Delta_B^2\ S}{B\ (B+\Delta_B^2)}\right]\right)^{\frac{1}{2}} \quad (2.12)$$

with $\Delta_B = xB$.

In Figure 2.2, we present the LHC sensitivity, as defined by Eqn. (2.12), to the signal for the different considered benchmark scenarios and for both the $N(b) = 2$ and $N(b) = 1$ signal regions. The normalization moreover corresponds to an integrated luminosity of 1000 fb^{-1}. All the selection cuts introduced above have been applied, with the exception of the one on the leading and next-to-leading leptons in the case of the **BP1** scenario, as indicated above. The results are shown for various levels of systematic uncertainties ranging from 0% to 50%. They are found stable with respect to the systematics thanks to a very large signal and the almost background-free environment originating from our selection.

The results presented so far correspond to a signal cross section that has been

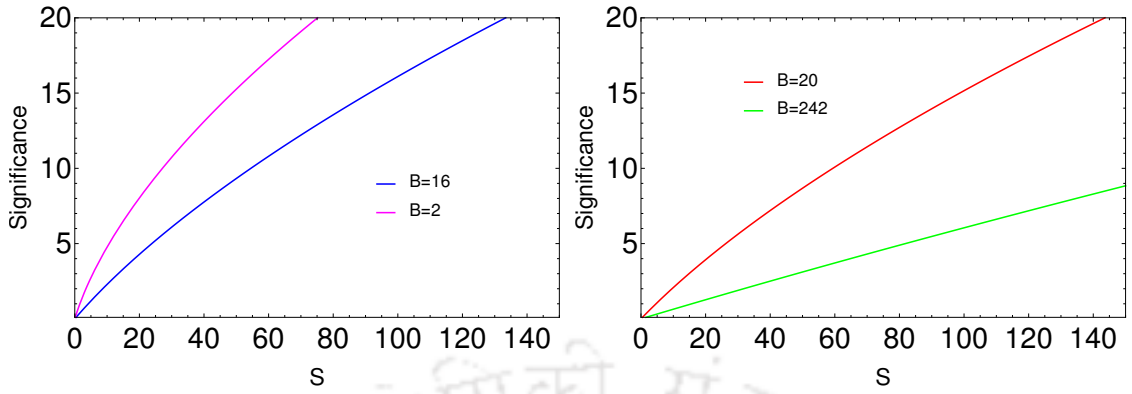

Figure 2.3: Variation of the significance with respect to the number of signal events S for the $N(b) = 2$ (left panel) and $N(b) = 1$ (right panel) signal regions, both when the cut on the transverse momentum of the leading and next-to-leading leptons is applied (purple and red) and ignored (blue and green). We consider a level of systematic uncertainties of 10%.

.

fixed to 5 fb. In Figure 2.3, we relax this hypothesis and show the dependence of the significance on the number of signal events S when 10% of systematic uncertainties is assumed. We again consider both the $N(b) = 2$ (left panel) and $N(b) = 1$ (right panel) signal regions, and study the dependence on the last cut on the transverse momentum of the two leading leptons. As expected, the effect of this selection increases the significance for a given number of signal events. Conversely, while about 25 and 85 signal events are required for a 5σ discovery without imposing any requirement on the leptons, for the $N(b) = 2$ and $N(b) = 1$ signal regions respectively, these numbers are reduced to 10 and 25 after constraining the transverse momentum of the leptons as in Eq. (2.11).

Translating these numbers in term of cross section, compressed scenarios like our **BP1** configuration could yield an observable signal in the $N(b) = 2$ and $N(b) = 1$ signal regions as long as the production rate is at least 0.78 fb and 0.49 fb, respectively. The reach of the $N(b) = 1$ signal region is found to be larger, by virtue of the efficiency to correctly identify one b-jet that is larger than the one to identify two b-jets. The two regions are however complementary, as even if the $N(b) = 1$ region is better for what concerns the reach, the $N(b) = 2$ analysis offers a way to uniquely reconstruct the intermediate heavy Higgs states as illustrated in Figure 2.4. For scenarios exhibiting a mass spectrum featuring larger splittings like in the **BP2** configuration, the final state objects are harder, which implies a better reconstruction efficiency. Accordingly, one obtains better expected limits on the production rate, the observable cross section being 0.25 fb and 0.19 fb in the $N(b) = 2$ and

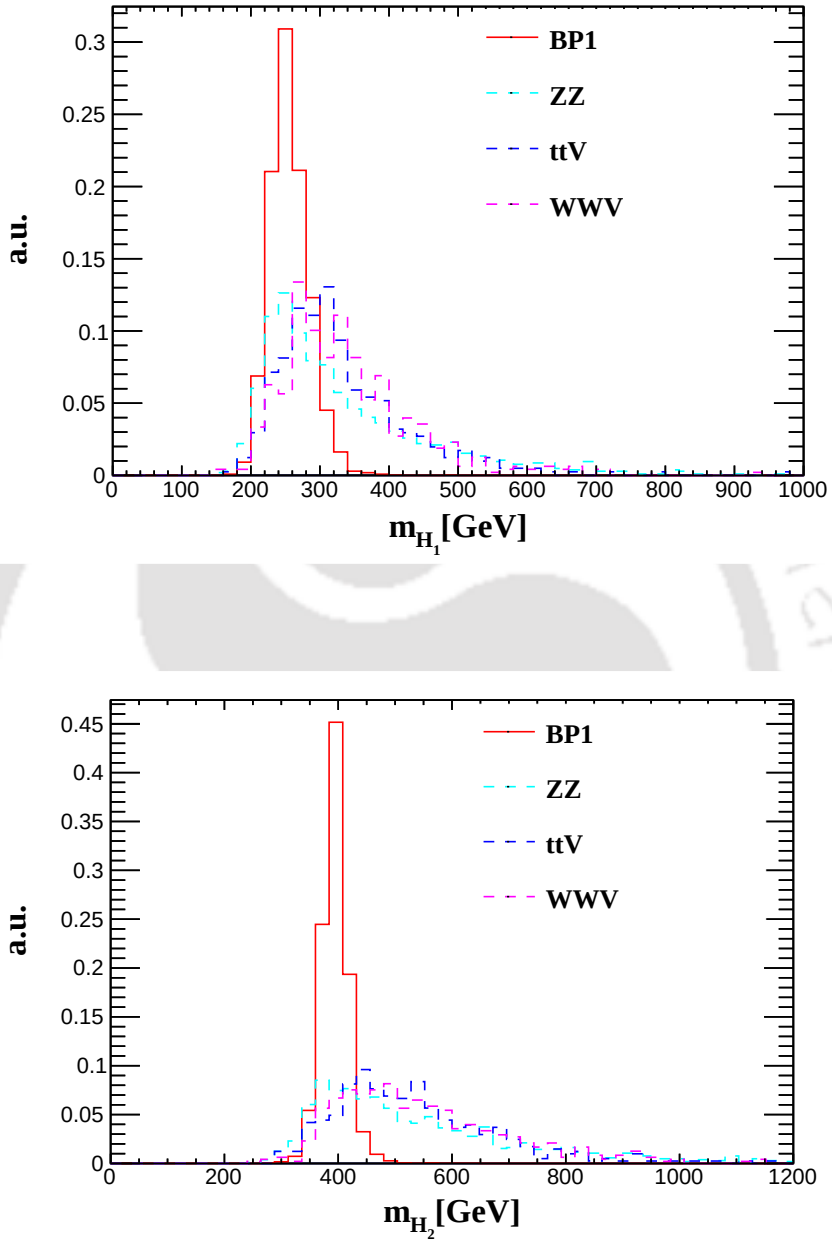

Figure 2.4: Normalized invariant-mass spectrum for the intermediate H_1 (upper panel) and H_2 (lower panel) states in the context of the $N(b) = 2$ analysis (the last cut being omitted) and for the **BP1** scenario. The results are derived from the reconstruction of the $2b\ell^+\ell^-$ and $2b4\ell$ systems. Whilst the spread in the H_1 invariant mass spectrum stems from the different possible combinations of the leptons, the distribution is found similar to the one obtained for any other lepton combination.

Background	$\ell^+\ell^-$ + jets	W^+W^- + jets	$t\bar{t}h^0$
$\sigma\times$ BR	3.2 pb	109.1 fb	14 fb

Table 2.4: Leading-order cross section for the different SM processes contributing to the background of our $2\ell + 4b$ analysis. They include the the relevant branching ratios and the preselection cuts of Eq. (2.5) and Eq. (2.6).

$N(b) = 1$ analysis, respectively. For scenarios featuring a smaller mass splitting like in the **BP3** case (where one of the decays has to occur close to threshold) or in the **BP4** case (where both decays have less available phase space than in the **BP2** case), the final state objects are softer, which results in degraded expected limits on the signal cross section, but still in the 1 fb regime.

2.1.3 Probing Higgs Cascades in the $2\ell 4b$ final state

The Higgs cascade signal that we consider in this work could also give rise to a final-state signature comprised of four b-jets and one pair of opposite-sign leptons of the same flavor,

$$pp \to H_2 \to H_1 Z \to h^0 Z Z \to b\bar{b}\; b\bar{b}\; \ell^+\ell^- \ . \tag{2.13}$$

The combinatorics induced by the final state reconstruction and the more abundant SM background renders the task of discriminating the signal from the background complicated. We however verify, in this section, the existence of any potential corresponding handle. The dominant contributions to the SM background arise from the associated production of a Drell-Yan pair of leptons with jets, W-boson pair production with jets and $t\bar{t}h^0$ production. The leading-order cross sections as returned by MadGraph5_aMC@NLO are shown in Table 2.4.

In our analysis, jet and lepton candidates are selected as in Eq. (2.5) and Eq. (2.6). We preselect events containing one positively-charged and one negatively-charged lepton regardless of the lepton flavor,

$$N(\ell^+) = N(\ell^-) = 1 \ , \tag{2.14}$$

and we require in addition the presence of at least four jets out of which three should be b-tagged,

$$N(j) \geq 4 \qquad \text{with} \qquad N(b) = 3 \ . \tag{2.15}$$

	Selection step	**BP1**	**BP2**	**BP3**	**BP4**	Background
0	Initial	5000	5000	5000	5000	6.657×10^6
1	$N(\ell^+) = N(\ell^-) = 1$	2815	3006	2747	2971	3.695×10^6
2	$N(j) \geq 4$	2811	3004	2735	2970	3.644×10^6
3	$N(b) = 3$	228	506	302	394	25062
4	80 GeV$< M_{\ell\ell} <$100 GeV	201	434	258	343	13072
5a	300 GeV$< m_{H_2} <$500 GeV	121	–	–	–	1954
5b	900 GeV$< m_{H_2} <$1400 GeV, $p_T^\ell > 70$ GeV	–	192	–	–	455
5c	900 GeV$< m_{H_2} <$1400 GeV, $p_T^\ell > 60$ GeV	–	–	94	–	649
5d	500 GeV$< m_{H_2} <$700 GeV , $p_T^\ell > 50$ GeV	–	–	–	91	552

Table 2.5: Number of events surviving each selection step for the four considered benchmark scenarios, as well as for the SM background. The results are normalized to an integrated luminosity of 1000 fb^{-1} and include a conservative K-factor of 2 for the background.

Whilst four b-tagged jets are expected, the loss in signal efficiency induced by the requirement of a fourth b-tag would make the signal unobservable (see the discussion in Section 2.1.2). The combined signal efficiency for these preselection cuts is of about 5–6%, for a background rejection factor of about 250. We then impose the lepton pair to be compatible with the decay of a Z-boson, constraining its invariant mass $m_{\ell\ell}$ to satisfy

$$80 \text{ GeV} \leq m_{\ell\ell} \leq 100 \text{ GeV}. \tag{2.16}$$

This allows for the reduction of the diboson and Higgs backgrounds without impacting the signal too much. At this stage, the number of background events is of about 13000, while the number of signal events is expected to be in the 200–450 window for the different scenarios, as illustrated in Table 2.5. The signal is thus not visible over the background. The fact that all final state objects are not fully identified and the combinatorics that may result from the reconstruction of the intermediate H_1 and Z-bosons make a kinematic fit complicated, in particular once detector effects are accounted for. We therefore approximate the invariant-mass spectrum of the H_2 boson by the invariant-mass distribution of the system comprised of the four leading jet candidates and the selected pair of leptons, m_{H_2}. As illustrated in Figure 2.5, this variable serves as a good discriminator of the signal from the background. The

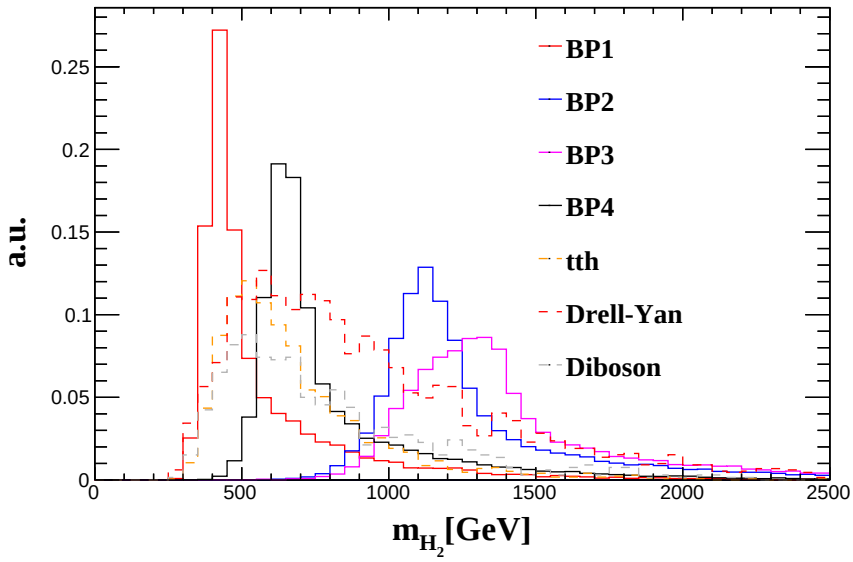

Figure 2.5: Normalised invariant-mass distribution of the heavy H_2 boson for the main contributions to the SM background and the four signal scenarios, once all other selection cuts have been applied.

distribution turns to be very broad for some scenarios, the distortion being larger for new physics scenarios featuring larger mass splittings as this configuration could induce extra radiation and thus more jets in the final state. There is no perfect scenario-independent selection that would allow for the observation of the signal from the overwhelming background. Such a potential cut indeed strongly depends on the mass splittings between the different Higgs states. We therefore propose four different cuts,

$$\begin{aligned}
&\text{(5a)} \quad 300\ \text{GeV} < m_{H_2} < 500\ \text{GeV}\ , \\
&\text{(5b)} \quad 900\ \text{GeV} < m_{H_2} < 1400\ \text{GeV}, \quad p_T^\ell > 70\ \text{GeV}\ , \\
&\text{(5c)} \quad 900\ \text{GeV} < m_{H_2} < 1400\ \text{GeV}, \quad p_T^\ell > 60\ \text{GeV}\ , \\
&\text{(5d)} \quad 500\ \text{GeV} < m_{H_2} < 700\ \text{GeV}, \quad p_T^\ell > 50\ \text{GeV}\ ,
\end{aligned} \tag{2.17}$$

where the extra selection on the leptons allow for a better signal discrimination in the case of a not too light spectrum (as this yields harder leptons). The first of these selection target setups similar to the configuration of the **BP1** scenario where the spectrum is compressed and light, while the second selection aims for scenarios featuring heavier Higgs boson with enough mass splittings to guarantee the presence of very hard leptons in the final state. The third choice is also appropriate for heavier spectra, but it potentially allows for intermediate decays being close to threshold.

Finally, the last selection targets spectra where the Higgs bosons are not too heavy but where the decays can occur far from threshold.

For an integrated luminosity of 1000 fb^{-1}, these cuts lead to an LHC sensitivity to the **BP1**, **BP2**, **BP3** and **BP4** scenarios of 2.7σ, 8.5σ, 3.6σ and 3.8σ respectively, when 10% of systematic uncertainties is also factored in. These results are however found not to depend on the systematics. Although potentially promising, the $4b2\ell$ signature does not provide as clear a handle on the signal as the $2b4\ell$ channel and will therefore be not considered in what follows.

2.2 Model Implications

We now turn to the understanding of the implications of the analyses that have been designed in Section 2.1 in a simplified model context. We investigate below how the simplified spectra introduced in the previous section can be realized in a concrete model with an enlarged scalar spectrum, and investigate the reach of our analysis. As an operating example, we choose the Type-II 2HDM. For details about the model and the couplings, we refer to Ref. [22] and to Section 2.2.1 where we sketch the essential details. Our phenomenological results are given in Section 2.2.2.

2.2.1 The Two-Higgs-Doublet Model - Spectrum and Couplings

The 2HDM has been extensively studied during the last decades, both as a standalone model and also often as the scalar sector of a larger model like the MSSM. Unlike the SM, the 2HDM contains two weak doublets of Higgs fields ϕ_1 and ϕ_2 of hypercharge $Y = 1$. At the minimum of the potential, the neutral components of both doublets develop VEV,

$$\langle \phi_1^0 \rangle = \frac{1}{\sqrt{2}} v_1 \qquad \text{and} \qquad \langle \phi_2^0 \rangle = \frac{1}{\sqrt{2}} v_2 \ , \tag{2.18}$$

where the vev of the SM Higgs fields v is obtained through $v_1^2 + v_2^2 \equiv v^2 = (\sqrt{2} G_F)^{-1}$ with G_F being the Fermi constant. The two vevs v_1 and v_2 are thus not arbitrary as their quadratic sum is connected to the mass scale of the electroweak bosons. We have thus here a single free parameter that is often chosen as the ratio $v_2/v_1 = \tan\beta$.

The breaking of the electroweak symmetry induces a mixing of the scalar degrees

of freedom that reads, at tree-level,

$$\begin{pmatrix} H^0 \\ h^0 \end{pmatrix} = \begin{pmatrix} \cos\alpha & \sin\alpha \\ -\sin\alpha & \cos\alpha \end{pmatrix} \begin{pmatrix} \Re\{\phi_1^0\} \\ \Re\{\phi_2^0\} \end{pmatrix} , \qquad A = -\sin\beta\, \Im\{\phi_1^0\} + \cos\beta\, \Im\{\phi_2^0\} , \tag{2.19}$$

$$H^\pm = -\sin\beta\ \phi_1^\pm + \cos\beta\ \phi_2^\pm , \tag{2.20}$$

where h^0 and H^0 are CP-even mass-eigenstates, A is a CP-odd mass-eigenstate and $H^\pm$ are the physical charged Higgs bosons. In the notation of Section 2.1, the H_2 boson can in principle equally be mapped to the heavier scalar state H^0 or the pseudoscalar state A, whereas we impose the lightest CP-even state h^0 to be the SM Higgs boson of mass $m_{h^0} = 125$ GeV. While the model features in general many free parameters, they can all be reduced, for our purposes, to the value of the mixing angle α and $\tan\beta$.

The way in which the mixing angles enter the couplings of the Higgs bosons to the SM particles depends on the 2HDM configuration under consideration. For the sake of the example, we consider in this section the CP-conserving version of the Type II 2HDM, where the first Higgs field ϕ_1 couples to the down-type quarks and the charged leptons, and the second Higgs field ϕ_2 couples to the up-type quarks, as in the MSSM.

Whereas two different Higgs cascades can in principle be considered,

$$pp \to H^0 \to AZ \to h^0 ZZ \qquad \text{and} \qquad pp \to A \to H^0 Z \to h^0 ZZ , \tag{2.21}$$

the absence of a $H^0 h^0 Z$ coupling in the Type II 2HDM implies that the second of the above processes is forbidden. In the notation of Section 2.1, this thus means that $H_1 \equiv A$ and $H_2 \equiv H^0$. The corresponding production cross section depends on the α and β angle through the off-diagonal coupling strengths of the Higgs bosons to the Z-boson $g_{H^0 AZ}$ and $g_{Ah^0 Z}$,

$$g_{H^0 AZ} = -\frac{g\sin(\beta-\alpha)}{2\cos\theta_w} \qquad \text{and} \qquad g_{Ah^0 Z} = \frac{g\cos(\beta-\alpha)}{2\cos\theta_w} , \tag{2.22}$$

with g being the weak coupling and θ_w the electroweak mixing angle and the coupling of the Higgs bosons to $t\bar{t}$ and $b\bar{b}$ - see Sec. 2.2.2. While other Higgs production process could be relevant as potentially yielding an observable signal (like the vector-boson fusion production of an A boson), we opt to ignore them all as they would require

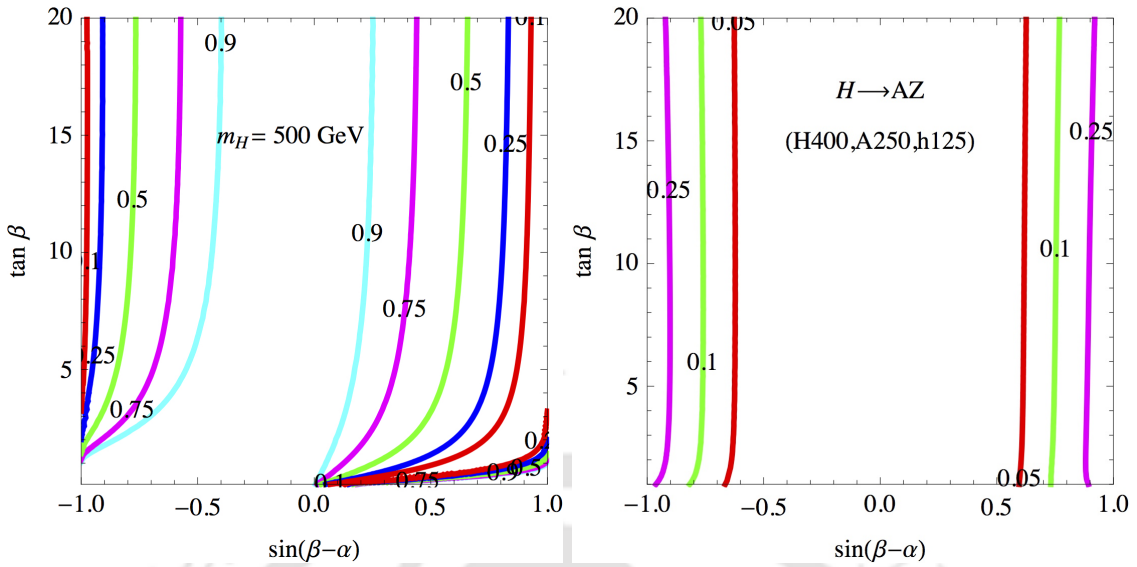

Figure 2.6: Dependence of the $\sigma(pp \to H^0)$ cross section (left panel) and the $H^0 \to AZ$ (right panel) branching ratio on the Higgs mixing angles α and β. The results are shown in the $(\sin(\beta-\alpha), \tan\beta)$ plane and for the Higgs boson masses introduced in Section 2.1. The cross section values (in the left panel figure) are normalized to the corresponding SM value for a SM Higgs-boson of 500 GeV.

dedicated analyses which goes beyond the scope of this work.

2.2.2 Higgs-Boson Production Cross Sections and Branching Ratios

In order to evaluate the constraints that could be imposed on the 2HDM parameter space from H^0 cascades, we first need to calculate the $pp \to H^0$ cross section. We make use of the SM results [70, 71] that we rescale by an appropriate loop factor,

$$\sigma(pp \to H^0) = \sigma_{\rm SM} \times \frac{\left|\frac{\sin\alpha}{\sin\beta} F^h_{1/2}(\tau_t) + \frac{\cos\alpha}{\cos\beta} F^h_{1/2}(\tau_b)\right|^2}{|F^h_{1/2}(\tau_t) + F^h_{1/2}(\tau_b)|^2}, \tag{2.23}$$

where $\tau_f = 4m_f^2/m_{H^0}^2$ (with $f = t,\, b$) and where the loop function $F^h_{1/2}$ is given by

$$F^h_{1/2} = -2\tau\Big[1+(1-\tau)f(\tau)\Big] \qquad \text{with} \qquad f(\tau) = \begin{cases} \left[\sin^{-1}(1/\sqrt{\tau})\right]^2 & \tau \geq 1\ , \\ -\frac{1}{4}\left[\ln\frac{1+\sqrt{1-\tau}}{1-\sqrt{1-\tau}} - i\pi\right]^2 & \tau < 1\ . \end{cases} \tag{2.24}$$

In Figure 2.6 (upper panel), we present, in a convenient $(\sin(\beta-\alpha), \tan\beta)$ plane, the dependence on the H^0 gluon fusion production cross section on the mixing

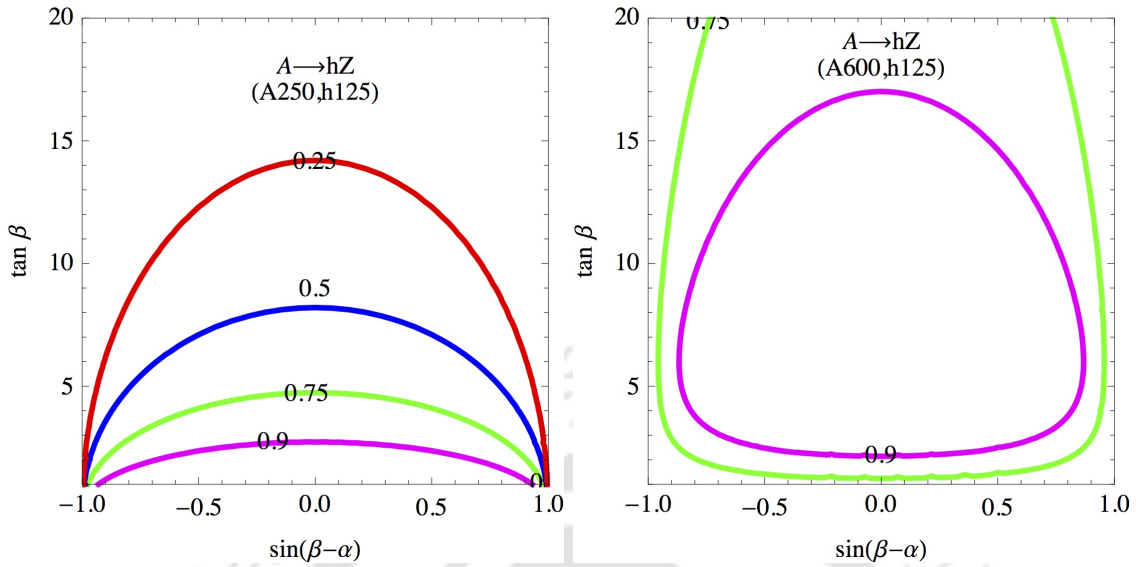

Figure 2.7: Dependence of the $A \to h^0 Z$ branching ratios on the Higgs mixing angles α and β. The results are shown in the $(\sin(\beta-\alpha), \tan\beta)$ plane and for the Higgs boson masses introduced in Section 2.1.

angles for a heavy Higgs boson mass of 500 GeV. The results are normalized to the corresponding SM Higgs boson production cross section, and we observe that the cross section is maximum when $\sin(\beta-\alpha) \to 0$ and tends to vanish for $\sin(\beta-\alpha) \to \pm 1$. As the lightest Higgs boson h^0 has to be SM-like, $\sin(\beta-\alpha) \sim \pm 1$, some slight deviations being however still allowed by current measurements [72]. This constraint will nevertheless be omitted from our analysis in which we aim to determine the constraints on the parameter space that are issued solely from Higgs cascades at the LHC. The asymmetry of the cross section dependence on $\sin(\beta-\alpha)$ (relatively to $\sin(\beta-\alpha)=0$) originates from the α and β dependence in Eq. (2.23). The cross section is hence enhanced both for small values of $\tan\beta$ (due to an enhancement of the contributions of the top-quark loops) and large values of $\tan\beta$ (due to an enhancement of the contributions of the bottom-quark loops). The top-loop enhancement is more pronounced in the positive $\sin(\beta-\alpha)$ half-plane, while the bottom-loop one impacts the negative $\sin(\beta-\alpha)$ half-plane. Moreover, any further increase of $\tan\beta$ beyond 20 does not lead to any appreciable effect via the bottom loops, so that we impose $\tan\beta < 20$ in the following analysis.

The partial widths associated with the $H^0 \to AZ$ and $A \to h^0 Z$ decays are controlled by the scaling factors $\sin(\beta-\alpha)$ and $\cos(\beta-\alpha)$ respectively, as illustrated by Eq. (2.22). As a result, the intermediate region in which $\sin(\beta-\alpha)$ is different both from 0 and ± 1 features an interesting enhancement of the $H^0 \to h^0 ZZ$ decay.

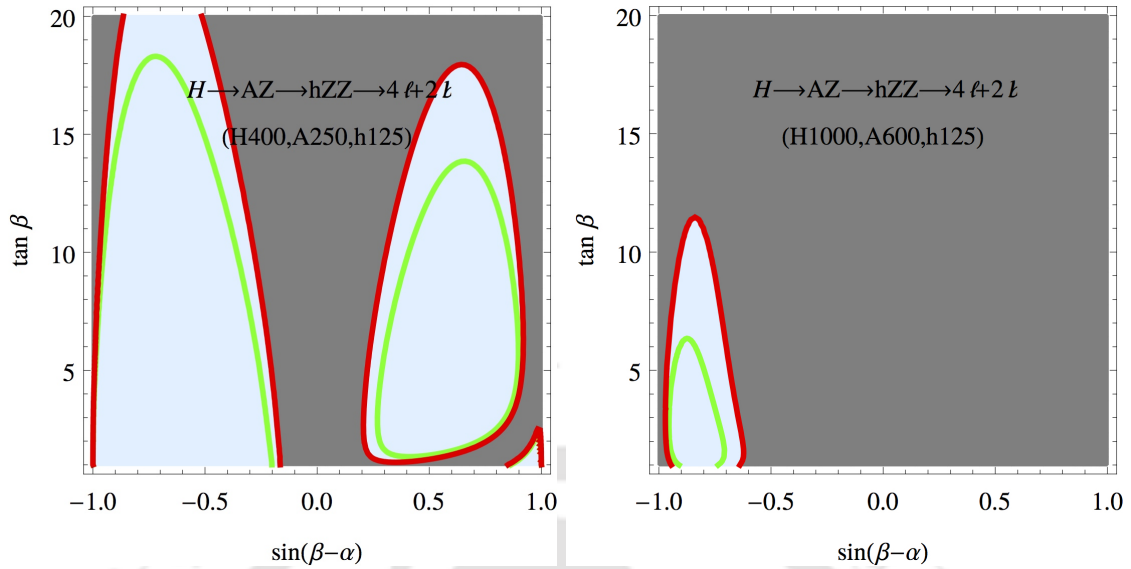

Figure 2.8: Sensitivity of the LHC in the 2HDM parameter space once all Higgs masses have been fixed as in the **BP1** (left panel), **BP2** (right panel) scenarios. The green and red contours respectively correspond to the region covered by the $N(b) = 2$ and $N(b) = 1$ signal regions for an integrated luminosity of 1000 fb^{-1}.

In the lower panel of Figure 2.6 and in Figure 2.7, we present contours of specific branching ratios values for the $H^0 \to AZ$ and $A \to h^0 Z$ decays for representative Higgs boson mass choices corresponding to the benchmark points introduced in Section 2.1. As expected, we observe that the $H^0 \to AZ$ decay becomes prominent for $\sin(\beta - \alpha) \sim \pm 1$, while the $A \to h^0 Z$ one exhibits a complementary behavior and becomes smaller in this region. The qualitative difference in the behavior of the pseudoscalar decay into a $h^0 Z$ pair for the **BP1**-like (lower left panel) and **BP2**-like (lower right panel) configurations stems from the $t\bar{t}$ channel that is kinematically open in the **BP2** case and is dominant for low values of $\tan\beta$. On the other hand, the decays into $b\bar{b}$ and $\tau^+\tau^-$ systems are enhanced for larger $\tan\beta$ values, and the partial width of the $A \to h^0 Z$ decay increases for $\sin(\beta - \alpha) \to 0$, as shown in Eq. (2.22). Consequently, the branching ratio associated with the $A \to h^0 Z$ decay is bounded from above in the large $\tan\beta$ region for both scenarios, as well as for small $\tan\beta$ values in the **BP2** case. This explains the origins of the closed contours of given branching ratio values obtained for the **BP2** scenario. On different grounds, we have found that there is no qualitative differences across scenarios for the $H^0 \to AZ$ branching ratio.

In Figures 2.8 and 2.9, we show the allowed regions in the $(\sin(\beta - \alpha), \tan\beta)$ plane for mass configurations equal to those of the benchmark scenarios introduced in the former section. If the final state topology is similar to the one encountered in

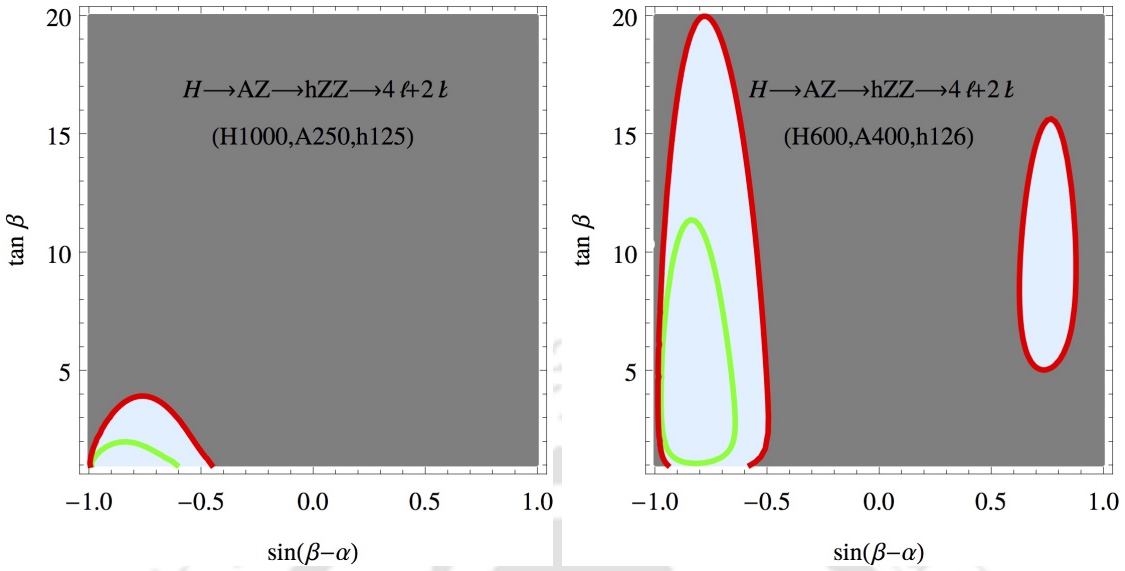

Figure 2.9: Sensitivity of the LHC in the 2HDM parameter space once all Higgs masses have been fixed as in the **BP3** (left panel) and **BP4** (right panel) scenarios. The green and red contours respectively correspond to the region covered by the $N(b) = 2$ and $N(b) = 1$ signal regions for an integrated luminosity of 1000 fb^{-1}.

the case of the considered benchmarks, the already-computed upper limits on the signal cross section could be applied. On the other hand, new limits could also be obtained after deriving the selection efficiency that would be associated with the new signal, following the different analysis strategies introduced in Section 2.1.

The light blue regions shown on Figures 2.8 and 2.9 correspond to parameter space configurations in which the cross section associated with the heavy Higgs boson cascade process is large enough to yield a 5σ discovery. The results are based on the numbers quoted in the previous section and are related to an integrated luminosity of 1000 fb^{-1}. The green contours determine the reach of the $N(b) = 2$ signal region of the $4\ell 2b$ analysis while the red ones refer to the $N(b) = 1$ signal region of the same analysis. As mentioned previously, the $4b2\ell$ analysis is not considered as it is expected to lead to weaker bounds.

By virtue of a larger heavy-Higgs production cross section, the **BP1** and **BP4** scenarios are much better covered, the H^0 boson being indeed lighter than in the other cases. Moreover, while the functional form of the production cross section favors the $\sin(\beta - \alpha) \approx 0$ region, the product of the two branching ratio and their dependence on $\sin(\beta-\alpha)$ and $\cos(\beta-\alpha)$ moves the parameter space region of interest away from the $\sin(\beta - \alpha) \sim 0$ region. The bulk of the discovery reach is located, for the four benchmark, close to $\sin(\beta - \alpha) \sim 1$ that is precisely the region favored by current Higgs data. On the other hand, the dependence on $\tan\beta$ directly originates

from the branching ratio results of Figure 2.6 that show that large and small $\tan\beta$ values may respectively imply a reduced sensitivity due to the importance of the $A \to b\bar{b}$ decay and $A \to t\bar{t}$ decay (if relevant). While the rates of the cascade-decay processes undergone by heavier Higgs bosons may be suppressed, it is seen that they are indeed a viable option to find these additional Higgs bosons at the LHC particularly if they are moderately heavy. The expected suppression of the branching ratio has indeed been found not to be sufficient to balance the strength of simple selection cuts allowing for the separation of the signal from the background.

2.3 Conclusions

While the spectrum of the SM has been established firmly today, physics beyond the SM still remains a mystery. On the theoretical side, creative model building has explored avenues with an enlarged gauge group, extended matter representations and often a richer Higgs sector. While dedicated analyses are necessary to probe specific models of new physics, many models share common features (at least in terms of their spectra) so that they could be explored simultaneously in a general manner. In this spirit, this work aims to study heavy neutral Higgs bosons that cascade decay into SM particles via intermediate lighter scalar states, as could occur in varied new physics theories. While exotic Higgs boson decays have been investigated in the literature, doubly-exotic modes involving several Higgs bosons have mostly not been targeted widely so far although they are an interesting probe for potential discovery.

In this chapter, we have discussed the generic cascade decay process $pp \to H_2 \to H_1 Z \to h^0 ZZ$ where a heavy Higgs boson H_2 decays into a lighter Higgs boson H_1 and a Z-boson, and where the H_1 boson further decays into a SM Higgs boson h^0 and a Z-boson. Investigating a final state signature made of either two b-jets and four charged leptons, or of four b-jets and two charged leptons, we have found that the discovery potential of such a process heavily depends on the magnitude of the mass splittings between the different scalar states, which directly impacts final state object identification. It turned out that the $2b4\ell$ channel is very promising, in particular when the requirement on the number of b-tagged jets is relaxed to $N(b) = 1$. Although this channel does however not allow for the proper reconstruction of the heavy Higgs bosons, it provides an excellent handle for exhibiting the presence of a new physics signal. In contrast, the $4b+2\ell$ final state turns to be less promising, due to the non-perfect b-jet identification and the larger backgrounds.

We have begun with performing our collider analysis in a simplified-model approach inspired by the 2HDM, without resorting to specific values for the new physics couplings. This has allowed us to design several dedicated analyses, optimizing them for a good Higgs-cascade signal selection efficiency and an important associated background rejection. We have then applied our findings to assess the LHC discovery potential of a specific model that has been taken for the sake of the example to be the Type-II 2HDM. In this theoretical framework, we have found that the LHC is sensitive to Higgs-to-Higgs cascades in particular if the heaviest scalar state mass is moderate and for couplings close to those currently allowed by LHC Higgs data. This preferred configuration enhances on the one hand the heavy Higgs boson production cross section, and guarantees on the other hand that the decay products of the Higgs boson can properly be reconstructed. 2HDM compressed scenarios like our **BP1** benchmark point satisfy both these criteria and are understandably expected to be better covered by future LHC results. Scenarios with a slightly heavier spectrum but exhibiting not too large mass splittings, like our **BP4** scenario, are expected to be well probed too, however with a more limited reach. Finally, the sensitivity to scenarios like our **BP2** and **BP3** where the spectrum is much heavier (the heaviest state being at the TeV scale) is still appreciable but reduced as a consequence of the Higgs decay products being in a boosted regime for which our analysis is not sensitive to and the smaller production cross section.

Higgs cascade decays therefore offer a new channel to look for extended scalar sectors, complementing and potentially competing - at least in some models where heavier Higgs bosons for instance feature reduced couplings to fermions - with the more traditional approaches seeking heavier Higgs bosons.

Chapter 3

Exploring Inert Higgs Doublet Model via dijet plus MET analysis

In this chapter, we study dijet plus MET channel aiming to probe heavier masses of charged Higgs boson in the context of inert version of 2HDM at LHC. We perform a detailed signal versus background analysis which concludes that the channel we consider has the potential to probe heavier charged Higgs masses with a high luminosity at LHC.

The issue of DM, required by astrophysical observations but for which we lack a suitable candidate in the SM, is an important reason to attempt to go beyond the SM and, in these attempts, it is often the minimalism of the scalar sector of the SM that is sacrificed.

The IHDM, discussed in the Introduction, with one of the doublet fields not having any direct (at the level of the Lagrangian) interaction with the SM particles, except the gauge particles and SM-like Higgs boson, is a promising candidate model in this regard. This is achieved by the imposition of a Z_2 symmetry under which one of the doublets is odd, while all other fields are even. Such an IHDM [18] would have the Higgs phenomenology, quite different from that of the SM as well as the MSSM or the usual 2HDM scenarios. For example, in the physical Higgs boson sector, all neutral scalars except one are odd under the Z_2 symmetry and are, therefore, always produced in pairs. This also means that the lightest of these cannot decay, and thus could be a candidate for DM. Adding a Z_2-odd right-handed neutrino to this model can also generate small neutrino masses radiatively [73], and to generate leptogenesis [74], ideas which are followed up in further studies [75–83].

The model is shown to be helpful in explaining the LEP-paradox [84–86], and could also generate EWSB at one-loop level through Coleman-Weinberg mechanism [87].

With its interesting Higgs phenomenology, the IHDM has been studied in the context of the LHC [88–107], and in the context of ILC [108–110] in the past. The study in reference [94] considers the results of LUX [111], PLANCK [112], and include the updated results from LHC in references [95, 96], which has provided a comprehensible analysis to provide the available parameter space regions.[2] Most of these studies focus on the pair production of the inert scalars, and consider final states involving leptons and missing energy. The purely hadronic channels are generically marred by the large irreducible background owing to the hadronic environment of the LHC. A comprehensive report on the IHDM search at Run 2 of the LHC is provided by the Dark Matter Forum [114]. For the ILC, the effect of IHDM on the triplet Higgs couplings is studied by Ref. [115]. In this chapter, we consider the dijet along with missing energy as the signature of IHDM, and explore the possible parameter reach at the LHC, with moderate to high luminosity. Apart from the pair production and subsequent cascade decays, this channel receives significant contribution from the vector boson fusion (VBF) [116], t-channel with the invisible Higgs (H) radiating from the mixed propagator, and the s-channel with quartic coupling involving H and W/Z.

This chapter is organized in the following way. In Section 3.1, we describe the present theoretical and experimental constraints available on the model parameters. In Section 3.2, we discuss our analysis, and finally, in Section 3.3, we present the summary and conclusions of the study performed in this chapter.

3.1 Present Constraints on the Model Parameters

We have discussed the inert version of 2HDM i.e. IHDM in Chapter 1. The potential of the model is given in Eq. (1.42). We may note that the parameters are not completely free and independent of each other. There are theoretical constraints arising from the vacuum stability [99, 117], given by

$$\lambda_1 > 0, \quad \lambda_2 > 0, \quad \sqrt{\lambda_1\lambda_2} + \lambda_3 > 0 \ \text{ and } \ \sqrt{\lambda_1\lambda_2} + \lambda_3 + \lambda_4 - |\lambda_5| > 0, \qquad (3.1)$$

and to ensure perturbativity [85, 117] we need to keep $|\lambda_i| \leq 8\pi$. Eq. 1.44 gives $\lambda_5 < 0$ for $m_H < m_A$, and $\lambda_5 > 0$ for $m_A < m_H$. Thus, the sign of λ_5 dictates

[2] In the present study, benchmark points resulting from the analysis of [96] are used.

whether H or A is the DM candidate. Apart from these theoretical constraints, we have experimental constraints coming from LEP observations [118, 119]. From the non-observation of Z and W decays to dark Higgs bosons, we require $m_H + m_A > m_Z$, $2m_{H^\pm} > m_Z$ and $m_{H,A} + m_{H^\pm} > m_W$. The oblique parameter, T, receives contributions from the IHDM, which could be written in terms of the mass splittings as

$$\Delta T \simeq \frac{1.08}{v^2}\big(m_{H^\pm} - m_H\big)\big(m_{H^\pm} - m_A\big) = 0.07 \pm 0.08. \tag{3.2}$$

SUSY searches at LEP leads to constraints on the charged Higgs mass, $m_{H^\pm} \geq 70$ GeV [106, 120], and requires $|m_A - m_H| \leq 8$ GeV for $m_H \leq 80$ GeV and $m_A \leq 100$ GeV [95, 96]. Besides these collider constraints, dark matter relic abundance and direct searches [98, 121, 122] put a limit on the mass of the DM candidate, $40 \leq m_{DM} \leq 80$ GeV,[3] where m_{DM} is either m_H or m_A for the cases of H or A considered as the darkmatter, respectively.

Coming to the LHC experiments, the bound on the invisible decay width of an SM-like Higgs boson(h) is given to be, BR($h \to$ invisible) < 0.12 [124] at 95% confidence level[4] This restricts the relevant coupling for $m_H \leq m_h/2$. At the same time, $m_H < m_h/2$ region is ruled out considering the XENON100 and LUX measurements [93, 111, 126]. Also, the future Cherenkov Telescope Array (CTA) may be able to rule out heavier dark matter masses [127]. Previous studies of the LHC phenomenology include Refs. [89, 97, 98]. Most of these studies consider $m_{H^\pm} \leq 150$ GeV, for which the preferred processes are the pair productions, H^+H^-, $AH^\pm$ and $HH^\pm$. More recently, Ref. [105] studied the constraints of IHDM arising through the dilepton channels, considering two representative values of $m_{H^\pm} = 85$ and 150 GeV, focusing on the parameter region which are complementary to those accessible by dark matter direct searches and Higgs invisible decay channels. This include pair production of AH, HH, AH and $H^\pm H^\mp$ decaying through to the final state of two leptons and missing energy.

In this chapter, we focus on the dijet plus missing energy signal arising in the IHDM scenario. As we see in the next section, this signal can originate from the production of $H^\pm$ in association with H, with the subsequent decay of the charged Higgs boson, as well as from other VBF channels, and s-channels with quartic $VVHH$ couplings, where $V = Z, W$, and t-channel with mixed propagator, radiating HH.

[3]The present allowed range on the mass of the DM, $55 \leq m_{DM} \leq 75$ GeV [123]
[4]The present allowed value for BR($h \to$ invisible) ≤ 0.24 [125] at 95% confidence level.

3.2 Discussion

Discovery of the charged Higgs boson will provide a smoking gun signature of the multi-Higgs models. Compatibility of such a scenario, and further identification of the couplings would be one of the first steps in establishing a specific multi- Higgs model. The prominent production processes involving the charged Higgs bosons at the LHC are H^+H^-, H^+A, H^+H. In the IHDM, H^+ predominantly decay into W^+H, and A decays mostly to ZH, leaving missing energy in all cases and making it almost impossible to reconstruct the events. The magnitude of the cross section will depend on the masses and couplings of the scalars involved. The couplings are dictated by the gauge coupling, and therefore are fixed. Our interest is to explore the low, intermediate and high mass regions of m_{H^+} values. For our study we have taken $\{m_{H^+},\ m_A,\ m_H,\ m_h,\ \lambda_L, \lambda_2\ \}$ as our free parameter set, where masses can be expressed in terms of the parameters available in the potential as given by Eqn.(1.39), and $\lambda_L = \frac{1}{2}\ (\lambda_3+\lambda_4+\lambda_5)$ is the combination relevant to the couplings of the dark matter candidate, H. Considering all the dark matter and collider constraints available presently, the following benchmark points (BP) [5] are selected for our study. Here all the masses are given in GeV. Benchmark Points used in the Table:[6]

BP1: $m_{H^+} = 80$, $m_A = 75.4$, $m_H = 65$, $m_h = 125.1$, $\lambda_L = 0.006$, $\lambda_2 = 0.1$
BP2: $m_{H^+} = 150$, $m_A = 138.6$, $m_H = 65$, $m_h = 125.1$, $\lambda_L = 0.009$, $\lambda_2 = 0.1$
BP3: $m_{H^+} = 200$, $m_A = 189.5$, $m_H = 65$, $m_h = 125.1$, $\lambda_L = 0.009$, $\lambda_2 = 0.1$
BP4: $m_{H^+} = 300$, $m_A = 289.3$, $m_H = 65$, $m_h = 125.1$, $\lambda_L = 0.009$, $\lambda_2 = 0.1$
BP5: $m_{H^+} = 400$, $m_A = 397.6$, $m_H = 65$, $m_h = 125.1$, $\lambda_L = 0.009$, $\lambda_2 = 0.1$
BP6: $m_{H^+} = 500$, $m_A = 494.0$, $m_H = 65$, $m_h = 125.1$, $\lambda_L = 0.009$, $\lambda_2 = 0.1$

We have fixed the mass of the dark matter candidate to be $m_H = 65$ GeV, in order to avoid the invisible decay of the SM Higgs boson to a pair of DM. However, we have confirmed that, varying the mass slightly, within the window available, as described above does not bring in any significant change in our conclusions. We have then chosen different representative values of m_{H^+}, the main object of our study. From Eq. (3.2), this then naturally limits the value of m_A to be close to m_{H^+}. The

[5] The BP's are provided by A. Ilnicka and T. Robens. We acknowledge their help, and refer the reader to their work [95, 96] for a detailed study of the parameter space of the model compatible with the dark matter and collider considerations.

[6] The value of λ_L will not affect our analysis as the processes considered for this analysis is independent of λ_L.

Benchmark Points	cross sections in fb			
	$pp \to H^{\pm}H$	$pp \to H^{\pm}A$	$pp \to HA$	$pp \to H^{+}H^{-}$
BP1	1235.0	954.2	851.8	446.5
BP2	257.9	96.7	179.6	46.4
BP3	110.9	31.3	71.8	15.8
BP4	29.8	6.1	18.1	3.2
BP5	10.7	1.7	5.8	0.9
BP6	4.6	0.6	2.5	0.3

Table 3.1: The production cross section for different Higgs pairs at the LHC ($\sqrt{s} = 13$ TeV) for different BPs considered.

values considered in the BP's are obtained from a random scan, satisfying all the dark matter and collider constraints mentioned above. The production cross section of the Higgs boson pairs at the LHC with $\sqrt{s} = 13$ TeV[7] for these benchmark points are given in Table 3.1. H^+ dominantly decay to W^+H with a BR of almost 100% for $m_{H^+} > (m_H + m_W)$. For masses below this, both $W^{+*}H$ and W^+A^* could contribute. For the BP's considered here, m_A is close to m_{H^+} in all cases, and therefore the decay channel W^+A^* has a maximum contribution of around 2% for $m_{H^+} = 80$ GeV case (BP1). The detector-level final states, considering the

Benchmark Points	$2j + HH$ cross sections in fb (different channels)				$2j + \nu\bar{\nu}HH$ cross sections in fb (different channels)		
	(i) $H^{\pm}H$	(ii): HA	total cascade (i)+(ii)	(A):$pp \to 2j + HH$ (all inclusive)	$H^{\pm}A$	(B):$pp \to 2j + \nu\bar{\nu}HH$ (all inclusive)	(A)+(B)
BP1	1.2	0.008	1.2	1.9	0.2	27.5	29.4
BP2	134.5	36.3	170.8	184.4	9.2	17.5	201.9
BP3	53.1	29.0	82.1	86.7	2.9	6.5	93.2
BP4	15.3	7.8	23.1	27.5	0.6	1.6	29.1
BP5	5.5	2.5	8.0	13.9	0.2	0.5	14.4
BP6	2.3	1.1	3.4	10.5	0.005	0.2	10.7

Table 3.2: Cross section(in fb) at $\sqrt{s} = 13$ TeV for specific benchmark points, showing the significance of the VBF and $t-$channel contributions.

decay of W and Z, are (i) the purely hadronic with jets and missing energy, (ii)

[7]The cross sections do not change significantly at 14 TeV LHC, and the conclusions drawn in this work are expected to be valid at this centre of mass energy as well.

jets and leptons with missing energy, and (iii) purely leptonic with missing energy. H^+H^- thus leads to the final states with $4j+MET$, $2j+l+MET$ and $2l+MET$, with the W pair from the $H^\pm$ decay hadronically, semileptonically, and leptonically, respectively. The H^+A, similarly, leads to $4j+MET$, $2j+2l+MET$, $2j+l+MET$, $2j+MET$, $3l+MET$ and $l+MET$, with W and Z decaying into hadronic jets and leptons, as is the case may be. The other two pairs, H^+H and AH give the final states, $2j+MET$, $2l+MET$, and $l+MET$. The $4j+MET$ final state signal is almost impossible to ressurect from the huge hadronic backgrounds at the LHC. The leponic final states are studied in the literature in the context of LHC. In this article, we shall focus on the dijet plus missing energy signal at the LHC. The $2j+MET$ arises through the cascade decays, $H^+A \to (W^+H)\ (ZH) \to (jjH)\ (\nu\bar{\nu}H)$, and $H^+H \to (W^+H)\ H \to (jjH)\ H$. Apart from these cascade decays, this final state could arise from the VBF to HH, and the t-channel with mixed propagator involving $W(Z)$ and $H^+(A)$, as shown in the illustrative example Feynman diagrams in Fig. 3.1 and 3.2. The contributions arising from the VBF and s-channel with

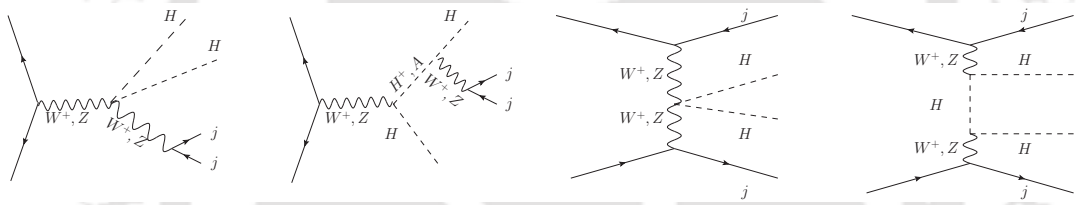

Figure 3.1: Typical Feynman diagrams from a set of such diagrams illustrate the production of $2j+HH$.

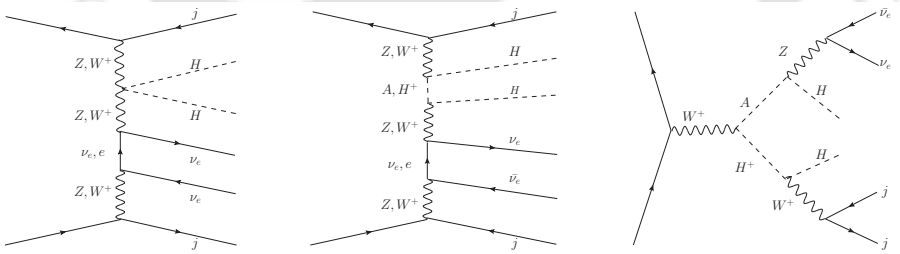

Figure 3.2: Typical Feynman diagrams from a set of such diagrams illustrate the production of $2j+\nu\bar{\nu}HH$.

quartic couplings, and the t-channel processes could be significant, depending on the mass ranges of the Higgs bosons considered. In Table 3.2, we compare the cross sections from cascade decays, separately, along with the total $2j+MET$ cross section, including any possible interference effects. The cross sections are obtained through MadGraph5_aMC@NLO, and after employing the basic cuts

on transverse momentum, $p_T(j) > 20$ GeV and pseudo rapidity, $|\eta_j| < 5.0$ to the two jets, and demanding a separation between the jets of $\Delta R_{j_1 j_2} > 0.4$. The cross sections quoted in Column 4 compared with that in Column 5 reveals the significance of contributions coming from other-than-cascade-decay processes in the case of $2j + HH$ final state, and the possible interference of these two categories. The trend is clear, that the contributions from cascade decay goes down drastically, as m_{H^+} increases, whereas, the other contributions seem to remain steady within the range of 5 to 7 fb. The slightly different behaviour at $m_{H^+} = 150$ GeV is possibly due to the very large and dominating contribution from the cascade-decay channel, where even the interference effects could play a significant role. The case of $2j + \nu\bar{\nu} + HH$ on the other hand gives a slightly different picture. Beyond $m_{H^+} = 300$ GeV, the contributions are very small. On the contrary, it contributes significantly at lower m_{H^+} values. Looking at the t-channel topology of the additional contributions, it is likely that the two jets are produced with large p_T, and therefore the cross section is not reduced by removing the soft jets, as is employed in getting the cross sections in Table 3.2. Background to the process $pp \to 2j + MET$ in IHDM arises through the SM processes of $2j + \nu\bar{\nu}$ and $W + 2j$, where the latter contribute in the leptonic decay of W with soft leptons, or leptons missing into the beam pipe. The cross section for these background processes at the 13 TeV LHC are 955 pb and 51 pb, respectively. In the following we shall discuss the signal and background, including the kinematic distributions, and establish the reach of the LHC in probing IHDM through this channel. We have used MadGraph5_aMC@NLO [57] for our analysis with the IHDM imported through the UFO generated from the publicly available FeynRules [60] interface. The signal and background processes are generated through MadGraph5_aMC@NLO along with basic acceptance cuts employed. For hadronization, we have considered Pythia 6 [62] inside MadGraph5_aMC@NLO with the options of ISR and FSR included. A study of the $p_T(jets)$ of the signal concluded that we can employ the basic cuts of $p_T(j_1) > 80$ GeV, and $p_T(j_2) > 50$ GeV, $|\eta_{jets}| < 5.0$, and a jet separation of $0.4 < \Delta R_{j_1 j_2} < 2.0$, at the generation level, without compromising the signal events significantly. This reduces the effective fiducial cross sections of the signal to 1.3 fb, 14 fb, 16 fb, 9.8 fb, 4.8 fb and 2.5 fb, for the cases of BP1, BP2, BP3, BP4, BP5 and BP6, respectively. We generated 50000 signal events in all cases. The background cross sections are reduced to 12.94 pb and 0.405 pb for $jj + \nu\bar{\nu}$ and Wjj, respectively. We generated 1300000, and 100000 events for these two backgrounds respectively, which provides sufficient statistics at 100 fb^{-1} luminosity. The events thus generated are then analysed with

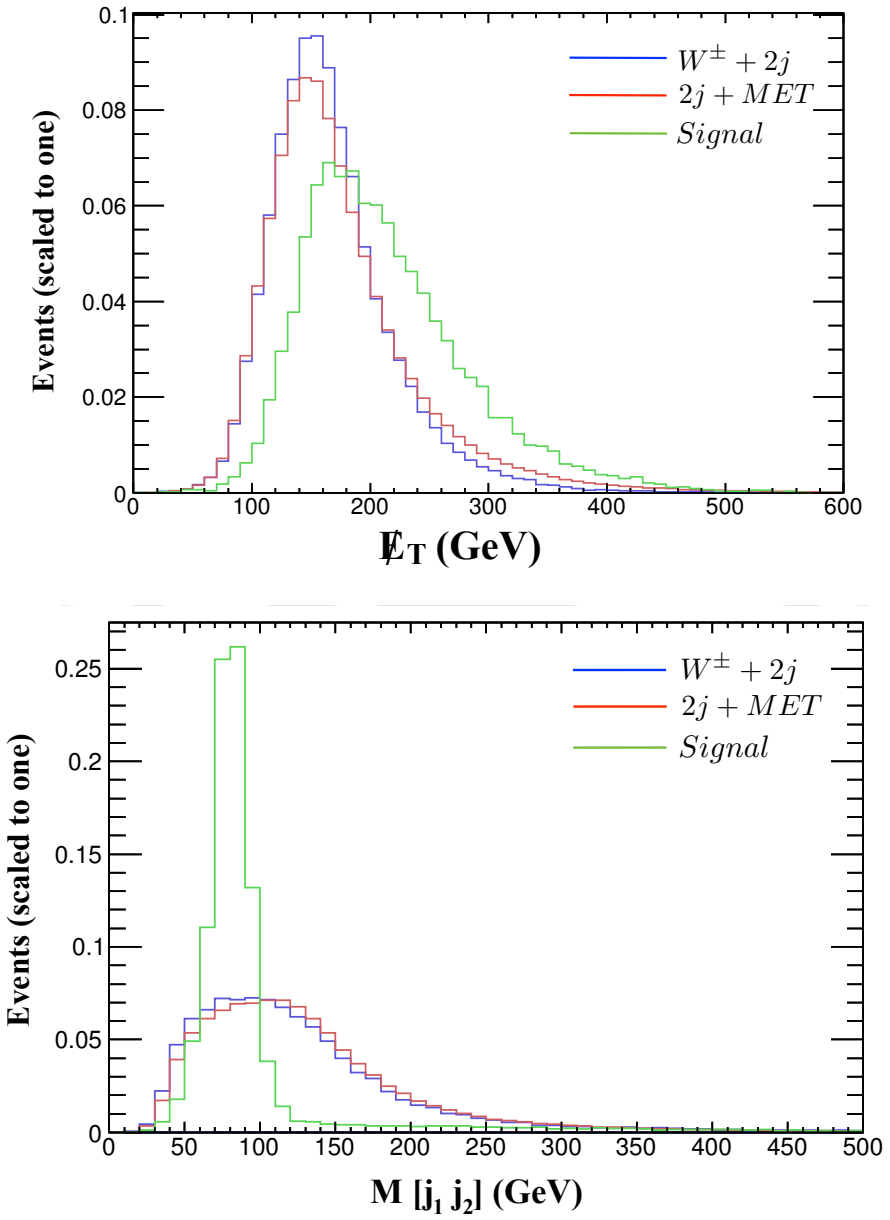

Figure 3.3: Kinematic distributions of the $2j + MET$ events for the scenario of BP4 corresponding to $m_{H^+} = 300$ GeV at 13 TeV LHC, after applying the basic selection criteria as discussed in the text.

the help of MadAnalysis 5 [66], using the inbuilt interface with FastJet and Delphes 3 with the CMS card. For jet reconstruction with Fastjet, we used anti-k_t algorithm with $\Delta R = 0.5$. The following selection cuts are applied to optimise the signal over the background. The events are cleaned from soft-jets and leptons that could arise in the detector simulation, by removing the jets softer than $p_T < 20$ GeV, and $|\eta| > 5.0$. Events with two jets are then selected ($N(j) = 2$), and also

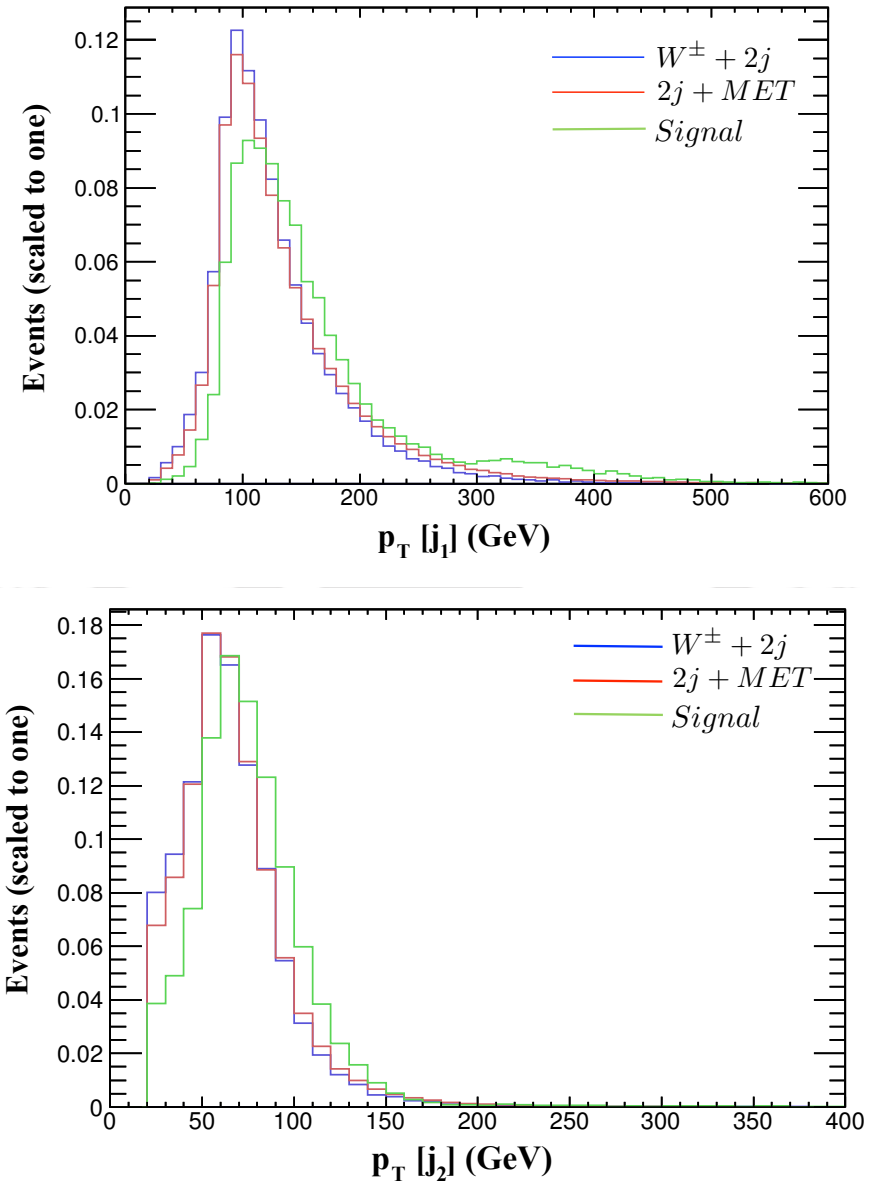

Figure 3.4: Kinematic distributions of the $2j + MET$ events for the scenario of BP4 corresponding to $m_{H^+} = 300$ GeV at 13 TeV LHC, after applying the basic selection criteria as discussed in the text.

demanded that the events do not contain b-jets ($N(b) = 0$) or leptons ($N(l) = 0$). In Figs. 3.3 and 3.4, we present some of the kinematic distributions corresponding to the case of $m_{H^+} = 300$ GeV, after employing the above selection. The other BP's have similar distributions, which are not presented here. Learning from the distributions, we employ further selection cuts on the kinematic distributions with the aim of improving the signal significance. A set of final selection cuts, with transverse momenta of the jets, $p_T(j_1) > 120$ GeV and $p_T(j_2) > 90$ GeV, jet

separation of $\Delta R_{j_1 j_2} < 1.8$, missing transverse energy $MET > 260$ GeV, and the invariant mass of the two jets, $75 < M_{j_1 j_2} < 90$ GeV are considered. With the above selection criteria, the case with low $m_{H^+} = 80$ GeV of BP1 is very difficult to probe due to very small cross section available after the basic cuts employed mentioned above. Considering other BP's, we are left with 90 signal events (S) for BP2 corresponding to $m_{H^+} = 150$ GeV, over a background (B) of 8500 SM events at 1000 fb^{-1} integrated luminosity. This means a significance of $\frac{S}{\sqrt{S+B}} = 0.97$, which is improved to 1.68 with 3000 fb^{-1} luminosity. The signal events are about 1% of the background events, and it requires a very controlled systematics to see the events. However, when we move on to larger m_{H^+} values, situation gets better. At BP3, BP4 and BP5 with $m_{H^+} = 200,\ 300$ and the 400 GeV, respectively, the signal events are 198, 168 and 120 with a luminosity of 1000 fb^{-1}. This corresponds to a signal significance of 2.12, 1.80 and 1.29, which are improved to 3.68, 3.13 and 2.24, respectively, at 3000 fb^{-1} luminosity. The ratio of the signal to background events is now a somewhat better 2.32%, 1.97% and 1.41%, for the respective cases. The other BP with $m_{H^+} = 500$ GeV (BP6) does not spare that well with these selection criteria. The number of signal events at 1000 fb^{-1} corresponding to this BP is 70, giving a significance of 0.76, which is improved to 1.31 at 3000 fb^{-1}. The signal to background ratio is now 0.82%, which is less than the expected systematic uncertainty. We have summarised the above results in Table 3.3. We have employed a uniform selection criteria for all the BP's considered, keeping in mind that such analysis will be easier from the point of view of data analysis. We understand that, the systematic uncertainties could play a critical role while looking for BSM effects with such large SM background events expected. While we do not attempt an involved analysis including the effects of the systematic uncertainties, we have looked at the effects on the significance with an assumed uncertainty of 1% on the background, and 10% systematic uncertainty on the signal events. The resulting significance computed using the formula $\frac{S}{\sqrt{B+(0.01\times B)^2+(0.1\times S)^2}}$ is presented in the Table 3.3. Clearly, the BP3 leaves a significance of about 2, which is sufficient to give a clear hint of a possible BSM signal. The significance corresponding to BP4 and BP5 lie between 1 and 2, while the other two BP's (BP2 and BP6) provide significance less than one. Please note that the above analysis is performed, keeping in mind a generic set of selection criteria that could be employed while searching for signals of the BSM scenarios, the presence of IDM in the present case. We conclude that, in contrast to the phenomenological studies involving leptonic final states, our analysis present a way to probe the large m_{H^+} regions up to a value of around 300 -

Cuts employed	B	BP's	S	$\frac{S}{B}$ %	$\frac{S}{\sqrt{S+B}}$		$\frac{S}{\sqrt{B+(0.01\times B)^2+(0.1\times S)^2}}$	
					1 /ab	3 /ab	1 /ab	3 /ab
$N(j) = 2$, $N(b) = 0$, $N(l) = 0$,	8500	BP2	90	1.05	0.97	1.68	0.72	0.89
$MET > 260$ GeV,		BP3	198	2.32	2.12	3.68	1.56	1.94
$p_T(j_1) > 120$, $p_T(j_2) > 90$,		BP4	168	1.97	1.80	3.13	1.33	1.65
$75 \leq M_{j_1 j_2} \leq 90$ GeV,		BP5	120	1.41	1.29	2.24	0.95	1.19
$\Delta R_{j_1 j_2} < 1.8$		BP6	70	0.82	0.76	1.31	0.56	0.70

Table 3.3: Generic selection cuts employed to optimise the S/B ratio and the signal significance at a 13 TeV LHC, along with the number of signal events (S), number of background events (B) corresponding to the different Benchmark Points (BP's) considered at integrated luminosity of 1000 fb^{-1}. Significances corresponding to a luminosity of 3000 fb^{-1} are also quoted. Significance with assumed systematic uncertainties are given in the last two columns.

400 GeV with high, but achievable, luminosity at the LHC through the $dijet+MET$ channel. Beyond these masses, establishing signals above background is somewhat difficult. However, upto even 500 GeV mass ranges, it is possible to probe the model with somewhat smaller significance.

3.3 Conclusion

The IHDM presents an interesting scenario within the multi-Higgs models, with a candidate dark matter, resulting in distinct phenomenology compared to other models like the 2HDM and MSSM. The model is compatible with all the experimental constraints arising from dark matter searches, as well as from collider experiments including the recent LHC measurements. In a specific scenario, we have considered the mass hierarchy of $m_{H^+} > m_A > m_H$, so that the neutral scalar is the dark matter candidate. We have considered the possibility to probe the model through $2j + MET$ signal at the LHC with high luminosity. This signal arises in IHDM through the cascade decay of pair production of Higgs bosons of the dark sector, along with other production mechanism like VBF, s-channel with quartic Higgs-gauge couplings, t-channel with two H radiating from the gauge-Higgs mixed propagator.

Contributions of cascade alone are significantly reduced at larger m_{H^+} values, whereas the contributions from other channels are somewhat independent of the Higgs mass, and remains at a few fb level throughout. This provides a promising

possibility to probe scenarios with $m_{H^+} > 150$ GeV, which is almost impossible with other channels studied in the literature.

We have specifically considered a few benchmark points with m_{H^+} ranging from 80 GeV to 500 GeV. The effect of systematics are included through an assumed 1% and 10% uncertainties on the background and signal events. The best case scenarios are the cases with m_{H^+} around 200 - 400 GeV, which could be probed at the LHC with about 3000 fb^{-1} integrated luminosity with a signal significance of about 2 for $m_{H^+} = 200$ GeV, and slightly lower, but still better than one for the larger mass regions. For higher mass case of $m_{H^+} = 500$ GeV, the significance is smaller than one, and cases with m_{H^+} beyond this range are harder to probe even at such high luminosity. The low mass scenarios with $m_{H^+} = 80$ GeV is also very difficult, mainly owing to the fact that the jets arising from these are too soft, and hard to isolate from the QCD background.

In summary, it is clear that probing $2j+MET$ provides good handle on the search for inert doublet scalars at LHC, and complements search through other leptonic channels. For scenarios like intermediate range of charged Higgs mass, this channel adds to other searches through leptonic and semi-leptonic channels. For larger mass range, where the leptonic channels become inefficient, the dijet plus missing energy channel discussed here proves to be an effective probe mechanism, albeit with the need of large luminosity of the order of 3000 fb^{-1}.

Chapter 4

Lepton Portal Limit of Inert Higgs Doublet Dark Matter with Radiative Neutrino Mass

In this chapter, we make an attempt to explain DM and non-zero neutrino mass in a single framework. For this, we extend the IHDM by adding 3 copies of right handed neutrinos and 3 copies of vector like leptons. With tiny Higgs-DM coupling, we explain correct dark matter relic abundance by suitably choosing other parameters available in the model. Also we highlight the modifications in the collider phenomenology in this model compared to pure IHDM.

The observational evidence suggesting the presence of DM in the Universe are irrefutable, with the latest data from the Planck experiment [112] indicating that approximately 27% of the present Universe is composed of dark matter. The observed abundance of DM is usually represented in terms of density parameter Ω as[8]

$$\Omega_{\rm DM}h^2 = 0.1187 \pm 0.0017 \tag{4.1}$$

where h = (Hubble Parameter)/100 is a parameter of order unity. In spite of astrophysical and cosmological evidences confirming the presence of DM, the fundamental nature of DM is not yet known. Since none of the particles in the SM can fulfil the criteria of a DM candidate, several BSM proposals have been put forward in the last few decades. Among them, the weakly interacting massive particle (WIMP)

[8]The current value of $\Omega_{\rm DM}h^2$ is 0.120 ± 0.001 [113]. This will not affect much to our analysis.

paradigm is the most popular one. Such WIMP dark matter candidates can interact with the SM particles through weak interactions and hence can be produced at the LHC or can scatter off nuclei at dark matter direct detection experiments like the ongoing LUX [128] and PandaX-II experiment [129].

Among different BSM proposals to incorporate dark matter, the IHDM [85, 130, 131] is one of the simplest extensions of the SM with an additional scalar field transforming as doublet under $SU(2)$ and having hypercharge $Y = 1$, odd under an imposed Z_2 discrete symmetry. As shown by the earlier works on IHDM, there are typically two mass ranges of DM mass satisfying the correct relic abundance criteria: one below the W boson mass and the other around 550 GeV or above. Among these, the low mass regime is particularly interesting due to stronger direct detection bounds. For example, the latest data from the LUX experiment rules out DM-nucleon spin independent cross section above around 2.2×10^{-46} cm^2 for DM mass of around 50 GeV [128]. In this mass range, as we discuss in details below, the tree level DM-SM interaction through the SM Higgs (h) portal is interesting as it can simultaneously control the relic abundance as well as the DM-nucleon scattering cross section. In this mass range, only a narrow region near the resonance $m_{\rm DM} \approx m_h/2$ is currently allowed by the LUX data. Though future DM direct detection experiments will be able to probe this region further, it could also be true that the DM-Higgs interaction is indeed too tiny to be observed at experiments. Such a tiny Higgs portal interaction will also be insufficient to produce the correct relic abundance of DM in this low mass regime. This almost rules out the low mass regime of DM in IHDM $m_{\rm DM} \lessapprox 70$ GeV.

Here we consider a simple extension of IHDM by singlet leptons (both neutral and charged) odd under the Z_2 symmetry such that the inert scalar dark matter can interact with the SM particles through these singlet leptons. This new interaction through lepton portal can revive the low mass regime of inert scalar DM even if future direct detection experiment rules out the Higgs portal interaction completely. The lepton portal interactions can also remain unconstrained from the limits on DM-nucleon interactions. Such a scenario is particularly interesting if LHC finds some signatures corresponding to the low mass regime of inert scalar DM while the direct detection continues to give null results. The dominant lepton portal interactions can explain correct relic abundance, null results at direct detection experiments and also give rise to interesting signatures at colliders. The neutral leptons added to IHDM can also give rise to tiny neutrino masses at one-loop level through scotogenic fashion [73]. We discuss the constraints on the model parameters from neutrino mass, DM

constraints and also make some estimates of some interesting collider signatures while comparing them with the pure IHDM.

This chapter is organised as follows. In Section 4.1, we discuss the lepton portal extension of IHDM. In Section 4.2, we discuss the dark matter related studies followed by our collider estimates in Section 4.3. We finally conclude in Section 4.4.

4.1 Lepton Portal Extensions of IHDM

As discussed earlier, considering lepton portal extensions of IHDM is very well motivated, specially from the origin of neutrino mass, DM direct detections and other flavour physics observables in the lepton sector. The inert Higgs doublet of the IHDM can couple to the SM leptons, if the model is suitably extended either by Z_2 odd neutral Majorana fermions or by charged vector like leptons, none of which introduce any chiral anomalies. The addition of three copies of neutral heavy singlet

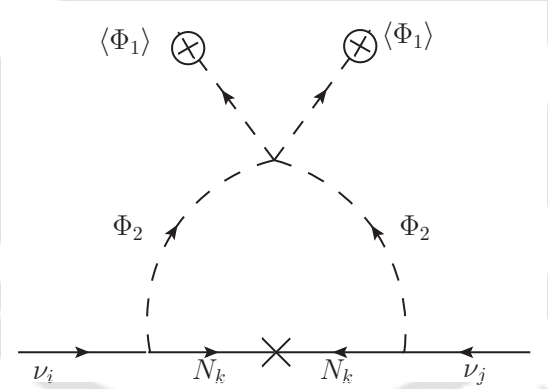

Figure 4.1: One-loop contribution to neutrino mass

fermions N_i, odd under the Z_2 symmetry leads to the upgradation of the IHDM to the scotogenic model [73]. Apart from providing another DM candidate in terms of the lightest N_i, the model also can explain tiny neutrino masses at one loop level. In the set up we study here, all of these singlet neutral fermions are assumed to be heavier than the neutral component of the inert Higgs doublet and hence our DM analysis is confined to the scalar DM only. The relevant interaction terms of these singlet fermions can be written as

$$\mathcal{L} \supset M_N NN + \Big((Y_N)_{ij}\, \bar{L}_i \tilde{\Phi}_2 N_j + \text{h.c.} \Big) \ . \tag{4.2}$$

The Feynman diagram for such one loop neutrino mass is shown in Figure 4.1. Using the expression from [73] of one loop neutrino mass

$$(m_\nu)_{ij} = \frac{(Y_N)_{ik}(Y_N)_{jk}M_k}{16\pi^2}\left(\frac{m_R^2}{m_R^2-M_k^2}\ln\frac{m_R^2}{M_k^2} - \frac{m_I^2}{m_I^2-M_k^2}\ln\frac{m_I^2}{M_k^2}\right) \tag{4.3}$$

Here $m_{R,I}^2 = m_{H,A}^2$ are the masses of scalar and pseudo-scalar part of Φ_2^0 and M_k the mass of singlet fermion N in the internal line. The index $i,j = 1,2,3$ runs over the three fermion generations as well as three copies of N. For $m_H^2 + m_A^2 \approx M_k^2$, the above expression can be simply written as

$$(m_\nu)_{ij} \approx \frac{\lambda_5 v^2}{32\pi^2}\frac{(Y_N)_{ik}(Y_N)_{jk}}{M_k} = \frac{m_A^2 - m_H^2}{32\pi^2}\frac{(Y_N)_{ik}(Y_N)_{jk}}{M_k} \tag{4.4}$$

In this model for the neutrino mass to match with experimentally observed limits (~ 0.1 eV), very tiny Yukawa couplings are required for the right handed neutrino mass of order of 1 TeV. Taking the mass difference $m_A - m_H = m_{H^\pm} - m_H = 60$ GeV, we show the constraints on neutral singlet fermion mass and corresponding Yukawa coupling from correct neutrino mass requirement in Figure 4.2. It can be seen that for low mass regime of DM, the neutrino mass constraints force the Yukawa couplings to be smaller than 10^{-4}, too small to have any impact on dark matter relic abundance calculation, to be discussed below. These neutral fermions can also contribute to charged lepton flavour violation (LFV) at one loop involving $N, \Phi_2^\pm$. The LFV processes like $\mu \to e\gamma$ remain suppressed in the SM due to the smallness of neutrino masses. Such LFV decays like $\mu \to e\gamma$ are being searched for at experiments like MEG [132]. The latest bound from the MEG collaboration is $\mathrm{BR}(\mu \to e\gamma) < 4.2 \times 10^{-13}$ at 90% confidence level [132]. However, due to small Yukawa couplings, as required by tiny neutrino mass constraints discussed above, keeps this new contribution to $\mu \to e\gamma$ way below this latest experimental bound, as discussed in the recent works [133, 134].

Similar to neutral singlet fermions, one can also incorporate charged singlet leptons $\chi_{L,R}$ with hypercharge $Y = -2$ and odd under the Z_2 symmetry. The relevant Lagrangian is

$$\mathcal{L} \supset M_\chi \bar{\chi}_L \chi_R + (Y_\chi)_{ij}\, \bar{L}_i \Phi_2 \chi_{R_j} + \text{h.c.} \tag{4.5}$$

These leptons can contribute both to DM relic abundance as well as LFV decays mentioned above. Since the corresponding Yukawa couplings are not restricted to be small from neutrino mass constraints, they can be sizeable and hence play a non-trivial role in generating DM relic abundance as we discuss below. Such large

Yukawa couplings can however give a large contribution to LFV decays like $\mu \to e\gamma$, with χ, Φ_2^0 in loop. As shown in a recent work [135], the above MEG bound can constrain the product of two relevant Yukawa couplings to be below 10^{-9} for χ mass around 100 GeV-1 TeV, too small to have any impact on DM relic abundance. These strict bounds from MEG can however be evaded by choosing diagonal structure of singlet lepton mass matrix M_χ and relevant Yukawa coupling Y. Such a structure can still have non-trivial impact on DM relic abundance, to be discussed below.

Although the addition of singlet fermions in this fashion may appear ad-hoc, they have very interesting phenomenological consequences as we discuss below. From UV completeness point of view, such low energy set up can in principle, be realised within well motivated BSM frameworks. For example, such exotic fermions can be realised within E_6 grand unified theories [136]. In the recent work [135], within the framework of left-right symmetric model it was shown that gauge singlet vector like fermions are necessary in order to generate all charged fermion masses through a common universal seesaw. The vector like charged leptons in the model discussed by [135] can generate light charged lepton masses at tree level and light Dirac neutrino masses at one loop. Thus, the low energy effective theory we study in this chapter from phenomenological point of view can have very well motivated UV completions. In another recent work [137], within the framework of an $SU(6)/Sp(6)$ little Higgs model, it is discussed how the vector like fermions appear along with an extended scalar sector, stabilizing the Higgs mass at electroweak scale. Even if this model (similar to all little Higgs models) has its own cut off scale which is incompatible with a strict idea of UV completion, it can naturally accommodate the vector like fermions instead of including it in an ad-hoc manner.

4.2 Dark Matter

The relic abundance of a DM particle ψ which was in thermal equilibrium at some earlier epoch can be calculated by solving the Boltzmann equation

$$\frac{dn_\psi}{dt} + 3Hn_\psi = -\langle\sigma v\rangle(n_\psi^2 - (n_\psi^{\rm eqb})^2), \tag{4.6}$$

where n_ψ is the number density of the DM particle ψ and n_ψ^{eqb} is the number density when ψ was in thermal equilibrium. H is the Hubble expansion rate of the Universe and $\langle\sigma v\rangle$ is the thermally averaged annihilation cross section of the DM particle ψ. In terms of partial wave expansion $\langle\sigma v\rangle = a + bv^2$. Clearly, in the case of thermal

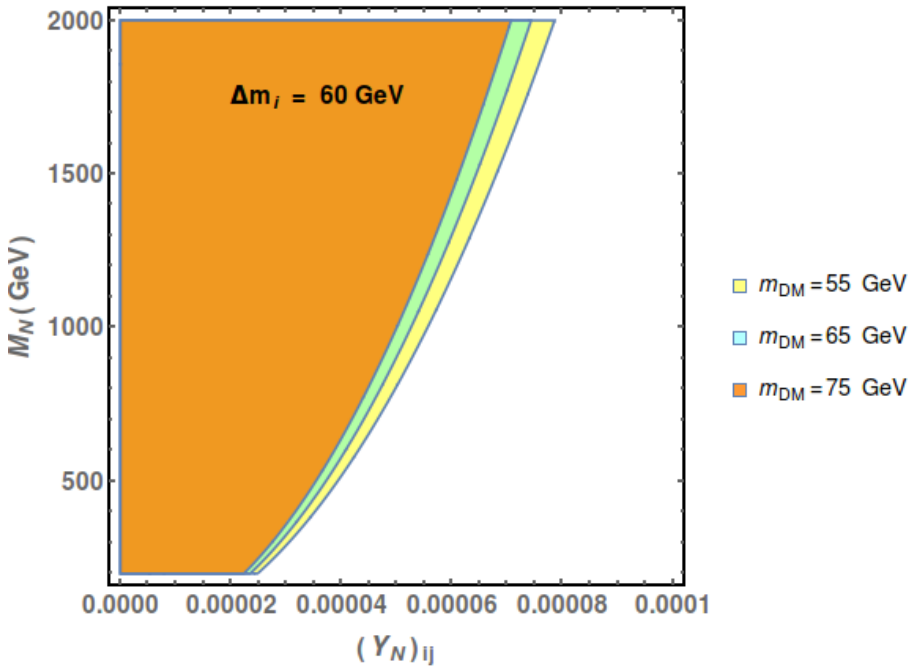

Figure 4.2: Allowed model parameters for neutrino mass generation

equilibrium $n_\psi = n_\psi^{\rm eqb}$, the number density is decreasing only by the expansion rate H of the Universe. The approximate analytical solution of the above Boltzmann equation gives [138, 139]

$$\Omega_\psi h^2 \approx \frac{1.04 \times 10^9 x_F}{M_{Pl}\sqrt{g_*}(a + 3b/x_F)}, \tag{4.7}$$

where $x_F = m_\psi/T_F$, T_F is the freeze-out temperature, g_* is the number of relativistic degrees of freedom at the time of freeze-out and $M_{Pl} \approx 10^{19}$ GeV is the Planck mass. Here, x_F can be calculated from the iterative relation

$$x_F = \ln \frac{0.038 g M_{\rm Pl} m_\psi < \sigma v >}{g_*^{1/2} x_F^{1/2}}. \tag{4.8}$$

The expression for relic density also has a more simplified form given as [140]

$$\Omega_\psi h^2 \approx \frac{3 \times 10^{-27} {\rm cm}^3 {\rm s}^{-1}}{\langle \sigma v \rangle}. \tag{4.9}$$

The thermal averaged annihilation cross section $\langle \sigma v \rangle$ is given by [141]

$$\langle \sigma v \rangle = \frac{1}{8 m_\psi^4 T K_2^2(m_\psi/T)} \int_{4m_\psi^2}^{\infty} \sigma(s - 4m_\psi^2)\sqrt{s} K_1(\sqrt{s}/T) ds, \tag{4.10}$$

where K_i's are modified Bessel functions of order i, m_ψ is the mass of DM particle and T is the temperature.

If we consider the neutral component of the scalar doublet Φ_2 to be the DM candidate, the details of relic abundance calculation is similar to the inert Higgs doublet model studied extensively in the literature [73, 85, 131, 142–146]. In the low mass regime $m_H = m_{DM} \leq m_W$, dark matter annihilation into the SM fermions through s-channel Higgs mediation dominates over other channels. As pointed out by [147], the DM annihilations $HH \to WW^* \to Wf\bar{f}'$ can also play a role in the $m_{DM} \leq m_W$ region. Also, depending on the mass differences $m_{H^+} - m_H, m_A - m_H$, the coannihilations of H, H^+ and H, A can also play a role in generating the relic abundance of DM. The relic abundance calculation incorporating these effects were studied by several groups in [148–150]. Beyond the W boson mass threshold, the annihilation channel of scalar doublet DM into W^+W^- pairs opens up suppressing the relic abundance below what is observed by Planck experiment, unless the DM mass is heavier than around 500 GeV, depending on the DM-Higgs coupling. Apart from the usual annihilation channels of inert doublet DM, in this model there is another interesting annihilation channel where dark matter annihilates into a pair of neutrinos (charged leptons) through the heavy fermion N_i (χ) in the t-channel.

Apart from the relic abundance constraints from Planck experiment, there exists strict bounds on the DM nucleon cross section from direct detection experiments like Xenon100 [151] and more recently LUX [128, 152, 153]. For scalar dark matter considered in this chapter, the relevant spin independent scattering cross section mediated by SM Higgs is given as [85]

$$\sigma_{\rm SI} = \frac{\lambda_L^2 f^2}{4\pi} \frac{\mu^2 m_n^2}{m_h^4 m_{DM}^2} \tag{4.11}$$

where $\mu = m_n m_{DM}/(m_n + m_{DM})$ is the DM-nucleon reduced mass and $\lambda_L = (\lambda_3 + \lambda_4 + \lambda_5)$ is the quartic coupling involved in DM-Higgs interaction. A recent estimate of the Higgs-nucleon coupling f gives $f = 0.32$ [154] although the full range of allowed values is $f = 0.26 - 0.63$ [155]. The latest LUX bound [128] on $\sigma_{\rm SI}$ constrains the DM-Higgs coupling λ_L significantly, if λ_L gives rise to most of the DM in the Universe. According to this latest bound, at a DM mass of 50 GeV, dark matter nucleon scattering cross sections above 1.1×10^{-46} cm^2 are excluded at 90% confidence level. Similar but slightly weaker bound has been reported by the PandaX-II experiment recently [129]. We however include only the LUX bound in our analysis. One can also constrain the DM-Higgs coupling λ_L from the latest LHC

constraint on the invisible decay width of the SM Higgs boson. This constraint is applicable only for DM mass $m_{DM} < m_h/2$. The invisible decay width is given by

$$\Gamma(h \to \text{Invisible}) = \frac{\lambda_L^2 v^2}{64\pi m_h}\sqrt{1 - 4\,m_{DM}^2/m_h^2} \tag{4.12}$$

The latest constraint on invisible Higgs decay is [125]

$$\text{BR}(h \to \text{Invisible}) = \frac{\Gamma(h \to \text{Invisible})}{\Gamma(h \to \text{Invisible}) + \Gamma(h \to \text{SM})} < 24\%$$

As we will discuss below, this bound is weaker than the LUX 2016 and XENON1T 2017 bound.

It should be noted that, there can be sizeable DM-nucleon scattering cross section at one loop level as well, which does not depend on the Higgs portal coupling discussed above. Even in the minimal IHDM such one loop scattering can occur with charged scalar and electroweak gauge bosons in loop [157]. The contributions of such one loop scattering can be kept even below future direct detection experiments like Xenon-1T by choosing large mass differences between the components of the inert scalar doublet [157]. Such large mass splittings also minimise the role of coannihilation between different inert scalar components on the DM relic abundance. This is in the spirit of the present chapter's motivation, as the DM abundance is primarily determined by the lepton portal couplings, rather than gauge and Higgs portal couplings. Another one loop scattering can occur, in principle, due to the exchange of photons or Z boson. This is possible through an effective coupling of the form $C\partial^\mu\Phi_2^0\partial^\nu\Phi_2^{0\dagger}F_{\mu\nu}$ with C being the loop factor [158]. However, since we have broken the degeneracy of our complex DM candidate Φ_2^0 and reduced it to one scalar and pseudo scalar, we can avoid such one loop scattering by choosing a mass splitting. In fact, one requires a non-zero mass splitting, at least greater than of the order of $\mathcal{O}(100$ keV), typical kinetic energy of DM particles, in order to avoid tree level inelastic scattering of DM off nuclei mediated by Z boson [159]. We implement the model in FeynRules [60]. The corresponding Feynrules code is given in the Appendix- A. After obtaining the model files compatible with micrOMEGA. We have used micrOMEGA 4.3.1 [160] to calculate the relic abundance of DM. We first reproduce the known results in IHDM by considering the neutral scalar H to be the DM candidate having mass below the W boson mass threshold. In the left panel of Figure 4.3, we first show the parameter space of pure IHDM in $\lambda_L - m_{DM}$ plane that satisfies the condition $\Omega_{\rm DM}h^2 \leq 0.1187$. We have taken both the mass

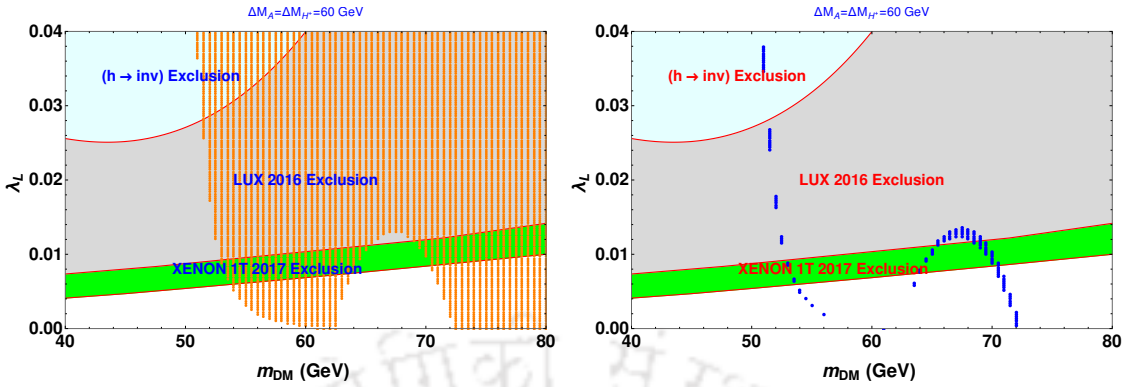

Figure 4.3: Parameter space in the $\lambda_L - m_{DM}$ plane giving rise to dark matter relic abundance $\Omega_{\rm DM}h^2 \leq 0.1187$ (left panel) and $\Omega_{\rm DM}h^2 \in 0.1187 \pm 0.0017$ (right panel) in pure IHDM. The points those lying below the second horizontal line are allowed points.

difference $m_A - m_H = m_{H^\pm} - m_H = 60$ GeV as a typical benchmark value satisfying all other constraints. Such a large benchmark point reduces the coannihilation effects and show the dependence of relic abundance on Higgs portal coupling λ_L in a visible manner.[9] The blue region in the left panel of Figure 4.3 therefore indicates the parameter space where the DM annihilation is either just enough or more than the required one to produce the correct relic abundance. Therefore, considering the additional lepton portal couplings for such values of λ_L will further suppress the relic abundance. Therefore, we choose benchmark values of $\lambda_L - m_{DM}$ for our next analysis, from that region of this plot which overproduces the DM in pure IHDM, so that an efficient lepton portal annihilation can bring down the relic abundance to the observed range. In the right panel of Figure 4.3, we further impose the relic abundance criteria $\Omega_{\rm DM}h^2 \in 0.1187 \pm 0.0017$ which reduces the number of allowed points significantly from the one in the left panel. In both the plots we also show the LUX-2016 and XENON1T (2017) exclusion line based on the upper bound on DM nucleon scattering cross section. We also show the LHC limit on Higgs invisible decay width which remains weaker than the LUX-2016 and XENON1T (2017) bound. The tiny allowed region near $m_{\rm DM} \approx m_h/2$ corresponds to the s-channel resonance mediated by the SM Higgs while the allowed region of $m_{\rm DM}$ close to W boson mass threshold corresponds to the dominance of DM annihilation into three body SM final states mentioned above.

After reproducing the known results of IHDM in the low mass regime for a benchmark value of mass splitting, we calculate the DM relic abundance by incorporating

[9] We have not considered low mass differences in this work as that will make the coannihilations more efficient reducing the dependence of relic abundance on Higgs or lepton portal couplings and here our main motivation is to show the importance of lepton portal couplings.

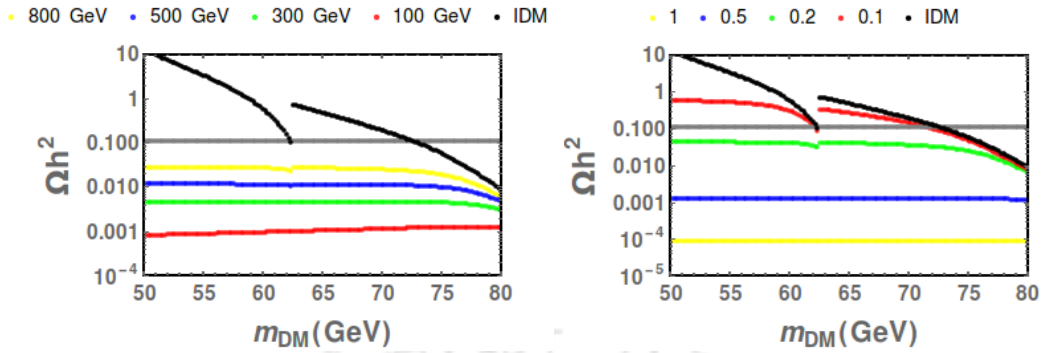

Figure 4.4: Effect of lepton portal couplings on dark matter relic abundance, for specific dark matter Higgs coupling λ_L. Left : Relic density vs. m_{DM} for different M_N with fixed $Y_N = 0.2$. Right : Relic density vs. m_{DM} for different Y_N with fixed M_N=1000 GeV.

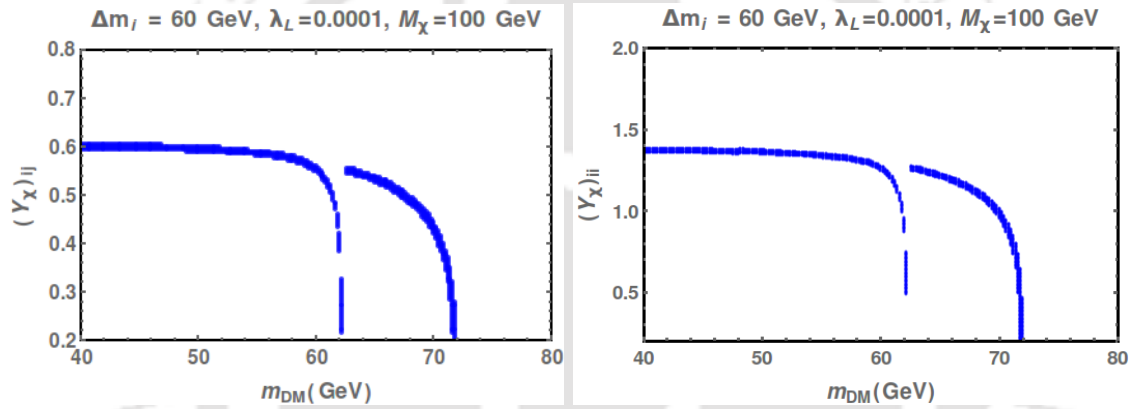

Figure 4.5: Parameter space in the $Y_\chi - m_{DM}$ plane giving rise to the correct dark matter relic abundance with 3σ range for specific choice of $\lambda_L = 0.0001$ and $M_\chi = 100$ GeV. Left : nonzero off-diagonal Yukawa coupling scenario, Right : Diagonal Yukawa coupling scenario.

the Z_2 odd heavy leptons. In Figure 4.4, we show the effect of vector like neutral heavy leptons on relic abundance. To make DM annihilations through lepton portal more efficient, we choose the Higgs portal coupling to be very small $\lambda_L = 0.0001$ and also keep both the mass splitting within the components of the inert scalar doublet as 60 GeV like before. In the left panel of Figure 4.4, the effect of heavy neutral fermion mass on the relic abundance is shown for a fixed value of Yukawa coupling $Y_N = 0.2$. In the right panel of Figure 4.4, the effect of lepton portal Yukawa couplings on DM relic abundance is shown for fixed value of heavy neutral fermion mass $M_N = 1000$ GeV. From both these panels of Figure 4.4, it is clear that the leptonic portal can play a non-trivial role in generating the DM relic abundance. While the benchmark values of Higgs portal coupling and mass splitting chosen above produce correct DM abundance only for two different masses, the introduction of lepton por-

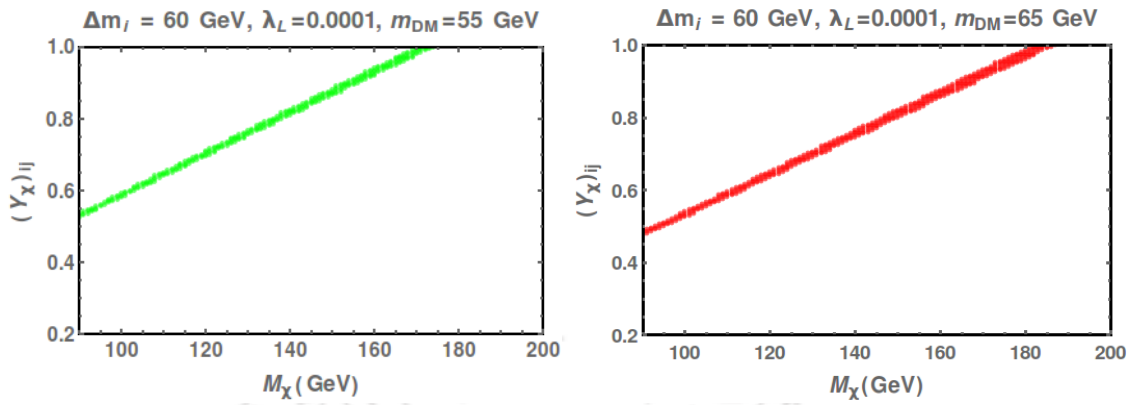

Figure 4.6: Parameter space in the $Y_\chi - M_\chi$ plane giving rise to the correct dark matter relic abundance with 3σ range for specific choice of $\lambda_L = 0.0001$ and m_{DM} for nonzero off-diagonal Yukawa coupling scenario. Left : for m_{DM}= 55 GeV, Right : for m_{DM}= 65 GeV.

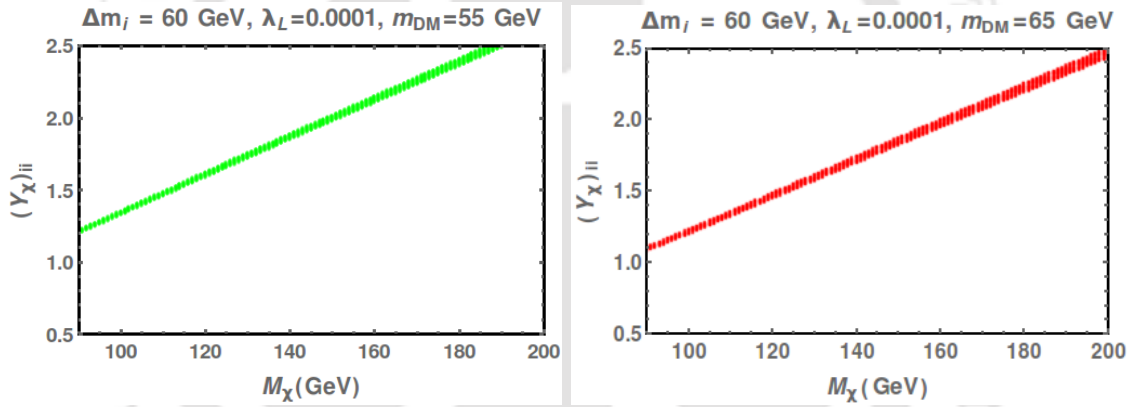

Figure 4.7: Parameter space in the $Y_\chi - M_\chi$ plane giving rise to the correct dark matter relic abundance with 3σ range for specific choice of $\lambda_L = 0.0001$ and m_{DM} for Diagonal Yukawa coupling scenario. Left : for m_{DM}= 55 GeV, Right : for m_{DM}= 65 GeV.

tal can result in new allowed region of DM masses. As expected, the maximum effect of lepton portal on DM relic abundance occurs for smaller values of heavy lepton mass or equivalently large values of Yukawa couplings. Since neutral heavy fermion couplings with SM leptons are required to be tiny from neutrino mass constraints as can be seen from Figure 4.2, we consider only the effect of heavy charged leptons on DM relic abundance. The effect of charged lepton portal on DM relic abundance will be similar to that of neutral case discussed above.

After showing the effect of lepton portal on DM relic abundance for specific values of Yukawa and heavy neutral fermion masses, we do a general scan of these two parameters from the requirement of generating correct abundance. Since neutral heavy fermion portal is not efficient after neutrino mass constraints are incorporated, we

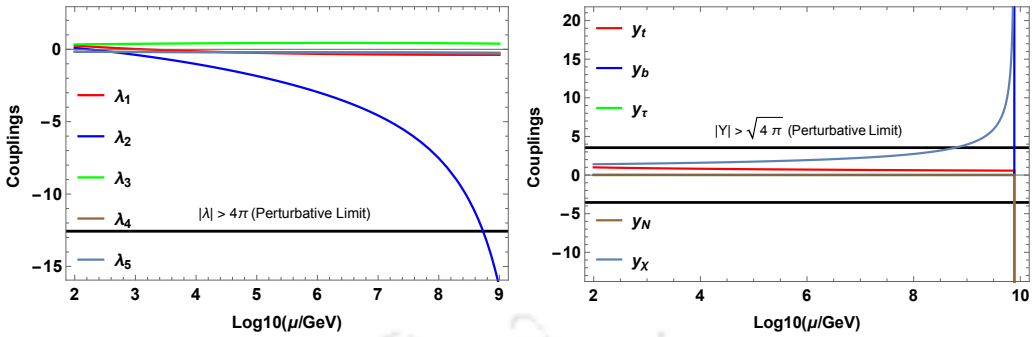

Figure 4.8: Evolution of quartic (left panel) and Yukawa (right panel) couplings under RGE. The benchmark values chosen at low energy which satisfy all relevant constraints are $m_{DM} = 55$ GeV, $m_A = m_{H^+} = 115$ GeV, $\lambda_L = 0.0001, \lambda_1 = 0.258, \lambda_2 = 0.1, \lambda_3 = 0.338, \lambda_4 = \lambda_5 = -0.1685$.

do the general scan only for charged heavy lepton portal here. In Figure 4.5, we show the allowed parameter space satisfying relic density in the $Y_\chi - m_{DM}$ plane for a benchmark point of IHDM parameters like before and taking the heavy charged fermion mass to be 100 GeV. The left panel of Figure 4.5 considers the lepton portal couplings to be of general non-diagonal type while the right panel considers the couplings to be diagonal. As discussed before, such diagonal couplings will evade the constraints from LFV decay. Since a diagonal structure of Yukawa couplings reduces the total number of annihilation channels, one requires larger values of Yukawa couplings to produce the correct relic abundance, compared to the ones in the non-diagonal case. In Figure 4.6, we show the allowed parameter space in $Y_\chi - M_\chi$ plane for two specific dark matter masses $m_{DM} = 55, 65$ GeV with general non-diagonal Yukawa couplings. The corresponding result for diagonal Yukawa couplings are shown in Figure 4.7. It should be noted that these two benchmark values of DM masses in pure IHDM can not give rise to correct relic abundance for small values of Higgs portal couplings as seen from Figure 4.3. However, after allowing the lepton portal couplings, we can generate correct relic abundance for such values of DM masses which remain disallowed in the pure IHDM.

The large lepton portal Yukawa couplings of order one required for giving correct relic abundance of dark matter can have serious implications for the renormalisation group evolution (RGE) of the quartic couplings of the scalar potential. Several works have appeared in the literature studying the implications of vector like fermions on the RGE of couplings some of which can be found in [169–171]. Using the RGE equations for the IHDM given in [83] and extending it by three copies of vector like charged leptons we study the evolution of different parameters of the model. The

RGE equations used in our numerical analysis are given in Appendix B. We choose benchmark values of couplings at low energy that satisfy all relevant constraints. We consider $m_{DM} = 55$ GeV, $m_A = m_{H^+} = 115$ GeV, $\lambda_L = 0.0001, \lambda_1 = 0.258, \lambda_2 = 0.1, \lambda_3 = 0.338, \lambda_4 = \lambda_5 = -0.1685$ with the Higgs boson mass being kept at 125 GeV. The vector like charged lepton mass is 100 GeV with the corresponding Yukawa coupling being $Y_\chi = 1.4$. The neutral heavy fermion mass is also kept at 100 GeV with the corresponding Yukawa couplings being fixed to 0.001. The evolution of the quartic and the Yukawa couplings with energy μ is shown in Figure 4.8. It can be seen that some of the Yukawa couplings including the one involving vector like charged leptons χ become non-perturbative around $\mu \approx 10^9$ GeV implying that some new dynamics should take over at that energy scale. This is due to the large value of Yukawa coupling between χ and Φ_2 chosen at low energy scale. The same non-perturbative nature is also seen in quartic coupling λ_2 around $\mu \approx 10^9$ GeV. Due to the coupled nature of the RGE equations, all other couplings including quartic and gauge also become non-perturbative beyond $\mu \approx 10^{10}$ GeV.

From Figure 4.8, it can be seen that λ_1 and λ_2 are going to negative. So, stability of vacuum is a concern here. However, the stability is possible with suitable modification of the model we considered here.

4.3 Collider Implications

In pure IHDM, the pseudo scalar A can decay into Z and H whereas $H^\pm$ can decay to either $W^\pm H$ or $W^\pm A$. When $m_{H^\pm}$ is close to m_A, then the first decay mode of $H^\pm$ almost dominates. Depending upon the decay mode of $W^\pm$ and Z, we have either pure leptonic plus MET or hadronic plus MET or mixed final states from pair production of the inert scalars. Earlier studies in the IHDM [97, 98, 161] focused on pair production of inert scalars and their decays into leptons and MET. In another recent work [162], the authors studied dijet plus MET final states in the context of IHDM at LHC. The dilepton plus dijet plus MET and trilepton plus MET final states have also been studied in a recent work [163]. The 8 TeV constraints and 13 TeV projection from monojet plus MET are discussed in another work [164].

In the presence of both Z_2 odd neutral and charged vector like leptons, additional channels open up. For example, now $H^\pm$ can decay to $\chi^\pm\ \nu_i$ or $N_i\ l^\pm$. Similarly, A can decay into $l^\pm\ \chi^\mp$ or $N_i\ \bar{\nu}_i$. Since neutrino mass constraints push the mass of neutral leptons typically to the order of TeV range, both $H^\pm$ and A will mainly decay through charged vector like leptons (VLL) $\chi^\pm$. Then $\chi^\pm$ will further decay into

$l^{\pm}H$. One can find earlier studies in the context of vector like leptons in references [165–169]. To highlight the difference in collider signatures with comparison to pure IHDM, we have considered a few benchmark points. We choose the following benchmark points all of which correspond to the fixed values of m_h = 125 GeV, λ_L = 0.0001 , λ_2 = 0.1, M_N=1000 GeV, Y_N=0.001.

BP1: m_H = 55 GeV, $m_{H^+} = m_A$ = 115 GeV, M_χ=100 GeV, $(Y_\chi)_{ii}$=1.5
BP2: m_H = 65 GeV, $m_{H^+} = m_A$ = 125 GeV, M_χ=100 GeV, $(Y_\chi)_{ii}$=1.5
BP3: m_H = 65 GeV, $m_{H^+} = m_A$ = 200 GeV, M_χ=150 GeV, $(Y_\chi)_{ii}$=2.0
BP4: m_H = 65 GeV, $m_{H^+} = m_A$ = 300 GeV, M_χ=150 GeV, $(Y_\chi)_{ii}$=2.0.

In Table 4.1, we have listed the parton level cross sections for final states that contribute to dilepton+MET final states at detector level in both IHDM and IHDM+VLL models for the above benchmark points. It should be noted that for BP1 and BP2, $H^{\pm}$ will go through off-shell decay that is, $H^{\pm} \to W^{*\pm}H$ with $W^{*\pm}$ decaying leptonically in pure IHDM case due to limited phase space availability. But for BP3 and BP4, $H^{\pm}$ will go through on-shell decay that is, $H^{\pm} \to W^{\pm}H$ with $W^{\pm}$ decaying leptonically in pure IHDM case. In IHDM+VLL model, $H^{\pm}$ will decay to $\chi^{\pm}$ that is, $H^{\pm} \to \chi^{\pm}\ \nu_l$ with $\chi^{\pm}$ further decaying into $l^{\pm}H$. It is clearly evident from this table that we have enhancement of the cross section in IHDM+VLL due to opening of new decay modes of $H^{\pm}$. We must highlight one point that it is very difficult to probe heavier charged Higgs mass (like the ones in BP3 and BP4) in pure IHDM case due to small cross section. But in the IHDM+VLL model discussed here, we have sufficient cross section to probe these heavier masses of charged Higgs. Apart from the channels listed in Table 4.1, there is another process which contributes to dilepton plus MET final states that is $\chi^+\chi^-$ production with $\chi^{\pm}$ decays to $l^{\pm}H$. So as a whole, the dilepton plus MET final state will be an important collider signature to probe the modified IHDM that we discussed in this chapter.

4.4 Conclusion

We have studied a very specific region of parameter space in IHDM where the Higgs portal coupling of DM is very small, as suggested by null results in dark matter direct detection experiments so far. In the low mass regime of DM that is $m_{DM} < m_W$, such small value of Higgs portal coupling λ_L may not be sufficient to produce the correct relic abundance of DM except for a few specific values of m_{DM}.

We have then extended this model by heavy neutral and charged leptons which

Benchmark	$\sigma(pp \to H^+H^- \to 2l + 2\nu + 2H)$(in fb)	
Points	IHDM	IHDM+VLL
BP1	8.1	126
BP2	6.1	93.5
BP3	1.7	13.8
BP4	0.3	2.1

Table 4.1: The parton level cross section for final states that contribute to dilepton+MET final states at detector level in both IHDM and IHDM+VLL models at the LHC ($\sqrt{s} = 14$ TeV) for different BPs considered.

are also odd under the Z_2 symmetry of the IHDM. These heavy leptons can be motivating from neutrino mass as well as LHC phenomenology point of view, apart from their role in producing the correct DM relic abundance in those region of parameter space which can not produce correct relic in pure IHDM. The neutral heavy fermions can generate tiny neutrino masses at one loop level via scotogenic mechanism, requiring the corresponding Yukawa couplings to be small ($< 10^{-4}$) for TeV scale heavy neutral fermion masses. This kept the contribution of neutral heavy leptons to DM abundance suppressed. The heavy charged fermion couplings to DM are however, not constrained to be tiny from neutrino mass point of view and hence can be sizeable enough to play a role in DM abundance. We have showed that the entire low mass regime of IHDM is allowed from relic abundance criteria if the lepton portal parameters are suitably chosen. This did not affected the DM direct detection scattering rates as there are no tree level or one loop couplings of DM with nuclei through leptons. The heavy leptons can also give rise to observable LFV decay rates like $\mu \to e\gamma$ as well as interesting collider signatures like dilepton plus missing energy. Although for simplicity, we have choosen particular type of Yukawa structure which does not contribute to LFV decay rates, it is in principle possible to choose some structure of the Yukawa couplings which can simultaneously produce correct DM abundance as well as keep the decay rate of LFV decays like $\mu \to e\gamma$ within experimental reach. We have checked the evolution of different couplings of the model under RGE and find that the model remains perturbative all the way upto around 10^9 GeV. Due to the requirement of large order one Yukawa coupling to keep the lepton portal annihilation of dark matter more efficient, different couplings of the model receive large corrections from RGE leading to non-perturbative nature at high energy scale.

We have also showed how the lepton portal extension of IHDM enhances dilepton

plus missing energy signals at the LHC, for chosen benchmark points. There can also be lepton number violating signal like same sign dilepton plus dijet plus missing energy in this model, but remain suppressed for the benchmark values chosen in our analysis.

Chapter 5

Summary and Conclusions

In this chapter, we summarize all the studies carried out in the thesis.

The discovery of Higgs boson by ATLAS and CMS in 2012 completes the particle spectrum of the SM. It is widely believed that SM is the most successful theory in terms of explaining elementary particles and their interactions. Despite its numerous successes, it is far from being the ultimate theory of nature, and there are many issues to be addressed. For example, SM is unable to explain non-zero neutrino mass, hierarchy problem, dark matter, matter-antimatter asymmetry.

To explain the unsolved issues one has to go beyond the SM. Out of many possible alternatives, the multi-Higgs models receive lot of attentions among particle physics community after the Higgs discovery. Because, one can still accommodate the observed Higgs in multi-Higgs models satisfying all theoretical and experimental constraints. One main feature of such scenarios is the presence of additional scalar degrees of freedom. To probe the additional Higgs bosons is one of the main interests of the phenomenologists as well as of the experimentalists.

In Chapter 1, SM of particle physics is discussed along with its difficulties. Then, we have mentioned some of the BSM approaches, aiming to explain these difficulties. Further, 2HDM is discussed in great detail along with its inert version. In the end, we have sketched the content of the remaining chapters.

In Chapter 2, we have explored collider signatures of the additional scalars of the multi-Higgs models in model independent way. For this, we have focused on the cascade decay of a heavy Higgs boson in the model with masses up to TeV range. We have considered two possible final states signatures i.e. four charged leptons and two b-jets or of four b-jets and two charged leptons. We have performed a signal versus background study and showed that indeed a 5σ discovery is possible

for various combinations of the parent and daughter Higgs boson masses. In the end, we have translated the model independent results to Type-II 2HDM and identified the regions of parameter space to which 14 TeV LHC is sensitive.

In Chapter 3, we have studied the signatures of the inert version of the 2HDM through the dijet final state along with large missing transverse energy. Our main aim was to probe heavier masses of charged Higgs bosons which is impossible via leptonic and semi-leptonic final states discussed in the literature. We have performed the analysis through selected BPs satisfying all the DM and relevant collider constraints. Performing a detailed analysis of the signal events against the background events, it is found that indeed a charged Higgs of mass around 200 GeV is possible to probe with a signal significance about 2σ at an integrated luminosity about $3000 fb^{-1}$.

In Chapter 4, we have explored a possible scenario which would address both the dark matter problem and the generation of tiny neutrino mass with minimal extensions of the IHDM with relevant fermionic degrees of freedom. Considering the neutral scalar of inert Higgs doublet as the dark matter candidate and assuming tiny Higgs-DM coupling, we demonstrated that it is possible to obtain correct relic abundance by tuning the lepton portal couplings. Also, it is noticed that we can probe heavier charged Higgs in this model compared to that of pure IHDM due to the presence of these additional leptons. We have presented the summary of all the works of this thesis in the Chapter 5.

In summary, we have focused on probing the additional scalars of some simplest multi-Higgs models. We hope, the analysis performed in the thesis will be helpful to the particle physics community. Especially, the experimental colleagues can adopt the strategies developed in the thesis to probe BSM scenarios related to multi-Higgs models more effectively.

Appendix A

Feynrules Model File used in Chapter 4

```
(*************************************************************)
(*This is the FeynRules mod-file for
****3 Neutral VLLs and 3 Charged VLLs**)
(******                                                ******)
******   We will use this model file together with
******   Inert Higgs Doublet Model file                ******)
******                                                ******)
(*************************************************************)
(**********************)
(***  VLLN Part ***)
(**********************)
(*External Parameters , neutral Vector-like lepton *)
M$ExtPrmVLL = {
ye1 == {
          TeX -> Subscript[y,e1],
          ParameterType -> External,
          InteractionOrder -> {NP,1},
          BlockName     -> VLL,
          ComplexParameter -> True,
          Value -> 1 ,
          Description -> "N1  -Darkmatter - left Handed SM
                          electron coupling"
       },
```

```
ye2 == {
          TeX -> Subscript[y,e2],
          ParameterType -> External,
          InteractionOrder -> {NP,1},
          BlockName     -> VLL,
          ComplexParameter -> True,
          Value -> 1 ,
          Description -> "N2  -Darkmatter - left Handed SM
                          electron coupling"
       },
ye3 == {
          TeX -> Subscript[y,e3],
          ParameterType -> External,
          InteractionOrder -> {NP,1},
          BlockName     -> VLL,
          ComplexParameter -> True,
          Value -> 1 ,
   Description -> "N3  -Darkmatter - left Handed SM
                   electron coupling"
       },
ym1 == {
          TeX -> Subscript[y,m1],
          ParameterType -> External,
          InteractionOrder -> {NP,1},
          BlockName     -> VLL,
          ComplexParameter -> True,
          Value -> 1 ,
          Description -> "N1  -Darkmatter - left Handed SM
                          muon coupling"
       },
ym2 == {
          TeX -> Subscript[y,m2],
          ParameterType -> External,
          InteractionOrder -> {NP,1},
          BlockName     -> VLL,
          ComplexParameter -> True,
```

```
          Value -> 1 ,
          Description -> "N2  -Darkmatter - left Handed SM
                          muon coupling"
       },

ym3 == {
          TeX -> Subscript[y,m3],
          ParameterType -> External,
          InteractionOrder -> {NP,1},
          BlockName     -> VLL,
          ComplexParameter -> True,
          Value -> 1 ,
          Description -> "N3  -Darkmatter - left Handed SM
                          muon coupling"
       },

yt1 == {
          TeX -> Subscript[y,t1],
          ParameterType -> External,
          InteractionOrder -> {NP,1},
          BlockName     -> VLL,
          ComplexParameter -> True,
          Value -> 1 ,
          Description -> "N1  -Darkmatter - left Handed SM
                          tau coupling"
       },

yt2 == {
          TeX -> Subscript[y,t2],
          ParameterType -> External,
          InteractionOrder -> {NP,1},
          BlockName     -> VLL,
          ComplexParameter -> True,
          Value -> 1 ,
          Description -> "N2  -Darkmatter - left Handed SM
                          tau coupling"
```

```
        },

yt3 == {
           TeX -> Subscript[y,t3],
           ParameterType -> External,
           InteractionOrder -> {NP,1},
           BlockName     -> VLL,
           ComplexParameter -> True,
           Value -> 1 ,
           Description -> "N3  -Darkmatter - left Handed SM
                           tau coupling"
        },
(*External Parameters , Charged Vector-like lepton *)
ye1lp == {
           TeX -> Subscript[ye1,VL1],
           ParameterType -> External,
           InteractionOrder -> {NP,1},
           BlockName     -> VLL,
           ComplexParameter -> True,
           Value -> 1 ,
           Description -> "VLL1  -Darkmatter - left Handed SM
                           electron coupling"
        },
 ye2lp == {
           TeX -> Subscript[ye2,VL2],
           ParameterType -> External,
           InteractionOrder -> {NP,1},
           BlockName     -> VLL,
           ComplexParameter -> True,
           Value -> 1 ,
           Description -> "VLL2  -Darkmatter - left Handed SM
                           electron coupling"
        },

 ye3lp == {
           TeX -> Subscript[ye3,VL3],
```

```
          ParameterType -> External,
          InteractionOrder -> {NP,1},
          BlockName     -> VLL,
          ComplexParameter -> True,
          Value -> 1 ,
          Description -> "VLL3  -Darkmatter - left Handed SM
                          electron coupling"
       },

ym1lp == {
          TeX -> Subscript[ym1,VL1],
          ParameterType -> External,
          InteractionOrder -> {NP,1},
          BlockName     -> VLL,
          ComplexParameter -> True,
          Value -> 1 ,
          Description -> "VLL1  -Darkmatter - left Handed SM
                          muon coupling"
       },
 ym2lp == {
          TeX -> Subscript[ym2,VL2],
          ParameterType -> External,
          InteractionOrder -> {NP,1},
          BlockName     -> VLL,
          ComplexParameter -> True,
          Value -> 1 ,
          Description -> "VLL2  -Darkmatter - left Handed SM
                          muon coupling"
       },

 ym3lp == {
          TeX -> Subscript[ym3,VL3],
          ParameterType -> External,
          InteractionOrder -> {NP,1},
          BlockName     -> VLL,
          ComplexParameter -> True,
```

```
          Value -> 1 ,
          Description -> "VLL3  -Darkmatter - left Handed SM
                         electron coupling"
       },
 yt1lp == {
          TeX -> Subscript[yt1,VL1],
          ParameterType -> External,
          InteractionOrder -> {NP,1},
          BlockName     -> VLL,
          ComplexParameter -> True,
          Value -> 1 ,
          Description -> "VLL1  -Darkmatter - left Handed SM
                         tau coupling"
       },
 yt2lp == {
          TeX -> Subscript[yt2,VL2],
          ParameterType -> External,
          InteractionOrder -> {NP,1},
          BlockName     -> VLL,
          ComplexParameter -> True,
          Value -> 1 ,
          Description -> "VLL2  -Darkmatter - left Handed SM
                         tau coupling"
       },
yt3lp == {
          TeX -> Subscript[yt3,VL3],
          ParameterType -> External,
          InteractionOrder -> {NP,1},
          BlockName     -> VLL,
          ComplexParameter -> True,
          Value -> 1 ,
          Description -> "VLL3  -Darkmatter - left Handed SM
          tau coupling"
       }

        };
```

```
(************************************************************)
(* Neutral Vector-like leptons *)

M$VLLFields = {

F[5] == {
ClassName        -> N1,
SelfConjugate    -> True,
Mass             -> {MN1, 500},
Width            -> {WN1, 1},
PDG              -> 160002,
PropagatorLabel  -> {"N1"},
PropagatorType   -> Straight,
PropagatorArrow  -> Forward,
      FullName ->    {"N1-lepton"} },


 F[6] == {
ClassName        -> N2,
SelfConjugate    -> True,
Mass             -> {MN2, 600},
Width            -> {WN2, 1},
PDG              -> 160003,
PropagatorLabel  -> {"N2"},
PropagatorType   -> Straight,
PropagatorArrow  -> Forward,
       FullName ->    {"N2-lepton"} },

 F[7] == {
ClassName        -> N3,
SelfConjugate    -> True,
Mass             -> {MN3, 700},
Width            -> {WN3, 1},
PDG              -> 160004,
PropagatorLabel  -> {"N3"},
PropagatorType   -> Straight,
```

```
PropagatorArrow  -> Forward,
        FullName ->    {"N3-lepton"} } ,

 (* charged Vector-like leptons *)
 F[8] == {
ClassName        -> lp1,
SelfConjugate    -> False,
Mass             -> {Mlp1, 500},
Width            -> {Wlp1, 1},
QuantumNumbers   -> {Q-> -1},
PDG              -> 160005,
PropagatorLabel  -> {"lp1"},
PropagatorType   -> Straight,
PropagatorArrow  -> Forward,
        FullName ->    {"lp1-lepton"} },

 F[9] == {
ClassName        -> lp2,
SelfConjugate    -> False,
Mass             -> {Mlp2, 600},
Width            -> {Wlp2, 1},
QuantumNumbers   -> {Q-> -1},
PDG              -> 160006,
PropagatorLabel  -> {"lp2"},
PropagatorType   -> Straight,
PropagatorArrow  -> Forward,
        FullName ->    {"lp2-lepton"} },

 F[10] == {
ClassName        -> lp3,
SelfConjugate    -> False,
Mass             -> {Mlp3, 700},
Width            -> {Wlp3, 1},
QuantumNumbers   -> {Q-> -1},
PDG              -> 160007,
PropagatorLabel  -> {"lp3"},
```

```
PropagatorType   -> Straight,
PropagatorArrow  -> Forward,
        FullName ->    {"lp3-lepton"} }
};
(*************************************************************)
(* Inert doublet *)
(*Phi2 := {Hch, (H0 + I A0)/Sqrt[2]};
Phi2bar := {Hchbar, (H0 - I A0)/Sqrt[2]};*)
(*************************************************************)
(*Yukawa Interaction for Neutral VLL and Charged VLL *)
(* Neutral Case *)
 LNIntE := ye1(vebar.ProjP.N1 H0/Sqrt[2]- I vebar.ProjP.N1 A0/Sqrt[2]
        - ebar.ProjP.N1 Hchbar) + ye2(vebar.ProjP.N2 H0/Sqrt[2]
        - I vebar.ProjP.N2 A0/Sqrt[2] - ebar.ProjP.N2 Hchbar)
        + ye3 (vebar.ProjP.N3 H0/Sqrt[2] - I vebar.ProjP.N3 A0/Sqrt[2]
        - ebar.ProjP.N3 Hchbar) ;

 LNIntMu := ym1(vmbar.ProjP.N1 H0/Sqrt[2] - I vmbar.ProjP.N1 A0/Sqrt[2]
         - mbar.ProjP.N1 Hchbar) + ym2(vmbar.ProjP.N2 H0/Sqrt[2]
         - I vmbar.ProjP.N2 A0/Sqrt[2] - mbar.ProjP.N2 Hchbar)
         + ym3 (vmbar.ProjP.N3 H0/Sqrt[2] - I vmbar.ProjP.N3 A0/Sqrt[2]
         - mbar.ProjP.N3 Hchbar) ;

 LNIntTau := yt1(vtbar.ProjP.N1 H0/Sqrt[2] - I vtbar.ProjP.N1 A0/Sqrt[2]
          - tabar.ProjP.N1 Hchbar) + yt2 (vtbar.ProjP.N2 H0/Sqrt[2]
          - I vtbar.ProjP.N2 A0/Sqrt[2] - tabar.ProjP.N2 Hchbar)
          + yt3 (vtbar.ProjP.N3 H0/Sqrt[2] - I vtbar.ProjP.N3 A0/Sqrt[2]
          - tabar.ProjP.N3 Hchbar) ;
LNInt := LNIntE + LNIntMu + LNIntTau ;
(*Charged Case*)
LlpIntE := (ye1lp/Sqrt[2])(ebar.ProjP.lp1 H0 + I ebar.ProjP.lp1 A0)
        + ye1lp (vebar.ProjP.lp1 Hch)+(ye2lp/Sqrt[2]) (ebar.ProjP.lp2 H0
        + I ebar.ProjP.lp2 A0) + ye2lp (vebar.ProjP.lp2 Hch)
        + (ye3lp/Sqrt[2])(ebar.ProjP.lp3 H0 + I ebar.ProjP.lp3 A0)
        + ye3lp (vebar.ProjP.lp3 Hch);
```

```
LlpIntMu := (ym1lp/Sqrt[2])(mbar.ProjP.lp1 H0 + I mbar.ProjP.lp1 A0)
          + ym1lp (vmbar.ProjP.lp1 Hch) +(ym2lp/Sqrt[2])(mbar.ProjP.lp2 H0
          + I mbar.ProjP.lp2 A0) + ym2lp (vmbar.ProjP.lp2 Hch)
          + (ym3lp/Sqrt[2])(mbar.ProjP.lp3 H0 + I mbar.ProjP.lp3 A0)
          + ym3lp ( vmbar.ProjP.lp3 Hch );

LlpIntTau := (yt1lp/Sqrt[2])(tabar.ProjP.lp1 H0 + I tabar.ProjP.lp1 A0)
           + yt1lp(vtbar.ProjP.lp1 Hch)+(yt2lp/Sqrt[2])(tabar.ProjP.lp2 H0
           + I tabar.ProjP.lp2 A0) + yt2lp (vtbar.ProjP.lp2 Hch )
           + (yt3lp/Sqrt[2])(tabar.ProjP.lp3 H0 + I tabar.ProjP.lp3 A0)
           + yt3lp (vtbar.ProjP.lp3 Hch);
LlpInt  := LlpIntE +  LlpIntMu +  LlpIntTau;
(*Total Yukawa*)
LYukTot := LNInt + LlpInt;
(*************************************************************)
(*Kinetic term for Neutral VLL and charged VLL *)
(*Neutral Case*)
LNKin := I ( N1bar.Ga[mu].del[N1,mu] +  N2bar.Ga[mu].del[N2,mu]
        +  N3bar.Ga[mu].del[N3,mu] );
(*Charged Case*)
Llp1Kin := I lp1bar.Ga[mu].del[lp1,mu];
Llp2Kin := I lp2bar.Ga[mu].del[lp2,mu];
Llp3Kin := I lp3bar.Ga[mu].del[lp3,mu];
LlpKin  := Llp1Kin + Llp2Kin + Llp3Kin;
(*Total Kinetic*)
LKinTot := LNKin + LlpKin;
(*************************************************************)
(* Mass term for Neutral VLL and charged VLL*)
(*Neutral Case*)
LNMass := - 1/2 MN1 ( N1bar.N1 ) - 1/2 MN2 ( N2bar.N2 )
          - 1/2 MN3 ( N3bar.N3 );
(*Charged Case*)
Llp1Mass := - Mlp1 ( lp1bar. ProjP.lp1 + lp1bar. ProjM.lp1);
Llp2Mass := - Mlp2 ( lp2bar. ProjP.lp2 + lp2bar. ProjM.lp2);
Llp3Mass := - Mlp3 ( lp3bar. ProjP.lp3 + lp3bar. ProjM.lp3);
LlpMass  := Llp1Mass + Llp2Mass + Llp3Mass;
```

```
(*Total Mass Term*)
LMassTot := LNMass + LlpMass;
(************************************************************)
(*Interaction of lp with photon*)
Llp1QED := -ee lp1bar.Ga[mu].lp1 A[mu];
Llp2QED := -ee lp2bar.Ga[mu].lp2 A[mu];
Llp3QED := -ee lp3bar.Ga[mu].lp3 A[mu];
LlpQED  :=  Llp1QED + Llp2QED + Llp2QED;
(*Interaction of lp with Z boson*)
Llp1Z := (ee/CW*SW) ( SW2 lp1bar.ProjM[mu].lp1 Z[mu]
       + SW2 lp1bar.ProjP[mu].lp1 Z[mu]) ;
Llp2Z := (ee/CW*SW) ( SW2 lp2bar.ProjM[mu].lp2 Z[mu]
       + SW2 lp2bar.ProjP[mu].lp2 Z[mu]) ;
Llp3Z := (ee/CW*SW) ( SW2 lp3bar.ProjM[mu].lp3 Z[mu]
     + SW2 lp3bar.ProjP[mu].lp3 Z[mu]) ;
LlpZ  := Llp1Z + Llp2Z + Llp3Z;
(************************************************************)
( Total VLL Lagrangian)
LVLL := LKinTot + LlpQED + LlpZ + LMassTot -( LYukTot + HC [LYukTot] ) ;
(Total Lagrangian)
LTot := LIDM + LVLL;
(************************************************************)
```

Appendix B

RGE equations for different couplings in Chapter 4

Here we list the RGE equations for the model IHDM plus vector like charged lepton singlets discussed in the work. For the gauge couplings, they are given by

$$16\pi^2\frac{dg_c}{dt} = -7g_c^3, \;\; 16\pi^2\frac{dg_L}{dt} = -3g_L^3, \;\; 16\pi^2\frac{dg_y}{dt} = 11g_y^3 \tag{B.1}$$

where g_c, g_L, g_y are the gauge couplings of $SU(3)_c, SU(2)_L, U(1)_Y$ gauge groups respectively and $t = \ln\mu$, μ being the energy scale. The quartic couplings of the scalar potential evolve as

$$\begin{aligned}16\pi^2\frac{1}{2}\frac{d\lambda_1}{dt} = {} & 3\lambda_1^2 + 4\lambda_3^2 + 4\lambda_3\lambda_4 + 2\lambda_4^2 + 2\lambda_5^2 + \frac{3}{4}(3g_L^4 + g_y^4 + 2g_L^2g_y^2) \\ & -\frac{\lambda_1}{2}(9g_L^2 + 3g_y^2 - 12y_t^2 - 12y_b^2 - 4y_\tau^2) - 12y_t^4\end{aligned} \tag{B.2}$$

$$\begin{aligned}16\pi^2\frac{1}{2}\frac{d\lambda_2}{dt} = {} & 3\lambda_2^2 + 4\lambda_3^2 + 4\lambda_3\lambda_4 + 2\lambda_4^2 + 2\lambda_5^2 + \frac{3}{4}(3g_L^4 + g_y^4 + 2g_L^2g_y^2) \\ & -\frac{3}{2}\lambda_2(3g_L^2 + g_y^2 - \frac{4}{3}y_N^2) - 4y_N^4 - 4y_\chi^4\end{aligned} \tag{B.3}$$

$$\begin{aligned}16\pi^2\frac{d\lambda_3}{dt} = {} & (\lambda_1 + \lambda_2)(3\lambda_3 + \lambda_4) + 4\lambda_3^2 + 2\lambda_4^2 + 2\lambda_5^2 + \frac{3}{4}(3g_L^4 + g_y^4 - 2g_L^2g_y^2) \\ & -\lambda_3(9g_L^2 + 3g_y^2 - 6y_t^2 - 6y_b^2 - 2y_\tau^2 - 2y_N^2 - 2y_\chi^2)\end{aligned} \tag{B.4}$$

$$16\pi^2\frac{d\lambda_4}{dt} = (\lambda_1+\lambda_2)\lambda_4+8\lambda_3\lambda_4+4\lambda_4^2+8\lambda_5^2+3g_L^2g_y^2-\lambda_4(9g_L^2+3g_y^2-6y_t^2-6y_b^2-2y_\tau^2-2y_N^2-2y_\chi^2) \tag{B.5}$$

$$16\pi^2\frac{d\lambda_5}{dt} = (\lambda_1+\lambda_2+8\lambda_3+12\lambda_4)\lambda_5-\lambda_5(9g_L^2+3g_y^2-6y_t^2-6y_b^2-2y_\tau^2-2y_N^2-2y_\chi^2) \tag{B.6}$$

Here y_t, y_b, y_τ are the top quark, bottom quark and tau lepton Yukawa couplings with the Higgs field Φ_1. The Yukawa couplings have the following RGE equations

$$16\pi^2\frac{dy_t}{dt} = y_t\left(-8g_c^2-\frac{9}{4}g_L^2-\frac{17}{12}g_y^2+\frac{9}{2}y_t^2+y_\tau^2+\frac{3}{2}y_b^2\right) \tag{B.7}$$

$$16\pi^2\frac{dy_b}{dt} = y_b\left(-8g_c^2-\frac{9}{4}g_L^2-\frac{5}{12}g_y^2+\frac{9}{2}y_b^2+y_\tau^2+\frac{3}{2}y_t^2\right) \tag{B.8}$$

$$16\pi^2\frac{dy_\tau}{dt} = y_\tau\left(-\frac{9}{4}g_L^2-\frac{15}{4}g_y^2+3y_t^2+3y_b^2+\frac{1}{2}y_N^2+\frac{1}{2}y_\chi^2+\frac{5}{2}y_\tau^2\right) \tag{B.9}$$

$$16\pi^2\frac{dy_N}{dt} = y_N\left(-\frac{9}{4}g_L^2-\frac{3}{4}g_y^2-\frac{3}{4}y_\tau^2+\frac{5}{2}y_N^2\right) \tag{B.10}$$

$$16\pi^2\frac{dy_\chi}{dt} = y_\chi\left(-\frac{9}{4}g_L^2-\frac{3}{4}g_y^2-\frac{3}{4}y_\tau^2+\frac{5}{2}y_\chi^2\right) \tag{B.11}$$

Bibliography

[1] S. L. Glashow, *Partial Symmetries of weak Interactions* Nucl. Phys. **22**, 579 (1961).

[2] S. Weinberg, *A Model of Leptons*, Phys. Rev. Lett. **19**, 1264 (1967).

[3] A. Salam (1968), N. Svartholm, ed. *Elementary Particle Physics: Relativistic Groups and Analyticity* . Eighth Nobel Symposium. Stockholm: Almquvist and Wiksell. p. 367.

[4] F. Englert and R. Brout, *Broken Symmetry and the Mass of Gauge Vector Mesons*, Phys. Rev. Lett. **13**, 321 (1964).

[5] P. W. Higgs, *Broken Symmetries and the Masses of Gauge Bosons*, Phys. Rev. Lett. **13**, 508 (1964).

[6] G. S. Guralnik, C. R. Hagen and T. W. B. Kibble, *Global Conservation Laws and Massless Particles*, Phys. Rev. Lett. **13**, 585 (1964).

[7] ATLAS collaboration, G. Aad et al., *Observation of a new particle in the search for the Standard Model Higgs boson with the ATLAS detector at the LHC*, *Phys. Lett.* **B716** (2012) 1–29, [1207.7214].

[8] CMS collaboration, S. Chatrchyan et al., *Observation of a new boson at a mass of 125 GeV with the CMS experiment at the LHC*, *Phys. Lett.* **B716** (2012) 30–61, [1207.7235].

[9] M. Schmaltz, *Physics beyond the standard model (theory): Introducing the little Higgs*, Nucl. Phys. Proc. Suppl. **117**, 40 (2003) [hep-ph/0210415].

[10] S. P. Martin, *A Supersymmetry primer*, In *Kane, G.L. (ed.): Perspectives on supersymmetry II* 1-153 [hep-ph/9709356].

[11] M. Drees, *An Introduction to supersymmetry*, hep-ph/9611409.

[12] U. Ellwanger, C. Hugonie and A. M. Teixeira, *The Next-to-Minimal Supersymmetric Standard Model*, Phys. Rept. **496**, 1 (2010) [arXiv:0910.1785 [hep-ph]] and references therein.

[13] I. Antoniadis, *From extra-dimensions: Multiple brane scenarios and their contenders*, Int. J. Mod. Phys. A **25**, 5817 (2010).

[14] T. G. Rizzo, *Extended gauge sectors*, In *Tahoe City 1994, Proceedings, Beyond the standard model 4* 24-31, and SLAC Stanford - SLAC-PUB-6741 (95,rec.Jan.) 24 p [hep-ph/9501261].

[15] H. Murayama, *Dynamical (super)symmetry breaking*, hep-ph/0010021 and references therein.

[16] R. A. Diaz, *Phenomenological analysis of the two Higgs doublet* , hep-ph/0212237.

[17] J. F. Gunion, H. E. Haber and J. Wudka, *Sum rules for Higgs bosons*, Phys. Rev. D **43**, 904 (1991).

[18] N. G. Deshpande and E. Ma, *Pattern of Symmetry Breaking with Two Higgs Doublets*, Phys. Rev. D **18**, 2574 (1978).

[19] ATLAS, CMS collaboration, G. Aad et al., *Measurements of the Higgs boson production and decay rates and constraints on its couplings from a combined ATLAS and CMS analysis of the LHC pp collision data at* $\sqrt{s} = 7$ *and 8 TeV*, *JHEP* **08** (2016) 045, [1606.02266].

[20] ATLAS, CMS collaboration, G. Aad et al., *Combined Measurement of the Higgs Boson Mass in pp Collisions at* $\sqrt{s} = 7$ *and 8 TeV with the ATLAS and CMS Experiments*, *Phys. Rev. Lett.* **114** (2015) 191803, [1503.07589].

[21] T. D. Lee, *A Theory of Spontaneous T Violation*, *Phys. Rev.* **D8** (1973) 1226–1239.

[22] G. C. Branco, P. M. Ferreira, L. Lavoura, M. N. Rebelo, M. Sher and J. P. Silva, *Theory and phenomenology of two-Higgs-doublet models*, *Phys. Rept.* **516** (2012) 1–102, [1106.0034].

[23] H. P. Nilles, *Supersymmetry, Supergravity and Particle Physics*, *Phys. Rept.* **110** (1984) 1–162.

[24] H. E. Haber and G. L. Kane, *The Search for Supersymmetry: Probing Physics Beyond the Standard Model*, *Phys. Rept.* **117** (1985) 75–263.

[25] S. Moretti, R. Santos and P. Sharma, *Optimising Charged Higgs Boson Searches at the Large Hadron Collider Across* $b\bar{b}W^{\pm}$ *Final States*, *Phys. Lett.* **B760** (2016) 697–705, [1604.04965].

[26] A. Arhrib, R. Benbrik and S. Moretti, *Bosonic Decays of Charged Higgs Bosons in a 2HDM Type-I*, *Eur. Phys. J.* **C77** (2017) 621, [1607.02402].

[27] B. Coleppa, F. Kling and S. Su, *Charged Higgs search via* $AW^{\pm}/HW^{\pm}$ *channel*, *JHEP* **12** (2014) 148, [1408.4119].

[28] ATLAS collaboration, G. Aad et al., *Search for a CP-odd Higgs boson decaying to Zh in pp collisions at* $\sqrt{s} = 8$ *TeV with the ATLAS detector*, *Phys. Lett.* **B744** (2015) 163–183, [1502.04478].

[29] ATLAS collaboration, *Search for a CP-odd Higgs boson decaying to Zh in pp collisions at* $\sqrt{s} = 13$ *TeV with the ATLAS detector*, ATLAS-CONF-2016-015.

[30] ATLAS collaboration, *Search for heavy resonances decaying to a W or Z boson and a Higgs boson in final states with leptons and b-jets in 36.1* fb^{-1} *of pp collision data at* $\sqrt{s} = 13$ *TeV with the ATLAS detector*, ATLAS-CONF-2017-055.

[31] ATLAS collaboration, M. Aaboud et al., *Search for heavy resonances decaying to a W or Z boson and a Higgs boson in the* $q\bar{q}^{(\prime)}b\bar{b}$ *final state in pp collisions at* $\sqrt{s} = 13$ *TeV with the ATLAS detector*, *Phys. Lett.* **B774** (2017) 494–515, [1707.06958].

[32] CMS collaboration, V. Khachatryan et al., *Search for a pseudoscalar boson decaying into a Z boson and the 125 GeV Higgs boson in* $l^+l^-b\bar{b}$ *final states*, *Phys. Lett.* **B748**

(2015) 221–243, [1504.04710].

[33] CMS collaboration, V. Khachatryan et al., *Search for neutral resonances decaying into a Z boson and a pair of b jets or τ leptons*, *Phys. Lett.* **B759** (2016) 369–394, [1603.02991].

[34] CMS Collaboration, *Search for H to Z(ll)+A(bb) with 2015 data*, CMS-PAS-HIG-16-010.

[35] S. Yang and Q.-S. Yan, *Searching for Heavy Charged Higgs Boson with Jet Substructure at the LHC*, *JHEP* **02** (2012) 074, [1111.4530].

[36] N. Chen, J. Li, Y. Liu and Z. Liu, *LHC searches for the CP-odd Higgs by the jet substructure analysis*, *Phys. Rev.* **D91** (2015) 075002, [1410.4447].

[37] B. Coleppa, F. Kling and S. Su, *Exotic Decays Of A Heavy Neutral Higgs Through HZ/AZ Channel*, *JHEP* **09** (2014) 161, [1404.1922].

[38] B. Dumont, J. F. Gunion, Y. Jiang and S. Kraml, *Constraints on and future prospects for Two-Higgs-Doublet Models in light of the LHC Higgs signal*, *Phys. Rev.* **D90** (2014) 035021, [1405.3584].

[39] J. Bernon, J. F. Gunion, H. E. Haber, Y. Jiang and S. Kraml, *Scrutinizing the alignment limit in two-Higgs-doublet models. II. $m_H = 125$ GeV*, *Phys. Rev.* **D93** (2016) 035027, [1511.03682].

[40] J. Bernon, J. F. Gunion, H. E. Haber, Y. Jiang and S. Kraml, *Scrutinizing the alignment limit in two-Higgs-doublet models: $m_h = 125$ GeV*, *Phys. Rev.* **D92** (2015) 075004, [1507.00933].

[41] F. Kling, A. Pyarelal and S. Su, *Light Charged Higgs Bosons to AW/HW via Top Decay*, *JHEP* **11** (2015) 051, [1504.06624].

[42] T. Li and S. Su, *Exotic Higgs Decay via Charged Higgs*, *JHEP* **11** (2015) 068, [1504.04381].

[43] J. Li, R. Patrick, P. Sharma and A. G. Williams, *Boosting the charged Higgs search prospects using jet substructure at the LHC*, *JHEP* **11** (2016) 164, [1609.02645].

[44] R. Patrick, P. Sharma and A. G. Williams, *Exploring a heavy charged Higgs using jet substructure in a fully hadronic channel*, *Nucl. Phys.* **B917** (2017) 19–30, [1610.05917].

[45] D. Goncalves and D. Lopez-Val, *Pseudoscalar searches with dileptonic tops and jet substructure*, *Phys. Rev.* **D94** (2016) 095005, [1607.08614].

[46] F. Kling, J. M. No and S. Su, *Anatomy of Exotic Higgs Decays in 2HDM*, *JHEP* **09** (2016) 093, [1604.01406].

[47] N. Chakrabarty and B. Mukhopadhyaya, *High-scale validity of a two Higgs doublet scenario: predicting collider signals*, *Phys. Rev.* **D96** (2017) 035028, [1702.08268].

[48] P. M. Ferreira, S. Liebler and J. Wittbrodt, *Wrong or right: $pp \to A \to Zh$ and the sign of the Two-Higgs-Doublet Model*, 1711.00024.

[49] Z. Kang, J. Li, T. Li, D. Liu and J. Shu, *Probing the CP-even Higgs sector via $H_3 \to H_2 H_1$ in the natural next-to-minimal supersymmetric standard model*, *Phys.*

Rev. **D88** (2013) 015006, [1301.0453].

[50] J. Hajer, Y.-Y. Li, T. Liu and J. F. H. Shiu, *Heavy Higgs Bosons at 14 TeV and 100 TeV*, *JHEP* **11** (2015) 124, [1504.07617].

[51] M. Casolino, T. Farooque, A. Juste, T. Liu and M. Spannowsky, *Probing a light CP-odd scalar in di-top-associated production at the LHC*, *Eur. Phys. J.* **C75** (2015) 498, [1507.07004].

[52] E. Conte, B. Fuks, J. Guo, J. Li and A. G. Williams, *Investigating light NMSSM pseudoscalar states with boosted ditau tagging*, *JHEP* **05** (2016) 100, [1604.05394].

[53] R. Aggleton, D. Barducci, N.-E. Bomark, S. Moretti and C. Shepherd-Themistocleous, *Review of LHC experimental results on low mass bosons in multi Higgs models*, *JHEP* **02** (2017) 035, [1609.06089].

[54] U. Ellwanger and M. Rodriguez-Vazquez, *Simultaneous Search for Extra Light and Heavy Higgs Bosons via Cascade Decays*, 1707.08522.

[55] N. Craig, J. A. Evans, R. Gray, C. Kilic, M. Park, S. Somalwar et al., *Multi-Lepton Signals of Multiple Higgs Bosons*, *JHEP* **02** (2013) 033, [1210.0559].

[56] C. Gao, M. A. Luty, M. Mulhearn, N. A. Neill and Z. Wang, *Searching for Additional Higgs Bosons via Higgs Cascades*, 1604.03108.

[57] J. Alwall, R. Frederix, S. Frixione, V. Hirschi, F. Maltoni, O. Mattelaer et al., *The automated computation of tree-level and next-to-leading order differential cross sections, and their matching to parton shower simulations*, *JHEP* **07** (2014) 079, [1405.0301].

[58] C. Degrande, C. Duhr, B. Fuks, D. Grellscheid, O. Mattelaer and T. Reiter, *UFO - The Universal FeynRules Output*, *Comput. Phys. Commun.* **183** (2012) 1201–1214, [1108.2040].

[59] N. D. Christensen, P. de Aquino, C. Degrande, C. Duhr, B. Fuks, M. Herquet et al., *A Comprehensive approach to new physics simulations*, *Eur. Phys. J.* **C71** (2011) 1541, [0906.2474].

[60] A. Alloul, N. D. Christensen, C. Degrande, C. Duhr and B. Fuks, *FeynRules 2.0 - A complete toolbox for tree-level phenomenology*, *Comput. Phys. Commun.* **185** (2014) 2250–2300, [1310.1921].

[61] NNPDF collaboration, R. D. Ball et al., *Parton distributions for the LHC Run II*, *JHEP* **04** (2015) 040, [1410.8849].

[62] T. Sjostrand, S. Mrenna and P. Z. Skands, *PYTHIA 6.4 Physics and Manual*, *JHEP* **05** (2006) 026, [hep-ph/0603175].

[63] DELPHES 3 collaboration, J. de Favereau, C. Delaere, P. Demin, A. Giammanco, V. Lematre, A. Mertens et al., *DELPHES 3, A modular framework for fast simulation of a generic collider experiment*, *JHEP* **02** (2014) 057, [1307.6346].

[64] B. Dumont, B. Fuks, S. Kraml, S. Bein, G. Chalons, E. Conte et al., *Toward a public analysis database for LHC new physics searches using MADANALYSIS 5*, *Eur. Phys. J.* **C75** (2015) 56, [1407.3278].

[65] M. Cacciari, G. P. Salam and G. Soyez, *The Anti-k(t) jet clustering algorithm*, *JHEP* **04** (2008) 063, [0802.1189].

[66] E. Conte, B. Fuks and G. Serret, *MadAnalysis 5, A User-Friendly Framework for Collider Phenomenology*, *Comput. Phys. Commun.* **184** (2013) 222–256, [1206.1599].

[67] E. Conte, B. Dumont, B. Fuks and C. Wymant, *Designing and recasting LHC analyses with MadAnalysis 5*, *Eur. Phys. J.* **C74** (2014) 3103, [1405.3982].

[68] M. Cacciari, G. P. Salam and G. Soyez, *FastJet User Manual*, *Eur. Phys. J.* **C72** (2012) 1896, [1111.6097].

[69] G. Cowan, K. Cranmer, E. Gross and O. Vitells, *Asymptotic formulae for likelihood-based tests of new physics*, *Eur. Phys. J.* **C71** (2011) 1554, [1007.1727].

[70] LHC Higgs Cross Section Working Group collaboration, S. Dittmaier et al., *Handbook of LHC Higgs Cross Sections: 1. Inclusive Observables*, 1101.0593.

[71] LHC Higgs Cross Section Working Group collaboration, D. de Florian et al., *Handbook of LHC Higgs Cross Sections: 4. Deciphering the Nature of the Higgs Sector*, 1610.07922.

[72] B. Coleppa, F. Kling and S. Su, *Constraining Type II 2HDM in Light of LHC Higgs Searches*, *JHEP* **01** (2014) 161, [1305.0002].

[73] E. Ma, *Verifiable radiative seesaw mechanism of neutrino mass and dark matter*, Phys. Rev. D **73**, 077301 (2006) [hep-ph/0601225].

[74] E. Ma, *Common origin of neutrino mass, dark matter, and baryogenesis*, Mod. Phys. Lett. A **21**, 1777 (2006) [hep-ph/0605180].

[75] L. M. Krauss, S. Nasri and M. Trodden, *A Model for neutrino masses and dark matter*, Phys. Rev. D **67**, 085002 (2003) [hep-ph/0210389].

[76] J. Kubo, E. Ma and D. Suematsu, *Cold Dark Matter, Radiative Neutrino Mass, $\mu \to e\gamma$, and Neutrinoless Double Beta Decay*, Phys. Lett. B **642**, 18 (2006) [hep-ph/0604114].

[77] D. Aristizabal Sierra, J. Kubo, D. Restrepo, D. Suematsu and O. Zapata, *Radiative seesaw: Warm dark matter, collider and lepton flavour violating signals*, Phys. Rev. D **79**, 013011 (2009) [arXiv:0808.3340 [hep-ph]].

[78] D. Suematsu, T. Toma and T. Yoshida, *Reconciliation of CDM abundance and $\mu \to e\gamma$ in a radiative seesaw model*, Phys. Rev. D **79**, 093004 (2009) [arXiv:0903.0287 [hep-ph]].

[79] D. Suematsu, T. Toma and T. Yoshida, *Enhancement of the annihilation of dark matter in a radiative seesaw model*, Phys. Rev. D **82**, 013012 (2010) [arXiv:1002.3225 [hep-ph]].

[80] D. Suematsu, *Thermal Leptogenesis in a TeV Scale Model for Neutrino Masses*, Eur. Phys. J. C **72**, 1951 (2012) [arXiv:1103.0857 [hep-ph]].

[81] S. Kashiwase and D. Suematsu, *Baryon number asymmetry and dark matter in the neutrino mass model with an inert doublet*, Phys. Rev. D **86**, 053001 (2012)

[arXiv:1207.2594 [hep-ph]].

[82] S. Kashiwase and D. Suematsu, *Leptogenesis and dark matter detection in a TeV scale neutrino mass model with inverted mass hierarchy*, Eur. Phys. J. C **73**, 2484 (2013) [arXiv:1301.2087 [hep-ph]].

[83] N. Chakrabarty, D. K. Ghosh, B. Mukhopadhyaya and I. Saha, *Dark matter, neutrino masses and high scale validity of an inert Higgs doublet model*, Phys. Rev. D **92**, no. 1, 015002 (2015) [arXiv:1501.03700 [hep-ph]].

[84] R. Barbieri and A. Strumia, *The 'LEP paradox'*, hep-ph/0007265.

[85] R. Barbieri, L. J. Hall and V. S. Rychkov, *Improved naturalness with a heavy Higgs: An Alternative road to LHC physics*, Phys. Rev. D **74**, 015007 (2006) [hep-ph/0603188].

[86] J. A. Casas, J. R. Espinosa and I. Hidalgo, *Expectations for LHC from naturalness: modified versus SM Higgs sector*, Nucl. Phys. B **777**, 226 (2007) [hep-ph/0607279].

[87] T. Hambye and M. H. G. Tytgat, *Electroweak symmetry breaking induced by dark matter*, Phys. Lett. B **659**, 651 (2008) [arXiv:0707.0633 [hep-ph]].

[88] Q. H. Cao, E. Ma and G. Rajasekaran, *Observing the Dark Scalar Doublet and its Impact on the Standard-Model Higgs Boson at Colliders*, Phys. Rev. D **76**, 095011 (2007) [arXiv:0708.2939 [hep-ph]].

[89] E. Dolle, X. Miao, S. Su and B. Thomas, *Dilepton Signals in the Inert Doublet Model*, Phys. Rev. D **81**, 035003 (2010) [arXiv:0909.3094 [hep-ph]].

[90] A. Arhrib, R. Benbrik and N. Gaur, $H \to \gamma\gamma$ *in Inert Higgs Doublet Model*, Phys. Rev. D **85**, 095021 (2012) [arXiv:1201.2644 [hep-ph]].

[91] M. Krawczyk, D. Sokolowska and B. Swiezewska, *Inert Doublet Model with a 125 GeV Higgs*, arXiv:1304.7757 [hep-ph].

[92] M. Krawczyk, D. Sokolowska, P. Swaczyna and B. Swiezewska, *Constraining Inert Dark Matter by* $R_{\gamma\gamma}$ *and WMAP data*, JHEP **1309**, 055 (2013) [arXiv:1305.6266 [hep-ph]].

[93] A. Goudelis, B. Herrmann and O. Stål, *Dark matter in the Inert Doublet Model after the discovery of a Higgs-like boson at the LHC*, JHEP **1309**, 106 (2013) [arXiv:1303.3010 [hep-ph]].

[94] A. Arhrib, Y. L. S. Tsai, Q. Yuan and T. C. Yuan, *An Updated Analysis of Inert Higgs Doublet Model in light of the Recent Results from LUX, PLANCK, AMS-02 and LHC*, JCAP **1406**, 030 (2014) [arXiv:1310.0358 [hep-ph]].

[95] A. Ilnicka, M. Krawczyk and T. Robens, *Constraining the Inert Doublet Model*, arXiv:1505.04734 [hep-ph].

[96] A. Ilnicka, M. Krawczyk and T. Robens, *The Inert Doublet Model in the light of LHC and astrophysical data – An Update –*, Phys. Rev. D **93**, no. 5, 055026 (2016) [arXiv:1508.01671 [hep-ph]].

[97] X. Miao, S. Su and B. Thomas, *Trilepton Signals in the Inert Doublet Model*, Phys. Rev. D **82**, 035009 (2010) [arXiv:1005.0090 [hep-ph]].

[98] M. Gustafsson, S. Rydbeck, L. Lopez-Honorez and E. Lundstrom, *Status of the Inert Doublet Model and the Role of multileptons at the LHC*, Phys. Rev. D **86**, 075019 (2012) [arXiv:1206.6316 [hep-ph]].

[99] B. Świeewska, *Yukawa independent constraints for two-Higgs-doublet models with a 125 GeV Higgs boson*, Phys. Rev. D **88**, no. 5, 055027 (2013) Erratum: [Phys. Rev. D **88**, no. 11, 119903 (2013)] [arXiv:1209.5725 [hep-ph]].

[100] M. Sher, *Review of prospects for H^+ in non-SUSY multi-Higgs models in view of LHC results*, PoS CHARGED **2012**, 015 (2012) [arXiv:1212.0789 [hep-ph]].

[101] A. Celis, V. Ilisie and A. Pich, *LHC constraints on two-Higgs doublet models*, JHEP **1307**, 053 (2013) [arXiv:1302.4022 [hep-ph]].

[102] G. Belanger, B. Dumont, U. Ellwanger, J. F. Gunion and S. Kraml, *Global fit to Higgs signal strengths and couplings and implications for extended Higgs sectors*, Phys. Rev. D **88**, 075008 (2013) [arXiv:1306.2941 [hep-ph]].

[103] T. Abe, R. Kitano and R. Sato, *Discrimination of dark matter models in future experiments*, Phys. Rev. D **91**, no. 9, 095004 (2015) [arXiv:1411.1335 [hep-ph]].

[104] M. Krawczyk, M. Matej, D. Sokoĺowska and B. Świeżewska, *The Universe in the Light of LHC*, Acta Phys. Polon. B **46**, no. 1, 169 (2015) [arXiv:1501.04529 [hep-ph]].

[105] G. Belanger, B. Dumont, A. Goudelis, B. Herrmann, S. Kraml and D. Sengupta, *Dilepton constraints in the Inert Doublet Model from Run 1 of the LHC*, Phys. Rev. D **91**, no. 11, 115011 (2015) [arXiv:1503.07367 [hep-ph]].

[106] N. Blinov, J. Kozaczuk, D. E. Morrissey and A. de la Puente, *Compressing the Inert Doublet Model*, Phys. Rev. D **93**, no. 3, 035020 (2016) [arXiv:1510.08069 [hep-ph]].

[107] M. A. D EDaz, B. Koch and S. Urrutia-Quiroga, *Constraints to Dark Matter from Inert Higgs Doublet Model*, Adv. High Energy Phys. **2016**, 8278375 (2016) [arXiv:1511.04429 [hep-ph]].

[108] G. Moortgat-Pick *et al.*, *Physics at the e+ e- Linear Collider*, Eur. Phys. J. C **75**, no. 8, 371 (2015) [arXiv:1504.01726 [hep-ph]].

[109] M. Aoki, S. Kanemura and H. Yokoya, *Reconstruction of Inert Doublet Scalars at the International Linear Collider*, Phys. Lett. B **725**, 302 (2013) [arXiv:1303.6191 [hep-ph]].

[110] M. Hashemi, M. Krawczyk, S. Najjari and A. F. Żarnecki, *Production of Inert Scalars at the high energy e^+e^- colliders*, [arXiv:1512.01175 [hep-ph]].

[111] D. S. Akerib *et al.* [LUX Collaboration], *First results from the LUX dark matter experiment at the Sanford Underground Research Facility*, Phys. Rev. Lett. **112**, 091303 (2014) [arXiv:1310.8214 [astro-ph.CO]].

[112] P. A. R. Ade *et al.* [Planck Collaboration], *Planck 2015 results. XIII. Cosmological parameters*, arXiv:1502.01589 [astro-ph.CO].

[113] N. Aghanim *et al.* [Planck Collaboration], arXiv:1807.06209 [astro-ph.CO].

[114] D. Abercrombie *et al.*, *Dark Matter Benchmark Models for Early LHC Run-2 Searches: Report of the ATLAS/CMS Dark Matter Forum*, arXiv:1507.00966 [hep-

ex].

[115] A. Arhrib, R. Benbrik, J. El Falaki and A. Jueid, *Radiative corrections to the Triple Higgs Coupling in the Inert Higgs Doublet Model*, JHEP **1512**, 007 (2015) [arXiv:1507.03630 [hep-ph]].

[116] J. Brooke, M. R. Buckley, P. Dunne, B. Penning, J. Tamanas and M. Zgubic, *Vector Boson Fusion Searches for Dark Matter at the LHC*, Phys. Rev. D **93**, no. 11, 113013 (2016) [arXiv:1603.07739 [hep-ph]].

[117] M. Gustafsson, *The Inert Doublet Model and Its Phenomenology*, PoS CHARGED **2010**, 030 (2010) [arXiv:1106.1719 [hep-ph]].

[118] J. Beringer *et al.* [Particle Data Group Collaboration], *Review of Particle Physics (RPP)*, Phys. Rev. D **86**, 010001 (2012).

[119] K. A. Olive *et al.* [Particle Data Group Collaboration], *Review of Particle Physics*, Chin. Phys. C **38**, 090001 (2014).

[120] A. Pierce and J. Thaler, *Natural Dark Matter from an Unnatural Higgs Boson and New Colored Particles at the TeV Scale*, JHEP **0708**, 026 (2007) [hep-ph/0703056 [HEP-PH]].

[121] J.-M. Frere, F.-S. Ling, L. Lopez Honorez, E. Nezri, Q. Swillens and G. Vertongen, *MeV right-handed neutrinos and dark matter*, Phys. Rev. D **75**, 085017 (2007) [hep-ph/0610240].

[122] E. M. Dolle and S. Su, *The Inert Dark Matter*, Phys. Rev. D **80**, 055012 (2009) [arXiv:0906.1609 [hep-ph]].

[123] J. Kalinowski, W. Kotlarski, T. Robens, D. Sokolowska and A. F. Zarnecki, *Benchmarking the Inert Doublet Model for e^+e^- colliders*, JHEP **1812**, 081 (2018) [arXiv:1809.07712 [hep-ph]].

[124] J. Bernon, B. Dumont and S. Kraml, *Status of Higgs couplings after run 1 of the LHC*, Phys. Rev. D **90**, 071301 (2014) [arXiv:1409.1588 [hep-ph]].

[125] V. Khachatryan *et al.* [CMS Collaboration], *Searches for invisible decays of the Higgs boson in pp collisions at $\sqrt{s}$ = 7, 8, and 13 TeV*, JHEP **1702**, 135 (2017) [arXiv:1610.09218 [hep-ex]].

[126] E. Aprile *et al.* [XENON100 Collaboration], *Dark Matter Results from 225 Live Days of XENON100 Data*, Phys. Rev. Lett. **109**, 181301 (2012) [arXiv:1207.5988 [astro-ph.CO]].

[127] F. S. Queiroz and C. E. Yaguna, *The CTA aims at the Inert Doublet Model*, JCAP **1602** (2016) no.02, 038 [arXiv:1511.05967 [hep-ph]].

[128] D. S. Akerib *et al.* [LUX Collaboration], *Results from a search for dark matter in the complete LUX exposure*, Phys. Rev. Lett. **118**, no. 2, 021303 (2017) [arXiv:1608.07648 [astro-ph.CO]].

[129] A. Tan *et al.* [PandaX-II Collaboration], *Dark Matter Results from First 98.7 Days of Data from the PandaX-II Experiment*, Phys. Rev. Lett. **117**, no. 12, 121303 (2016) [arXiv:1607.07400 [hep-ex]].

[130] M. Cirelli, N. Fornengo and A. Strumia, *Minimal dark matter*, Nucl. Phys. B **753**, 178 (2006) [hep-ph/0512090].

[131] L. Lopez Honorez, E. Nezri, J. F. Oliver and M. H. G. Tytgat, *The Inert Doublet Model: An Archetype for Dark Matter*, JCAP **0702**, 028 (2007) [hep-ph/ 0612275].

[132] A. M. Baldini *et al.* [MEG Collaboration], *Search for the lepton flavour violating decay* $\mu^+ \to e^+\gamma$ *with the full dataset of the MEG experiment*, Eur. Phys. J. C **76**, no. 8, 434 (2016) [arXiv:1605.05081 [hep-ex]].

[133] D. Borah and A. Dasgupta, *Common Origin of Neutrino Mass, Dark Matter and Dirac Leptogenesis*, JCAP **1612**, no. 12, 034 (2016) [arXiv:1608.03872 [hep-ph]].

[134] D. Borah and A. Dasgupta, *Observable Lepton Number Violation with Predominantly Dirac Nature of Active Neutrinos*, JHEP **1701**, 072 (2017) [arXiv:1609.04236 [hep-ph]].

[135] D. Borah and A. Dasgupta, *Naturally Light Dirac Neutrino in Left-Right Symmetric Model*, JCAP **1706**, no. 06, 003 (2017) [arXiv:1702.02877 [hep-ph]].

[136] T. G. Rizzo, *Phenomenology of Exotic Particles in* $E(6)$ *Theories*, Phys. Rev. D **34**, 1438 (1986).

[137] S. Gopalakrishna, T. S. Mukherjee and S. Sadhukhan, *Status and Prospects of the Two-Higgs-Doublet SU(6)/Sp(6) little-Higgs Model and the Alignment Limit*, Phys. Rev. D **94**, no. 1, 015034 (2016) [arXiv:1512.05731 [hep-ph]].

[138] E. W. Kolb and M. S. Turner, *The Early Universe*, Front. Phys. **69**, 1 (1990).

[139] R. J. Scherrer and M. S. Turner, *On the Relic, Cosmic Abundance of Stable Weakly Interacting Massive Particles*, Phys. Rev. D **33**, 1585 (1986) Erratum: [Phys. Rev. D **34**, 3263 (1986)].

[140] G. Jungman, M. Kamionkowski and K. Griest, *Supersymmetric dark matter*, Phys. Rept. **267**, 195 (1996) [hep-ph/9506380].

[141] P. Gondolo and G. Gelmini, *Cosmic abundances of stable particles: Improved analysis*, Nucl. Phys. B **360**, 145 (1991).

[142] D. Majumdar and A. Ghosal, *Dark Matter candidate in a Heavy Higgs Model - Direct Detection Rates*, Mod. Phys. Lett. A **23**, 2011 (2008) [hep-ph/0607067].

[143] T. A. Chowdhury, M. Nemevsek, G. Senjanovic and Y. Zhang, *Dark Matter as the Trigger of Strong Electroweak Phase Transition*, JCAP **1202**, 029 (2012) [arXiv:1110.5334 [hep-ph]].

[144] D. Borah and J. M. Cline, *Inert Doublet Dark Matter with Strong Electroweak Phase Transition*, Phys. Rev. D **86**, 055001 (2012) [arXiv:1204.4722 [hep-ph]].

[145] A. Dasgupta and D. Borah, *Scalar Dark Matter with Type II Seesaw*, Nucl. Phys. B **889**, 637 (2014) [arXiv:1404.5261 [hep-ph]].

[146] L. Lopez Honorez and C. E. Yaguna, *A new viable region of the inert doublet model*, JCAP **1101**, 002 (2011) [arXiv:1011.1411 [hep-ph]].

[147] L. Lopez Honorez and C. E. Yaguna, *The inert doublet model of dark matter revisited*, JHEP **1009**, 046 (2010) [arXiv:1003.3125 [hep-ph]].

[148] K. Griest and D. Seckel, *Three exceptions in the calculation of relic abundances*,

Phys. Rev. D **43**, 3191 (1991).

[149] J. Edsjo and P. Gondolo, *Neutralino relic density including coannihilations*, Phys. Rev. D **56**, 1879 (1997) [hep-ph/9704361].

[150] N. F. Bell, Y. Cai and A. D. Medina, *Co-annihilating Dark Matter: Effective Operator Analysis and Collider Phenomenology*, Phys. Rev. D **89**, no. 11, 115001 (2014) [arXiv:1311.6169 [hep-ph]].

[151] E. Aprile *et al.* [XENON100 Collaboration], *Dark Matter Results from 225 Live Days of XENON100 Data*, Phys. Rev. Lett. **109**, 181301 (2012) [arXiv:1207.5988 [astro-ph.CO]].

[152] D. S. Akerib et al. [LUX Collaboration], Phys. Rev. Lett. **112**, 091303 (2014).

[153] D. S. Akerib *et al.* [LUX Collaboration], *First results from the LUX dark matter experiment at the Sanford Underground Research Facility*, Phys. Rev. Lett. **112**, 091303 (2014) [arXiv:1310.8214 [astro-ph.CO]].

[154] J. Giedt, A. W. Thomas and R. D. Young, *Dark matter, the CMSSM and lattice QCD*, Phys. Rev. Lett. **103**, 201802 (2009) [arXiv:0907.4177 [hep-ph]].

[155] Y. Mambrini, *Higgs searches and singlet scalar dark matter: Combined constraints from XENON 100 and the LHC*, Phys. Rev. D **84**, 115017 (2011) [arXiv:1108.0671 [hep-ph]].

[156] G. Aad *et al.* [ATLAS Collaboration], *Constraints on new phenomena via Higgs boson couplings and invisible decays with the ATLAS detector*, JHEP **1511**, 206 (2015) [arXiv:1509.00672 [hep-ex]].

[157] M. Klasen, C. E. Yaguna and J. D. Ruiz-Alvarez, *Electroweak corrections to the direct detection cross section of inert higgs dark matter*, Phys. Rev. D **87**, 075025 (2013) [arXiv:1302.1657 [hep-ph]].

[158] S. Chang, R. Edezhath, J. Hutchinson and M. Luty, *Leptophilic Effective WIMPs*, Phys. Rev. D **90**, no. 1, 015011 (2014) [arXiv:1402.7358 [hep-ph]];
Y. Bai and J. Berger, *Lepton Portal Dark Matter*, JHEP **1408**, 153 (2014) [arXiv:1402.6696 [hep-ph]].

[159] C. Arina, F. S. Ling and M. H. G. Tytgat, *IDM and iDM or The Inert Doublet Model and Inelastic Dark Matter*, JCAP **0910**, 018 (2009) [arXiv:0907.0430 [hep-ph]].

[160] G. Belanger, F. Boudjema, A. Pukhov and A. Semenov, *micrOMEGAs$_3$: A program for calculating dark matter observables*, Comput.Phys.Commun.**185**, 960 (2014) [arXiv:1305.0237 [hep-ph]].

[161] A. Datta, N. Ganguly, N. Khan and S. Rakshit, *Exploring collider signatures of the inert Higgs doublet model*, Phys. Rev. D **95**, no. 1, 015017 (2017) [arXiv:1610.00648 [hep-ph]].

[162] P. Poulose, S. Sahoo and K. Sridhar, *Exploring the Inert Doublet Model through the dijet plus missing transverse energy channel at the LHC*, Phys. Lett. B **765**, 300 (2017) [arXiv:1604.03045 [hep-ph]].

[163] M. Hashemi and S. Najjari, *Observability of Inert Scalars at the LHC*, Eur. Phys.

J. C **77**, no. 9, 592 (2017) [arXiv:1611.07827 [hep-ph]].

[164] A. Belyaev, G. Cacciapaglia, I. P. Ivanov, F. Rojas-Abatte and M. Thomas, *Anatomy of the Inert Two Higgs Doublet Model in the light of the LHC and non-LHC Dark Matter Searches*, Phys. Rev. D **97**, no. 3, 035011 (2018) [arXiv:1612.00511 [hep-ph]].

[165] S. Bhattacharya, N. Sahoo and N. Sahu, *Minimal vectorlike leptonic dark matter and signatures at the LHC*, Phys. Rev. D **93**, no. 11, 115040 (2016) [arXiv:1510.02760 [hep-ph]].

[166] N. Kumar and S. P. Martin, *Vectorlike Leptons at the Large Hadron Collider*, Phys. Rev. D **92**, no. 11, 115018 (2015) [arXiv:1510.03456 [hep-ph]].

[167] *Vector-like leptons: Higgs decays and collider phenomenology*, JHEP **1405**, 092 (2014) [arXiv:1312.5329 [hep-ph]]. and references therein.

[168] S. Gopalakrishna, T. S. Mukherjee and S. Sadhukhan, *Extra neutral scalars with vectorlike fermions at the LHC*, Phys. Rev. D **93**, no. 5, 055004 (2016) [arXiv:1504.01074 [hep-ph]].

[169] A. Angelescu and G. Arcadi, *Dark Matter Phenomenology of SM and Enlarged Higgs Sectors Extended with Vector Like Leptons*, Eur. Phys. J. C **77**, no. 7, 456 (2017) [arXiv:1611.06186 [hep-ph]].

[170] K. Blum, R. T. D'Agnolo and J. Fan, *Vacuum stability bounds on Higgs coupling deviations in the absence of new bosons*, JHEP **1503**, 166 (2015) [arXiv:1502.01045 [hep-ph]].

[171] E. Bertuzzo, P. A. N. Machado and M. Taoso, *Diphoton excess in the 2HDM: Hastening towards instability and the nonperturbative regime*, Phys. Rev. D **94**, no. 11, 115006 (2016) [arXiv:1601.07508 [hep-ph]].

.

Supplementary Informations

Feynman Diagrams for pair production of Inert Scalars as discussed in Chapter 3

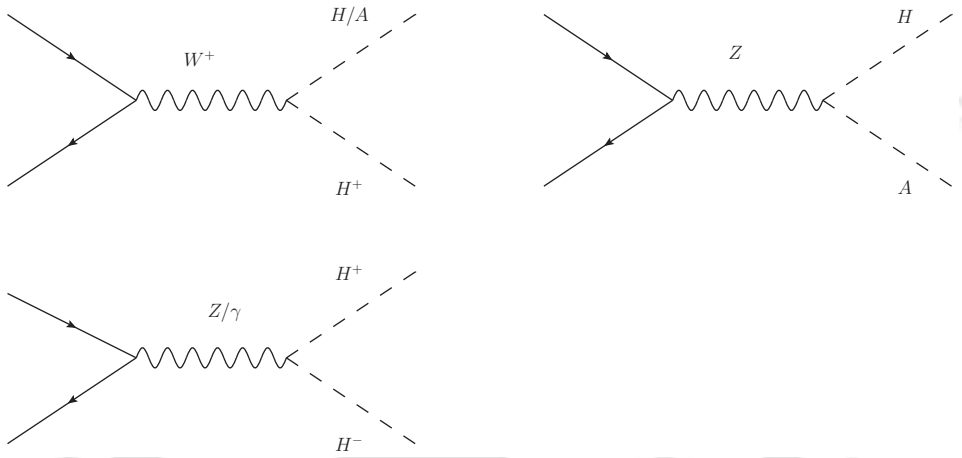

Feynman Diagrams those contributing to relic density as discussed in Chapter 4

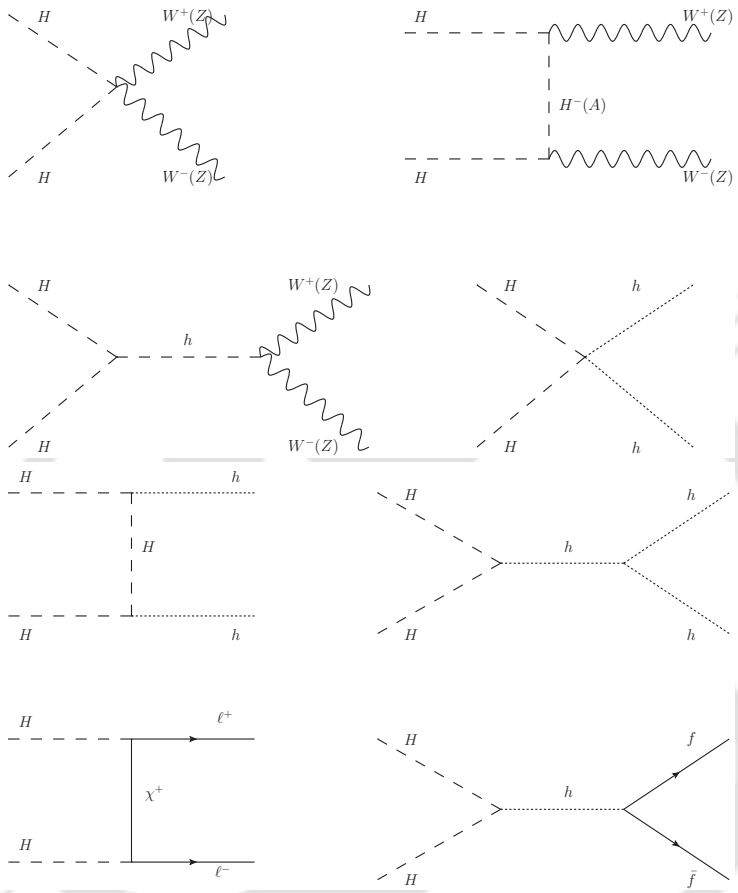

Vita

Shibananda Sahoo was born on 19th May, 1990 in Keonjhar, Odisha, India. He did his B.Sc. with Physics Honours in 2010 from Bhadrak Autonomous College, under Fakir Mohan University, Balasore and M.Sc. in physics from Utkal University, Bhubaneswar, Odisha in 2012. He had enrolled into the Ph.D programme at Indian Institute of Technology Guwahati in 2012. He had qualified Graduate Aptitude Test in Engineering (GATE) in 2012. He had earned the Senior Research Fellowship in 2014 by Indian Institute of Technology Guwahati.